



This is a repository copy of *Mechanisms underlying homeostatic plasticity in the Drosophila mushroom body in vivo*.

White Rose Research Online URL for this paper:  
<http://eprints.whiterose.ac.uk/162916/>

Version: Accepted Version

---

**Article:**

Apostolopoulou, A.A. [orcid.org/0000-0002-8174-4372](https://orcid.org/0000-0002-8174-4372) and Lin, A.C. [orcid.org/0000-0001-6310-9765](https://orcid.org/0000-0001-6310-9765) (2020) Mechanisms underlying homeostatic plasticity in the Drosophila mushroom body in vivo. *Proceedings of the National Academy of Sciences*. ISSN 0027-8424

<https://doi.org/10.1073/pnas.1921294117>

---

© 2020 The Author(s), Published under the PNAS license. This is an author-produced version of a paper subsequently published in *Proceedings of the National Academy of Sciences*. Uploaded in accordance with the publisher's self-archiving policy.

**Reuse**

Items deposited in White Rose Research Online are protected by copyright, with all rights reserved unless indicated otherwise. They may be downloaded and/or printed for private study, or other acts as permitted by national copyright laws. The publisher or other rights holders may allow further reproduction and re-use of the full text version. This is indicated by the licence information on the White Rose Research Online record for the item.

**Takedown**

If you consider content in White Rose Research Online to be in breach of UK law, please notify us by emailing [eprints@whiterose.ac.uk](mailto:eprints@whiterose.ac.uk) including the URL of the record and the reason for the withdrawal request.



[eprints@whiterose.ac.uk](mailto:eprints@whiterose.ac.uk)  
<https://eprints.whiterose.ac.uk/>

1 Mechanisms underlying homeostatic plasticity in the *Drosophila* mushroom body *in*  
2 *vivo*

3

4 Anthi A. Apostolopoulou<sup>1,2</sup>, Andrew C. Lin<sup>1,2\*</sup>

5

6 <sup>1</sup> Department of Biomedical Science, University of Sheffield, Sheffield S10 2TN, UK

7 <sup>2</sup> Neuroscience Institute, University of Sheffield, Sheffield S10 2TN, UK

8

9

10 \*For correspondence: [andrew.lin@sheffield.ac.uk](mailto:andrew.lin@sheffield.ac.uk), +44 114 222 3643

11

12 Classification: Biological Sciences: Neuroscience

13

14

15 **Abstract**

16

17 Neural network function requires an appropriate balance of excitation and inhibition  
18 to be maintained by homeostatic plasticity. However, little is known about  
19 homeostatic mechanisms in the intact central brain *in vivo*. Here, we study  
20 homeostatic plasticity in the *Drosophila* mushroom body, where Kenyon cells receive  
21 feedforward excitation from olfactory projection neurons and feedback inhibition from  
22 the APL neuron. We show that prolonged (4 d) artificial activation of the inhibitory  
23 APL causes increased Kenyon cell odor responses after the artificial inhibition is  
24 removed, suggesting that the mushroom body compensates for excess inhibition. In  
25 contrast, there is little compensation for lack of inhibition (blockade of APL). The  
26 compensation occurs through a combination of increased excitation of Kenyon cells  
27 and decreased activation of APL, with differing relative contributions for different  
28 Kenyon cell subtypes. Our findings establish the fly mushroom body as a model for  
29 homeostatic plasticity *in vivo*.

30

31 Keywords: *Drosophila*, olfaction, homeostatic plasticity, mushroom body

32

33 **Significance statement:** When a neuron fires, it excites or inhibits other neurons.  
34 These two opposing forces – excitation and inhibition – need to be carefully  
35 balanced in the brain for neural networks to function properly. Maintaining this  
36 balance requires homeostatic plasticity to compensate for perturbations in neural  
37 activity levels. Relatively little is known about how such homeostatic compensation  
38 works in the intact central brain *in vivo*. To address this problem, we developed a  
39 model for studying homeostatic plasticity *in vivo*: the *Drosophila* mushroom body (the  
40 fly’s olfactory memory center). We found that this brain structure compensates for  
41 prolonged excess inhibition through a combination of increased excitation and  
42 decreased inhibition, with these two mechanisms contributing differently for different  
43 types of neurons.

44

45 **Introduction**

46

47 Effective information coding in neural networks requires neuronal firing rates to stay  
48 within a certain dynamic range. At the extremes, networks carry no useful

49 information if neurons are completely silent or constantly fire at their highest possible  
50 rate. More subtle differences in activity levels can also affect information coding; for  
51 example, sparse coding of sensory stimuli helps to maximize associative memory  
52 capacity and to separate population representations of different stimuli, thereby  
53 enhancing learned discrimination (1, 2). Yet how do neural networks achieve such  
54 “Goldilocks” activity levels, and how do they maintain them in the face of external  
55 perturbations (e.g., temperature changes) or neural plasticity caused by  
56 development or learning (e.g., Hebbian plasticity, which risks destabilizing activity  
57 levels by strengthening active synapses and weakening inactive synapses)?  
58 Theoretical studies show that this problem can be solved by homeostatic plasticity,  
59 which compensates for changes in activity levels to restore neurons to a “set point”  
60 of activity (3, 4). Such homeostatic plasticity can occur through multiple mechanisms,  
61 including changes in intrinsic excitability, strength or number of excitatory or  
62 inhibitory synaptic inputs, or changes in the threshold between synaptic potentiation  
63 vs. depression (5, 6).

64

65 These findings have mostly come from dissociated neurons *in vitro* or *ex vivo*  
66 preparations like brain slices, sometimes following *in vivo* sensory deprivation like  
67 eyelid suture (e.g., (7-13)). Yet brain slices differ in important ways from the intact  
68 brain *in vivo*: compared to the intact brain, brain slices can have less spontaneous  
69 activity (14) and more synapses (15). Even *in vivo*, neural activity differs significantly  
70 between awake and anesthetized animals (16). Homeostatic compensation has  
71 been studied *in vivo* in the spinal cord (17, 18) and more recently in the brain (19-  
72 24), but the circuit mechanisms underlying homeostatic plasticity in the intact central  
73 brain *in vivo* remain relatively unknown.

74

75 This problem can be addressed in *Drosophila*, whose genetic toolkit and numerically  
76 simple brain allows greater specificity in manipulating and measuring neural activity  
77 *in vivo* than in mammals. These tools have revealed many examples at cellular  
78 resolution of plasticity underlying associative learning (25), non-associative learning  
79 (26-28), activity-dependent remodeling (29, 30) and developmental circuit refinement  
80 (31). However, relatively little is known about homeostatic regulation of activity levels  
81 (but see, e.g., (32)). In most examples of homeostatic compensation studied in  
82 *Drosophila*, the variable being controlled is not activity levels but synaptic strength. In

83 particular, in the most well-understood homeostatically controlled system, the  
84 neuromuscular junction (NMJ), the goal is to maintain constant synaptic strength so  
85 that the muscle can faithfully execute the motor neuron's commands, not to maintain  
86 constant average activity levels in the muscle (33) (see also (34) in the antennal  
87 lobe). It remains unclear whether or how the adult fly brain uses homeostatic  
88 plasticity to maintain activity levels in the correct range.

89

90 We address this question in the fly mushroom body, whose principal neurons, called  
91 Kenyon cells (KCs), receive both feedforward excitation from second-order olfactory  
92 neurons called projection neurons (PNs) and feedback inhibition from a single  
93 neuron called "APL" (anterior paired lateral; **Fig. 1A**) (1, 35-37). This balance of  
94 excitation and inhibition regulates the level of activity in KCs to enforce sparse  
95 coding, in which only a small fraction of KCs responds to each odor (38). This sparse  
96 coding reduces overlap between KC odor representations and enhances learned  
97 odor discrimination (1). However, it remains unclear how KCs set the relative  
98 strength of their excitatory and inhibitory inputs. We hypothesized that this balance  
99 might be set in an activity-dependent manner, in which case the mushroom body  
100 should homeostatically adapt to perturbations in activity levels.

101

102 Here we test the homeostatic capacity of the fly mushroom body *in vivo* and dissect  
103 the underlying circuit mechanisms. We find that the mushroom body compensates  
104 for excess inhibition from APL, but shows little compensation for lack of inhibition.  
105 Compensation for excess inhibition from APL requires multiple days and occurs by  
106 both weakening odor-evoked activity of APL and increasing odor-evoked excitation  
107 of KCs, with differing relative contributions of these two mechanisms in different  
108 subtypes of KCs. These findings establish the fly mushroom body as a model for  
109 studying homeostatic plasticity *in vivo*.

110

## 111 **Results**

112

### 113 **KCs show little compensation for loss of inhibition from APL**

114

115 We first tested whether the mushroom body circuitry adapts to lack of inhibition from  
116 APL. Previously we showed that blocking synaptic output from APL by acutely

117 expressing tetanus toxin (TNT) in APL dramatically increases odor-evoked  $\text{Ca}^{2+}$   
118 influx in KCs (1, 39). We now compared the effects of blocking inhibition from APL  
119 acutely (16-24 h) vs. constitutively (throughout development; **Fig. 1B**). As before, we  
120 expressed TNT in APL by intersecting the expression domains of NP2631-GAL4 and  
121 GH146-FLP, suppressing GAL4 activity in GH146-negative cells by including tubP-  
122 FRT-GAL80-FRT. The GAL80 is excised in GH146-positive cells by FLP  
123 recombinase approximately 50-70% of the time (1). This method drives expression  
124 of UAS-transgenes in APL and not in PNs or KCs ((1) and **Fig. S1A,B**). To express  
125 TNT acutely, we included tubP-GAL80<sup>ts</sup> to suppress GAL4 activity when flies were  
126 kept at 18 °C, and induced expression of TNT by heating the flies to 31 °C for 16–24  
127 h before the experiment. To express TNT in APL constitutively, we left out the tubP-  
128 GAL80<sup>ts</sup> but exposed the flies to the same temperatures as the “acute” flies (**Fig.**  
129 **1B**).

130

131 To confirm that tubP-GAL80<sup>ts</sup> effectively suppressed GAL4 activity in APL in “acute”  
132 flies, we drove CD8::GFP and mCherry in APL (see **Table S1** for full genotypes).  
133 These flies showed GFP expression in APL in 12/18 hemispheres when raised at 18  
134 °C and heated to 31 °C for 16–24 h before dissection (consistent with previous  
135 studies (1)), but in 0/15 hemispheres when kept at 18 °C. Given that both conditions  
136 have the same probability of GAL80 excision (excision occurs in development (40)  
137 so would be unaffected by heating during adulthood), it is extremely unlikely that  
138 GAL80 would be excised in APL in 12/18 hemispheres in one condition but 0/15 in  
139 the other ( $p < 0.0001$ , Fisher’s exact test). Thus, the most plausible explanation is  
140 that GAL80 was excised in APL even in the flies kept at 18 °C, but GAL4 activity was  
141 effectively suppressed by tubP-GAL80<sup>ts</sup>.

142

143 To measure KC odor responses, we expressed GCaMP6f in KCs under the control  
144 of MB247-LexA (41), and TNT in APL using the above-described intersectional  
145 strategy. MB247-LexA does not drive expression in APL ((1) and **Fig. S1C,D**). To  
146 test KC responses for different strengths of excitatory input, we recorded  $\text{Ca}^{2+}$  influx  
147 in KCs evoked by the “strong” odor isoamyl acetate and the “weak” odor  $\delta$ -  
148 decalactone (the former elicits more total activity in olfactory receptor neurons (42)  
149 and KCs (1)). We separately analyzed KC odor responses in the different lobes of  
150 the mushroom body, i.e., the  $\alpha'$  and  $\beta'$  lobes (made up of axons from  $\alpha'\beta'$  KCs), the  $\alpha$

151 and  $\beta$  lobes (axons from  $\alpha\beta$  KCs), and the  $\gamma$  lobe (axons from  $\gamma$  KCs; see diagrams  
152 in **Fig. 1C**), because the three main KC subtypes ( $\alpha'\beta'$ ,  $\alpha\beta$ , and  $\gamma$ ) have different  
153 functional properties (43-46).

154

155 We used two negative controls in which APL did not express TNT. First, we  
156 measured KC odor responses in brain hemispheres in which GAL80 was not excised  
157 in APL (i.e., identical genotype and treatment but no TNT in APL: “APL unlabeled”,  
158 black in **Fig. 1C,D**). We identified which hemispheres had GAL4 activity in APL by  
159 including UAS-mCherry or immunostaining brains for TNT after the experiment. (We  
160 pooled the APL-unlabeled hemispheres from flies with and without tubP-GAL80<sup>ts</sup>  
161 because their odor responses did not differ: **Fig. S2A**; conclusions from statistical  
162 analysis are unchanged if the two groups are separated: **Table S2**).

163

164 Second, to further confirm that tubP-GAL80<sup>ts</sup> suppressed TNT expression in APL to  
165 functionally insignificant levels, we measured KC odor responses in flies with tubP-  
166 GAL80<sup>ts</sup> that were kept at 18 °C throughout life (diagram in **Fig. 1B**, right; data  
167 labeled “18 °C”, green in **Fig. 1C,D**). These flies showed similar responses as the  
168 “APL unlabeled” controls. Although we could not confirm whether GAL80 had been  
169 excised from tubP-FRT-GAL80-FRT in APL in these flies (due to the continued  
170 activity of GAL80<sup>ts</sup>), it is unlikely that all “18 °C” flies would have had APL unlabeled  
171 by chance, given that 28/40 hemispheres had APL labeled in the corresponding  
172 experimental flies that were heated to 31 °C (0/10 at 18 °C vs. 28/40 at 31 °C,  $p <$   
173 0.0001, Fisher’s exact test), by the same logic as the GFP expression experiment  
174 above. This second negative control confirms that our “acute” expression of TNT  
175 was genuinely acute, with functionally no leaky expression of TNT during  
176 development.

177

178 Compared to both of these control groups, both acute and constitutive expression of  
179 TNT in APL dramatically increased odor-evoked Ca<sup>2+</sup> influx in KCs (**Fig. 1C,D**), with  
180 little evidence of homeostatic compensation. We did not observe any consistent  
181 differences in KC response amplitudes between acute vs. constitutive APL>TNT  
182 flies. In some cases, constitutive responses were lower than acute responses and in  
183 others, they were higher (KC responses imaged with GCaMP6f in **Fig. 1**, GCaMP3 in  
184 **Fig. S2B**). Other subtle differences occasionally appeared, e.g., smaller normalized

185 difference between responses to isoamyl acetate and  $\delta$ -decalactone in constitutive  
186 APL>TNT flies, potentially suggesting compensation to restore APL's gain control  
187 function, or reduced post-odor GCaMP signal in constitutive APL>TNT flies,  
188 potentially suggesting altered calcium export (**Fig. S3**). However, again, these  
189 differences were subtle and inconsistent, and thus do not provide clear evidence of  
190 functionally significant adaptation. Thus, taken together, our data indicate that  
191 Kenyon cells show little, if any, homeostatic compensation for prolonged lack of  
192 inhibition from APL.

193

### 194 **KC odor responses are higher following prolonged excess inhibition from APL**

195

196 We next tested the reverse manipulation: rather than blocking APL, we activated  
197 APL with the temperature-sensitive cation channel dTRPA1 (47). Acutely activating  
198 APL with dTRPA1 suppresses odor responses in KCs (1) and activation with  
199 dTRPA1 throughout development induces homeostatic plasticity in larval motor  
200 neurons (29). Given that mammalian cortical plasticity induced by sensory  
201 deprivation can take several days to appear (24, 48), we initially activated APL for 4  
202 d. We expressed GCaMP6f in KCs, and dTRPA1 and mCherry in APL, using the  
203 same drivers as in **Fig. 1**. We raised flies at 22 °C, collected them 0–1 d after  
204 eclosion, and either left them at 22 °C or heated them to 31 °C for 4 d (88–96 h)  
205 before recording KC odor responses at 22 °C (**Fig. 2A**).

206

207 If this prolonged artificial activation of APL induces homeostatic compensation, KC  
208 activity should rebound to abnormally high levels when the artificial activation is  
209 stopped. Indeed, KC odor responses recorded at 22 °C were significantly higher in  
210 hemispheres where APL expressed dTRPA1 when the flies had been pre-heated to  
211 31 °C for 4 d, compared to hemispheres where APL was unlabeled or to flies that  
212 had not been pre-heated. This effect occurred in all lobes, with both the “strong” odor  
213 isoamyl acetate and the “weak” odor  $\delta$ -decalactone (**Fig. 2B,C**). Similar effects were  
214 seen when measuring odor responses with GCaMP3 instead of GCaMP6f (**Fig. S4**),  
215 although the effect in  $\alpha'\beta'$  KCs was less consistent here and in later experiments (see  
216 below). Note that “APL unlabeled” and “APL>dTRPA1” hemispheres had the same  
217 genotype and in many cases were in the same fly, providing an ideal genetic control.

218



219 Increased responses in KC axonal lobes could reflect individual KCs responding  
220 more and/or more KCs responding. To test the latter possibility, we recorded KC  
221 somatic odor responses in pre-heated flies and measured the population sparseness  
222 of the resulting activity maps. Odor responses were less sparse (broader) in  
223 APL>dTRPA1 hemispheres compared to APL unlabeled hemispheres (**Fig. 2D,E,**  
224 **S5A**). We next asked if this broadening would also make KC odor responses more  
225 similar. Although inter-odor correlations between activity maps were somewhat  
226 higher in APL>dTRPA1 hemispheres, the effect was not statistically significant (**Fig.**  
227 **S5B,C**). We may lack statistical power to detect a modest effect, but our sample size  
228 provided 96% power to detect an effect as large as the increase in inter-odor  
229 correlations previously observed in APL>TNT flies (1). This difference could be  
230 explained by the fact that adaptation to APL activation causes a much smaller  
231 increase in KC odor responses than APL>TNT does (**Fig. S5D**).

232

233 The smaller effect of adaptation to APL>dTRPA1 (vs. blocking APL with TNT) also  
234 implies that the adaptation effect cannot be explained trivially as APL simply being  
235 killed or damaged by over-activation by dTRPA1 for 4 d. This trivial explanation is  
236 further excluded by the fact that even after we pre-activated APL with dTRPA1,  
237 heating flies to 31 °C during the imaging experiment to acutely activate APL still  
238 efficiently suppressed KC odor responses (**Fig. S6,S7**, see also **Fig. 5** below).  
239 Moreover, adaptation to APL>dTRPA1 caused no obvious changes in the gross  
240 morphology of KCs or APL (**Fig. S8**). Together, these results suggest that 4 d  
241 APL>dTRPA1 activation induces homeostatic compensation to counteract the  
242 excess activity in APL or insufficient activity in Kenyon cells.

243

244 **Adaptation to excess inhibition from APL is most prominent after 4 days and is**  
245 **temporary**

246

247 To further confirm these results, we repeated the APL>dTRPA1 adaptation  
248 experiments using a different APL driver, VT43924-GAL4, to express dTRPA1 in  
249 APL (49) (see **Fig. S1** for expression pattern). Kenyon cells' odor responses  
250 recorded after 4 d pre-activation of APL were significantly higher (except in the  $\alpha'$   
251 lobe) in flies where APL expressed dTRPA1, compared to flies with UAS-dTRPA1

252 alone (**Fig. 3A**, blue squares; **S9**), thereby reproducing the results obtained with the  
253 intersectional strategy for labeling APL.

254

255 Other model systems show homeostatic compensation in as little as 1 d (9, 19, 23,  
256 50-52). To test whether the mushroom body might similarly compensate within 1 d,  
257 we tested flies after 1 d of pre-activating APL instead of 4 d, while still imaging them  
258 4-5 d after eclosion (**Fig. 3**, blue squares; **S9**). Unlike with 4 d pre-heating, with 1 d  
259 pre-heating, APL>dTRPA1 flies did not have significantly higher KC odor responses  
260 than flies with UAS-dTRPA1 alone (although in some case there was a non-  
261 significant trend toward an increase).

262

263 This difference might arise not from the length of pre-heating but rather from the  
264 timing during the fly's life: perhaps there is a critical period for homeostatic plasticity  
265 in the first day after eclosion. To test this, we pre-heated newly eclosed flies for 1 d.  
266 These flies also showed no significant difference between APL>dTRPA1 flies and  
267 UAS-dTRPA1 controls (**Fig. S10**), suggesting that the difference between 1 d and 4  
268 d pre-heating is not due to a critical period (although there may still be a critical  
269 period such that, e.g., 10 d old flies would not show homeostatic plasticity).

270

271 To further probe when compensation occurs, we tested flies at multiple time points:  
272 1, 2, 3 and 4 d of heating (keeping the age of the fly at imaging constant). To  
273 reproduce our timescale results with a different driver, we returned to the  
274 NP2631/GH146-FLP intersectional driver (**Fig. 3**, black circles). Consistent with the  
275 results with VT43294-GAL4, only at 4 d did we consistently observe significantly  
276 higher KC odor responses in APL>dTRPA1 hemispheres compared to control 'APL  
277 unlabeled' hemispheres (although at 1-3 d there was a trend toward an increase that  
278 was sometimes significant at 2-3 d; **Fig. 3A, S11**). Here and in **Fig. S9**, we do not  
279 exclude the possibility that some small adaptation occurs before 4 d that couldn't be  
280 detected with our statistical power, but these results suggest that the effect is more  
281 prominent after 4 d.

282

283 We next tested how long homeostatic compensation lasts, by taking flies where APL  
284 had been activated for 4 d and leaving them at 22 °C for 1, 2, or 3 d to 'forget' the  
285 adaptation. The difference between APL>dTRPA1 and control hemispheres was no

286 longer statistically significant by 1-2 d (**Fig. 3B, S12**), suggesting that adaptation  
287 does not last more than 1-2 d after excess inhibition from APL stops.

288

### 289 **APL odor responses are reduced following adaptation**

290

291 We next asked what cellular or circuit mechanisms underlie the adaptation observed  
292 above, i.e., increased odor responses in KCs following excess inhibition from APL.

293 We postulated five broad, non-mutually-exclusive categories of mechanisms: (1)  
294 increased synaptic excitation from PNs to KCs, (2) increased intrinsic excitability of  
295 KCs, (3) decreased synaptic excitation from KCs to APL, (4) decreased intrinsic  
296 excitability of APL, and (5) decreased synaptic inhibition from APL to KCs (**Fig. 4A**).

297 Mechanisms 1, 2 and 5 center on KC activity while mechanisms 3 and 4 center on  
298 APL activity. To test these two broad groupings of hypotheses, we recorded odor  
299 responses in APL after adaptation (**Fig. 4B**). If adaptation only involves changes  
300 centered on KC activity (mechanisms 1, 2, 5), then the relation between KC activity  
301 and APL activity would be unchanged; therefore, because APL's odor input comes  
302 from KCs (1), APL should continue to copy whatever KCs do. Thus, APL odor  
303 responses should increase after adaptation just as KC odor responses do. Contrary  
304 to this prediction, after 4 d at 31 °C, APL>dTRPA,GCaMP6f flies showed *decreased*  
305 APL odor responses compared to APL>GCaMP6f (no dTRPA1) flies (**Fig. 4C**),  
306 particularly in the peak response (compare to steady-state responses in **Fig. S13**).  
307 These results suggest that increased KC odor responses after adaptation can be  
308 explained at least in part by decreased activity in the inhibitory APL neuron  
309 (mechanism 3 and/or 4).

310

### 311 **Different KCs show different effects of APL activation after adaptation**

312

313 These results do not rule out the possibility that, in addition to changes in APL  
314 activity, adaptation also involves changes centered on KC activity (mechanisms 1, 2  
315 and 5 above: increased intrinsic excitability, increased synaptic excitation from PNs,  
316 decreased sensitivity to inhibition from APL). To test this possibility, we re-examined  
317 data from **Fig. S6** to focus on KC odor responses during acute activation of APL  
318 (caused by heating APL>dTRPA1 flies to 31 °C during imaging) (**Fig. 5C,D**).

319 Artificially activating APL overrules the reduced odor-evoked activity in APL, making

320 APL activity equal in adapted and non-adapted flies, both before and during odor  
321 pulses (**Fig. 5A,B, S14**). Therefore, if adaptation was due only to reduced APL odor-  
322 evoked activity, then the difference in KC odor response between adapted and non-  
323 adapted flies should go away when we artificially activate APL.

324

325 We observed different results in different KCs. In  $\alpha\beta$  KCs, odor responses in adapted  
326 flies were generally still higher than in non-adapted flies even at 31 °C (**Fig. 5E**). In  
327 contrast, in  $\gamma$  KCs, although odor responses were higher in adapted than non-  
328 adapted flies when recorded at 22 °C, the odor responses declined approximately to  
329 the same level when recorded at 31 °C (**Fig. 5E**). (Note that **Fig. 5** shows mean  $\Delta F/F$   
330 rather than maximum  $\Delta F/F$  because in some cases activating APL with dTRPA1  
331 changed the dynamics of the KC odor responses; see **Fig. S15** for maximum  $\Delta F/F$ ,  
332 which gives similar results.) A power analysis indicates our sample sizes would  
333 detect an effect as strong as that observed in the  $\beta$  lobe with power >0.95. (Odor  
334 responses in  $\alpha'\beta'$  KCs are more difficult to interpret as they did not consistently  
335 decrease when APL was activated by dTRPA1; see **Fig. S6, S7, S15**.) These results  
336 indicate that while adaptation in  $\gamma$  KCs can be explained by decreased APL odor  
337 responses, adaptation in  $\alpha\beta$  KCs requires an additional mechanism.

338

### 339 **Adaptation in $\alpha\beta$ KCs occurs at least partly through non-inhibitory plasticity**

340

341 This additional mechanism in  $\alpha\beta$  KCs could be mechanism 1, 2 and/or 5: increased  
342 intrinsic excitability, increased synaptic excitation from PNs, and/or decreased  
343 sensitivity to inhibition from APL. To distinguish between these possibilities (**Fig. 6A**),  
344 we sought to block inhibition from APL in adapted flies (**Fig. 6B**). If adaptation  
345 occurred solely through weakening inhibition, whether through reducing APL activity  
346 (mechanisms 3 and 4) or reducing KC sensitivity to inhibition (mechanism 5), then  
347 blocking inhibition should remove the difference between adapted and non-adapted  
348 flies. To acutely block inhibition from APL in pre-heated APL>dTRPA1 flies, we  
349 expressed the histamine-gated  $\text{Cl}^-$  channel Ort (53) in APL, and bath-applied  
350 histamine. Ectopically expressing Ort in olfactory neurons allows histamine to  
351 potently inhibit them for at least several minutes (54). We again used the  
352 intersectional driver for APL to express dTRPA1 and Ort in APL, and mb247-LexA to  
353 express GCaMP6f in KCs. In hemispheres where APL was unlabeled, 2 mM

354 histamine did not affect KC odor responses (**Fig. 6C, Fig. S16**); this result is  
355 consistent with the relative absence of histamine and histamine receptors in the  
356 mushroom body (54-60), and argues against non-specific effects of histamine.

357

358 In **Fig. 2-3**, the adapted vs. non-adapted conditions were hemispheres in  
359 APL>dTRPA1 flies where APL was labeled or unlabeled, respectively. However, in  
360 this experiment, we could not use APL-unlabeled hemispheres as controls, because  
361 here we sought to compare adapted vs. non-adapted flies when APL was blocked by  
362 Ort, which is not expressed if APL is unlabeled. In theory, the non-adapted controls  
363 could be either APL>dTRPA1,Ort flies kept at 22 °C or APL>Ort flies (without  
364 dTRPA1) kept at 31 °C. However, in preliminary experiments, we found that in  
365 APL>dTRPA1,Ort flies kept at 22 °C for 4 d, histamine increased KC odor responses  
366 modestly, but not as strongly as in APL>dTRPA1,Ort or APL>Ort flies kept at 31 °C  
367 for 4 d (**Fig. S16**). This temperature dependence suggests that Ort expression was  
368 stronger at 31 °C than 22 °C because Gal4 activity is stronger at higher temperatures  
369 (61). Therefore, APL>dTRPA1,Ort flies kept at 22 °C were not a suitable control.  
370 Instead, we compared only flies kept at 31 °C for 4 d: APL>dTRPA1,Ort (adapted)  
371 and APL>Ort (non-adapted).

372

373 These genotypes replicated the adaptation effect: before adding histamine,  
374 responses in APL>dTRPA1,Ort hemispheres were higher than responses in  
375 APL>Ort (no dTRPA1) hemispheres. (In the  $\alpha'$  and  $\beta'$  lobes, this difference was not  
376 statistically significant (**Fig. S17**); it may be that any adaptation effect in  $\alpha'\beta'$  KCs is  
377 less robust than in  $\alpha\beta$  and  $\gamma$  KCs, as in **Fig. S4,S9,S11,S12**). After adding histamine,  
378 KC responses in both genotypes were dramatically increased, to a similar degree as  
379 that caused by tetanus toxin expression in APL (**Fig. S18**), suggesting that in flies  
380 kept at 31 °C, stimulating Ort in APL with 2 mM histamine suffices to block APL  
381 inhibition onto KCs.

382

383 In the  $\alpha$  and  $\beta$  lobes, after adding histamine, responses to isoamyl acetate in  
384 APL>dTRPA1,Ort hemispheres were still significantly higher than in APL>Ort  
385 hemispheres (**Fig. 6C,D**). That is, even without inhibition from APL, we still observed  
386 the adaptation effect, suggesting that the adaptation from excess APL inhibition  
387 occurs at least in part through non-inhibitory plasticity, i.e., increased synaptic

388 excitation or intrinsic excitability (mechanism 1 or 2), rather than entirely through  
389 decreased sensitivity to inhibition or decreased activity in APL (mechanisms 3-5). In  
390 contrast, in the  $\gamma$  lobe, although APL>dTRPA1,Ort responses were slightly higher  
391 than APL>Ort responses after adding histamine, this difference was not statistically  
392 different. This result suggests that in  $\gamma$  KCs, adaptation from excess APL inhibition  
393 mostly relies on reduced inhibition (mechanisms 3-5). Note that we do not exclude  
394 the possibility that APL>dTRPA1,Ort and APL>Ort  $\gamma$  lobe responses were actually  
395 different and we lacked the statistical power to detect a significant effect due to  
396 experimental variability. Still, this difference between  $\alpha\beta$  and  $\gamma$  KCs is consistent with  
397 the conclusion from APL activation during imaging (**Fig. 5**) that adaptation in  $\gamma$  KCs  
398 can be explained mostly by decreased APL activity (mechanisms 3 and 4) while  
399 adaptation in  $\alpha\beta$  KCs requires something extra.

400

## 401 **Discussion**

402

403 We have delineated the homeostatic capacity of the *Drosophila* mushroom body *in*  
404 *vivo* and revealed circuit mechanisms underlying homeostatic plasticity. We found  
405 that the mushroom body compensates for excess inhibition from APL, but not lack of  
406 inhibition. This compensation requires multiple days and occurs by two mechanisms  
407 — suppressed odor-evoked APL activity and increased odor-evoked excitation of  
408 KCs — which contribute differentially to adaptation in different subtypes of KCs.

409

410 We did not observe clear evidence of compensation for lack of inhibition in APL>TNT  
411 flies. Could this be because our “acute” manipulation (16-24 h TNT expression in  
412 APL) was already long enough to induce adaptation? Two lines of evidence argue  
413 against this possibility. First, the effect of blocking APL with 16-24 h of TNT  
414 expression is at least as strong as the effect of blocking APL with *shibire<sup>ts</sup>*, which  
415 occurs over only ~15 min (1). Second, we saw similar size effects for 16-24 h  
416 APL>TNT expression and APL>Ort + 5 min histamine bath application (**Fig. S18**).  
417 Because 16-24 h APL>TNT expression produces a similar effect on KCs as two  
418 separate acute blockades of APL, we consider it unlikely that a shorter TNT  
419 blockade would produce larger KC odor responses.

420

421 Why do KCs show little compensation for lack of inhibition in APL>TNT flies? For  
422 example, KCs could in theory increase expression of potassium channels to reduce  
423 their excitability (45), yet apparently they do not. It may be that the mushroom body  
424 normally tries to compensate for increased KC activity by increasing inhibition from  
425 APL (i.e., mechanisms 3-5 in the scheme in **Fig. 4A**, but in the opposite direction),  
426 but this strategy fails in APL>TNT flies because synaptic output from APL is  
427 permanently blocked. (Indeed, we observed anecdotally that prolonged APL>TNT  
428 expression appeared to make APL's neurites degenerate: **Fig. S19**.) This  
429 explanation would be consistent with findings in mammals that hyperexcitability is  
430 compensated for by increased synaptic inhibition (62-64). Such mechanisms would  
431 successfully adapt for variable APL activity; their only failure mode (complete  
432 inactivation of APL) might be rare enough not to be worth evolving compensation for.  
433 The lack of compensation for blockade of APL may not be surprising in light of other  
434 findings that even strong homeostatic compensation can be imperfect (65).

435

436 We imposed excess inhibition on KCs by activating APL with dTRPA1 for 4 d.  
437 Although it was not technically feasible to verify by *in vivo* recordings that APL was  
438 continuously activated throughout the 4 d, **Fig. 5A,S14** show that (1) dTRPA1  
439 activation drives  $Ca^{2+}$  influx in APL to a plateau lasting as long as a ~3-4 min heat  
440 stimulus and (2) APL activation during imaging is not affected by APL pre-activation  
441 for 4 d. APL is unlikely to enter depolarization block as it does not fire action  
442 potentials (66). Similarly, activating APL with dTRPA1 still suppresses KC odor  
443 responses after 4 d pre-activation (**Fig. 4,S6-7**). These results suggest that APL  
444 most likely was depolarized throughout the 4 d pre-activation.

445

446 What mechanisms underlie the observed compensation for excess inhibition from  
447 APL? We initially postulated five non-mutually-exclusive categories of mechanisms:  
448 (1) increased synaptic excitation from PNs to KCs, (2) increased intrinsic excitability  
449 of KCs, (3) decreased synaptic excitation from KCs to APL, (4) decreased intrinsic  
450 excitability of APL, and (5) decreased synaptic inhibition from APL to KCs (**Fig. 4A**).  
451 Our finding that APL shows decreased odor responses after adaptation (**Fig. 4**)  
452 implicates decreased synaptic excitation and/or intrinsic excitability of APL  
453 (mechanisms 3 and 4). The equal activation of APL by dTRPA1 in control vs.  
454 adapted flies (**Fig. 5A**) might argue against decreased intrinsic excitability of APL.

455 However, dTRPA1 activation might be so strong as to cause a ceiling effect, or  
456 GAL4-driven dTRPA1 expression in APL might be higher in pre-heated flies (61),  
457 cancelling out any decreased intrinsic excitability.

458

459 Our finding of decreased APL activity after APL over-activation is consistent with  
460 previous studies showing the converse result: that mammalian interneurons increase  
461 their excitability when their activity is blocked (67-69). Yet other studies found  
462 opposite effects: decreasing network activity *decreases* excitability of interneurons  
463 while increasing activity *increases* it (10, 21, 23, 51). These differences likely arise  
464 from whether the system's homeostatic set point focuses on single neurons (i.e.,  
465 inhibitory interneurons try to maintain their desired activity) or the network as a whole  
466 (i.e., if total network activity is decreased, even including decreased interneuron  
467 activity, interneurons should still decrease their excitability to disinhibit the network)  
468 (70). In our case, both scenarios point in the same direction, as our manipulation  
469 activates an inhibitory interneuron (APL) that then inhibits the principal excitatory  
470 neurons (KCs); both the primary and secondary effect demand decreased APL  
471 excitability as the correct homeostatic response.

472

473 We further found that  $\alpha\beta$  (but not  $\gamma$ ) KCs continue to show the adaptation effect when  
474 APL is artificially activated (**Fig. 5**) or blocked (**Fig. 6**), implicating increased synaptic  
475 excitation or intrinsic excitability of KC (mechanisms 1 and/or 2 in  $\alpha\beta$  KCs). These  
476 findings are consistent with other studies showing increased excitation/excitability of  
477 excitatory neurons in response to decreased activity (7, 12, 19, 52, 71, 72). Note that  
478 we do not exclude the possibility of decreased synaptic inhibition from APL to KCs  
479 (mechanism 5); such weakening of inhibition onto excitatory neurons commonly  
480 occurs in response to neuronal inactivity (7, 8, 11, 73). Finally, in contrasting  $\alpha\beta$  KCs  
481 and  $\gamma$  KCs, we do not claim that  $\gamma$  KCs show absolutely no changes in excitation,  
482 merely that we did not find evidence of such changes.

483

484 What molecular mechanisms may be involved? Neurons in the circuit might sense  
485 their abnormally high (APL) or low (KC) activity by reactive oxygen species via the  
486 redox sensor DJ-1 $\beta$  (29) or by  $Ca^{2+}$  levels via CaM kinase (9, 72). Our finding that  
487 adaptation takes more than 1 d suggests that the effector arm of the homeostatic  
488 mechanism may involve altered transcription or translation. Increased (KCs) or



489 decreased (APL) synaptic excitation (mechanisms 1 and 3 above) might occur  
490 through altered synapse size/number (30) or altered surface expression of post-  
491 synaptic nicotinic acetylcholine receptors, as occurs with AMPA receptors in  
492 plasticity of glutamatergic synapses (74, 75). Such changes could also occur by  
493 altered pre-synaptic release from PNs or KCs, respectively. However, we consider  
494 pre-synaptic plasticity in PNs less likely, as this would be expected to affect all KCs  
495 equally rather than only  $\alpha\beta$  KCs, whereas we only observed increased  
496 excitation/excitability in  $\alpha\beta$  KCs, not  $\gamma$  KCs. Increased (KCs) or decreased (APL)  
497 intrinsic excitability (mechanisms 2 and 4 above) might occur through altered ion  
498 channel expression, as observed in *Drosophila* larval motor neurons (32), or (for  
499 KCs) through moving the axon initial segment (76, 77).

500

501 We do not exclude the possibility that other neurons in the mushroom body could be  
502 involved in the observed homeostatic compensation. For example, DPM ('dorsal  
503 paired medial') also forms reciprocal synapses with KCs (78) and contains GABA  
504 (79), so it may be that DPM reduces inhibition of KCs to compensate for excess  
505 inhibition from APL. However, unlike APL, DPM shows little or no expression of  
506 GABAergic markers (56). Moreover, there is no published physiological evidence  
507 that DPM directly inhibits KCs; DPM and APL are connected by gap junctions (80) so  
508 findings that activating DPM increases chloride concentrations in KCs (79) could be  
509 explained by DPM activating APL. If increased KC activity arises in part from  
510 decreased DPM activity causing decreased APL activity via DPM-APL gap junctions,  
511 this could be considered a special case of decreased synaptic excitation from KCs to  
512 APL.

513

514 Our findings that adaptation occurs over multiple days (**Fig. 3, S9-S11**) fit in with  
515 diverse adaptation timescales in other *in vivo* studies. Following sensory deprivation  
516 in mammals, recovery of cortical activity levels from their nadir can take ~1-3 d (21,  
517 48, 81), even up to 7 d (24). In other cases, adaptation occurs within 24 h (19, 23,  
518 50, 51). It may be that the incomplete suppression of KC odor responses by  
519 APL>dTRPA1 activation (**Fig. 5, S6-7**) is a less drastic effect than, e.g., the effect of  
520 eyelid suture on visually evoked cortical activity. Intuitively, it is reasonable that  
521 homeostatic mechanisms may take longer to sense and respond to a less drastic  
522 activity perturbation. Alternatively, it may simply be that the mushroom body is less

523 efficient at compensating for activity perturbations than mammalian cortex, whether  
524 due to differences between species or types of brain structures. Future studies may  
525 address these and other questions about the timescale of adaptation, such as  
526 whether adaptation occurs in older flies, or whether different underlying mechanisms  
527 kick in at different times during the multi-day unfolding of homeostatic adaptation.

528

529 Finally, what is the behavioral significance of homeostatic adaptation in Kenyon  
530 cells? In the example studied here, increased KC activity following excess inhibition  
531 makes odor responses less sparse (**Fig. 2D**), which could impair learned odor  
532 discrimination (1). However, it is unclear if the relatively modest decrease in  
533 sparseness would measurably impair odor discrimination, especially as we did not  
534 detect a significant increase in inter-odor correlations. Indeed, the adaptation might  
535 even improve associative olfactory learning, given that improved learning is seen  
536 when KC activity is modestly increased by downregulating GABA synthesis in APL  
537 (vs. blocking APL output completely) (1, 36, 37). Future work may address which (if  
538 any) of these potential behavioral outcomes occurs. Conversely, given that  
539 homeostatic compensation following APL>dTRPA1 pre-activation allows  $\alpha\beta$  (but not  
540  $\gamma$ ) KC odor responses to approach normal amplitudes during acute APL>dTRPA1  
541 activation despite the excess inhibition (**Fig. 5**), it will be interesting to test whether  
542 pre-activating APL analogously allows flies to resist whatever learning impairment (if  
543 any) might normally result from acutely inhibiting KCs with APL>dTRPA1. If so,  
544 homeostatic adaptation might help flies avoid detection failures in the case of hyper-  
545 inhibition. Indeed, a greater need to avoid detection failures than discrimination  
546 failures could explain why the mushroom body compensates for KC hypo-activity but  
547 not hyper-activity. More generally, homeostatic plasticity may reflect broader activity-  
548 dependent parameter setting in KCs that helps achieve reliably distributed sparse  
549 odor coding (82).

550

551

552 **Methods**

553

554 See **SI Appendix, Supplementary Methods** for details.

555

556 **Fly strains**

557 Flies were raised on standard cornmeal agar at the temperatures described. Details  
558 of fly strains are given in **Supplementary Methods**.

559

560 **Imaging**

561 Brains were imaged by two-photon microscopy on a Movable Objective Microscope  
562 (Sutter) using ScanImage software (Vidrio), as described (1, 43). Volume imaging  
563 was performed in sawtooth mode (typically 10-16 z slices, volume rate ~3 Hz).  
564 Movies were motion-corrected in X-Y using the moco ImageJ plugin (83), and  
565 motion-corrected in Z by maximizing the pixel-by-pixel correlation between each  
566 volume and the average volume across time points (43).  $\Delta F/F$  traces were calculated  
567 in ImageJ using manually-drawn ROIs for the background and brain structure of  
568 interest, and smoothed with a 0.2 s boxcar filter and interpolated to common frame  
569 times for averaging traces in Igor Pro 7 (WaveMetrics).  $\Delta R/R$  in **Fig. 5, Fig. S14** was  
570 calculated by dividing GCaMP6f signal by dsRed signal, to remove motion artifacts  
571 caused by heating. Sparseness and correlation were analyzed as in (1). Histamine  
572 (2 mM, Sigma H7250) was added 5 min before imaging in APL>Ort experiments.

573

574 **Data availability statement**

575 All data necessary to reproduce our findings and figures is included in the SI  
576 Dataset. Analysis code is available at <https://github.com/aclinlab/calcium-imaging>.

577

578 **Acknowledgements**

579 We thank members of the Lin and Juusola labs for discussions, Moshe Parnas,  
580 Mikko Juusola, and Anton Nikolaev for comments on the manuscript, Lily Bolsover,  
581 Chloe Donahue, Kath Whitley, Josh Marston, Rachael Thomas, and Rachid Achour  
582 for technical assistance, and Chi-hon Lee (Academia Sinica), the Bloomington Stock  
583 Center, and the Vienna *Drosophila* Resource Center for flies. This work was  
584 supported by the European Research Council (639489) and the Biotechnology and  
585 Biological Sciences Research Council (BB/S016031/1).

586

587 **Figure legends**

588

589 **Fig. 1. Kenyon cells show little compensation for loss of inhibition from APL**

590 (A) Schematic of mushroom body circuitry: Kenyon cells (KCs) receive  
591 feedforward excitation from projection neurons (PNs) and feedback inhibition  
592 from APL.

593 (B) Diagram of genotype (green shows GCaMP6f expression; orange X shows  
594 blockade with TNT) and experimental protocol. Flies were raised at 18 °C,  
595 collected 0–1 d after eclosion, then kept at 18 °C for 3 d and heated to 31 °C  
596 for 16–24 h (middle panel) or kept at 18 °C for 4 d (right panel) before the  
597 imaging experiment, which was always done at 22 °C.

598 (C) Responses of different KC lobes to isoamyl acetate (IA, upper) or  $\delta$ -  
599 decalactone ( $\delta$ DL, lower), imaged with GCaMP6f. Black bars, 5 s odor pulse;  
600 shading, s.e.m. Diagrams show the locations of different lobes in the  
601 mushroom body (green; medial is left, dorsal is up). See also **Fig. S2-3**.

602 (D) Maximum  $\Delta F/F$  of data from C. Half-filled circles mean the category pools  
603 data, i.e., APL labeled and unlabeled (green), with GAL80<sup>ts</sup> and without  
604 (black). Mean  $\pm$  95% confidence interval. #  $p < 0.05$  between acute vs.  
605 constitutive, \*  $p < 0.001$  between TNT expressed (acute or constitutive) vs.  
606 TNT not expressed (18 °C or APL unlabeled), ANOVA (see **Table S2** for  
607 details). n, given as # hemispheres (# flies), left to right:  $\alpha'$  and  $\alpha$ , 9 (5), 9 (7),  
608 22 (15), 17 (10);  $\beta'$ ,  $\beta$  and  $\gamma$ , 10 (5), 19 (14), 28 (19), 26 (15).

609

610 **Fig. 2. Kenyon cell odor responses are higher following prolonged excess**  
611 **inhibition from APL**

612 (A) Diagram of genotype (green shows GCaMP6f expression; magenta shows  
613 activation with dTRPA1) and experimental protocol. Flies were raised at 22  
614 °C, collected 0–1 d after eclosion, kept at 22 °C (control) or 31 °C (pre-heated)  
615 for 4 d, and returned to 22 °C for the imaging experiment.

616 (B) Responses of the  $\gamma$  lobe to isoamyl acetate, for flies kept at 22 °C (upper) or  
617 31 °C (lower), where APL was unlabeled (grey/black) or expressed dTRPA1  
618 (pink/red). Black bars, 5 s odor pulse; shading, s.e.m. Responses of all lobes  
619 shown in **Fig. S4**.

620 (C) Maximum  $\Delta F/F$  of odor responses in all lobes to isoamyl acetate (IA) and  $\delta$ -  
621 decalactone ( $\delta$ DL). \*  $p < 0.05$ , \*\*  $p < 0.01$ , \*\*\*  $p < 0.001$ , ANOVA (see **Table**  
622 **S2** for details). n, given as # hemispheres (# flies), left to right within each  
623 graph: 9 (8), 15 (11), 11 (7), 13 (8).  
624 (D) Activity maps of responses to isoamyl acetate in KC somata. Grayscale  
625 shows baseline fluorescence of GCaMP6f; false-color overlay shows odor-  
626 responsive pixels. Scale bar 10  $\mu$ m.  
627 (E) Average sparseness to a panel of 6 odors ( $\delta$ -decalactone, isoamyl acetate,  
628 ethyl butyrate, methylcyclohexanol, 3-octanol, benzaldehyde; sparseness to  
629 each odor shown separately in **Fig. S5**). Mean  $\pm$  95% confidence interval. \*\*\*  
630  $p < 0.001$ , unpaired t-test.

631

632 **Fig. 3. Adaptation to excess inhibition from APL is most prominent after 4 days**  
633 **and is temporary**

634 (A) Adaptation after 1, 2, 3, or 4 d of APL activation. Flies were raised at 22 °C  
635 and collected 0-1 d after eclosion, then kept at 22 °C for 0-3 d, then kept at 31  
636 °C for 1-4 d, and imaged at 22 °C at 4-5 d post-eclosion. Graphs show effect  
637 size of adaptation (maximum  $\Delta F/F$  of KC response to isoamyl acetate,  
638 APL>dTRPA1 minus control), calculated using bootstrap-coupled estimation  
639 statistics (84), driving dTRPA1 expression in APL using NP2631+GH146-FLP  
640 (black circles; control is APL unlabeled) or VT43924-GAL4 (blue squares;  
641 control is UAS-dTRPA1/+). Error bars, 95% confidence intervals. In the  
642 diagram of the genotype (upper left), green shows GCaMP6f expression,  
643 magenta shows activation with dTRPA1. \*  $p < 0.05$  for APL>dTRPA1 vs.  
644 control, ANOVA (see **Table S2** for details). ns ( $p > 0.05$ ) applies to both  
645 drivers at 1 d. Full data and sample sizes for all lobes in **Fig. S9-11**.

646 (B) As in A, except flies were all kept at 31 °C for 4 d, then kept at 22 °C for 0-3 d  
647 before imaging. Data for 0 d is repeated from '4 d' in panel A for comparison.  
648 Full data in **Fig. S12**.

649

650 **Fig. 4. APL odor responses are reduced following adaptation**

651 (A) Diagrams of potential mechanisms that might underlie increased KC odor  
652 responses following adaptation. This figure tests mechanisms 1, 2, 5 vs.  
653 mechanisms 3-4, and shows evidence for mechanisms 3-4 (blue box).

654 (B) Diagram of genotype (APL expresses dTRPA1 and GCaMP6f) and  
 655 experimental protocol (all flies were raised at 22 °C and kept at 31 °C for 4 d  
 656 before imaging).

657 (C) Responses of different lobes of APL (as determined by the anatomical marker  
 658 mb247-dsRed) to isoamyl acetate in APL>GCaMP6f (“no dTRPA1”) or  
 659 APL>dTRPA1,GCaMP6f (“APL>dTRPA1”) flies kept at 31 °C for 4 d.  
 660 Diagrams show the locations of different lobes (green) within APL, which  
 661 innervates the whole mushroom body. Graphs show maximum  $\Delta F/F$ , mean  $\pm$   
 662 95% confidence interval; shading, s.e.m. \*  $p < 0.05$ , \*\*  $p < 0.01$ , unpaired t-  
 663 test or Mann-Whitney test (see **Table S2** for details). n, left to right:  $\alpha'$  and  $\alpha$ ,  
 664 12 (9 flies), 12(8 flies);  $\beta'$ ,  $\beta$  and  $\gamma$ , 12 (9 flies), 13 (8 flies).

666 **Fig. 5. Different KCs show different effects of APL activation after adaptation**

667 (A) APL is equally activated by dTRPA1 regardless of pre-heating. Upper traces  
 668 show GCaMP6f signal of  $\beta$  lobe of APL (as determined by the anatomical  
 669 marker mb247-dsRed), normalized to dsRed signal (hence  $\Delta R/R$ , not  $\Delta F/F$ ),  
 670 during perfusion heating of saline, in APL>TRPA,GCaMP6f flies kept at 22 °C  
 671 (black) or 31 °C (red) for 4 d. Blue shading shows periods used for  
 672 quantification in (B): After temperature reached a plateau (period 1), isoamyl  
 673 acetate (period 2) and  $\delta$ -decalactone (period 3) were presented. Lower traces  
 674 show the saline temperature corresponding to recordings in the upper traces  
 675 (same color scheme and time scale). Shading, s.e.m. Other lobes shown in  
 676 **Fig. S14.**

677 (B) Quantification of periods from A: average  $\Delta R/R$  during temperature plateau  
 678 (period 1) and maximum  $\Delta R/R$  during odors (periods 2, 3). Maximum  $\Delta R/R$  is  
 679 used for odors for consistency with **Fig. 4**. Graphs show mean  $\pm$  95%  
 680 confidence interval. n.s.  $p > 0.05$ , unpaired t-test or Mann-Whitney test. n: 22  
 681 °C, 10 (8 flies); 31 °C, 8 (6 flies).

682 (C) This figure tests mechanisms 1, 2, 5 vs. mechanisms 3-4, and shows  
 683 evidence for mechanisms 1, 2, 5 (blue box) in  $\alpha\beta$  KCs.

684 (D) Diagram of genotype (APL expresses dTRPA1, KCs express GCaMP6f) and  
 685 experimental protocol for (E).

686 (E) Traces show responses of the  $\alpha$ ,  $\beta$ , and  $\gamma$  lobes to isoamyl acetate (IA, left)  
 687 and  $\delta$ -decalactone ( $\delta$ DL, right) in KC>GCaMP6f, APL>dTRPA1 flies kept at

688 22 °C or 31 °C for 4 d, recorded at 22 °C (black) or 31 °C (magenta). Only  
689 paired recordings are shown (same fly recorded at both temperatures). Black  
690 bars, 5 s odor pulse; shading, s.e.m. Bar graphs quantify traces using mean  
691  $\Delta F/F$  during the odor pulse (same color scheme as traces; bars show mean,  
692 thin lines show paired data recorded at 22 °C and 31 °C). Data for  $\alpha\beta'$  KCs  
693 and maximum  $\Delta F/F$  given in **Fig. S15**. \*  $p < 0.05$ , \*\*  $p < 0.01$ , \*\*\*  $p < 0.001$ ,  
694 paired t-test or Wilcoxon test (22 °C vs. 31 °C), unpaired t-test or Mann-  
695 Whitney test (across flies), with Holm-Bonferroni correction (see **Table S2** for  
696 details). n as in **Fig. S6, S7**.

697

698 **Fig. 6. Adaptation effect remains in  $\alpha\beta$  KCs after removing inhibition from APL**

699 (A) This figure tests mechanisms 1-2 vs. mechanisms 3-5, and shows evidence  
700 for mechanisms 1-2 (blue box) in  $\alpha\beta$  KCs.

701 (B) Diagram of genotype and experimental protocol. Flies were raised at 22 °C,  
702 collected 0–1 d after eclosion, kept at 31 °C for 4 d, and returned to 22 °C for  
703 the imaging experiment. During the experiment, odor responses were  
704 recorded before and after bath-applying 2 mM histamine.

705 (C) Responses of  $\alpha$ ,  $\beta$  and  $\gamma$  lobes to isoamyl acetate before (black) and after  
706 (orange) bath-applying 2 mM histamine. Genotypes: mixture of hemispheres  
707 from APL>Ort and APL>dTRPA1,Ort flies where APL was unlabeled (left);  
708 APL>Ort, APL labeled (middle); APL>dTRPA1,Ort, APL labeled (right).  
709 Shading, s.e.m. Traces of other lobes and responses to  $\delta$ -decalactone are  
710 shown in **Fig. S16,S17**.

711 (D) Maximum  $\Delta F/F$  for traces in (C). Genotypes: APL>Ort (left), APL>dTRPA1,Ort  
712 (right). Bars show mean, thin lines show paired data (same hemisphere  
713 before and after histamine). The effect of histamine was statistically significant  
714 in all cases ( $p < 0.001$ , paired t-test or Wilcoxon test). \*  $p < 0.05$ , \*\*  $p < 0.01$ ,  
715 unpaired t-test or Mann-Whitney test, Holm-Bonferroni correction for multiple  
716 comparisons (see **Table S2** for details). n: no dTRPA1, 17 (11 flies);  
717 APL>dTRPA1, 16 (11 flies).

718

719

720

721 **References**

722

- 723 1. Lin AC, Bygrave AM, de Calignon A, Lee T, Miesenböck G (2014) Sparse,  
724 decorrelated odor coding in the mushroom body enhances learned odor  
725 discrimination. *Nat Neurosci* 17(4):559–568.
- 726 2. Olshausen BA, Field D (2004) Sparse coding of sensory inputs. *Curr Opin*  
727 *Neurobiol* 14(4):481–487.
- 728 3. Litwin-Kumar A, Doiron B (2014) Formation and maintenance of neuronal  
729 assemblies through synaptic plasticity. *Nature Communications* 5(1):1–12.
- 730 4. O'Leary T, Williams AH, Franci A, Marder E (2014) Cell Types, Network  
731 Homeostasis, and Pathological Compensation from a Biologically Plausible Ion  
732 Channel Expression Model.
- 733 5. Keck T, Hübener M, Bonhoeffer T (2017) Interactions between synaptic  
734 homeostatic mechanisms: an attempt to reconcile BCM theory, synaptic  
735 scaling, and changing excitation/inhibition balance. *Curr Opin Neurobiol*  
736 43:87–93.
- 737 6. Turrigiano G (2011) Too many cooks? Intrinsic and synaptic homeostatic  
738 mechanisms in cortical circuit refinement. *Annu Rev Neurosci* 34:89–103.
- 739 7. Maffei A, Nelson SB, Turrigiano GG (2004) Selective reconfiguration of layer 4  
740 visual cortical circuitry by visual deprivation. *Nat Neurosci* 7(12):1353–1359.
- 741 8. Maffei A, Turrigiano GG (2008) Multiple Modes of Network Homeostasis in  
742 Visual Cortical Layer 2/3. *J Neurosci* 28(17):4377–4384.
- 743 9. Goold CP, Nicoll RA (2010) Single-cell optogenetic excitation drives  
744 homeostatic synaptic depression. *Neuron* 68(3):512–528.
- 745 10. Chang MC, et al. (2010) Narp regulates homeostatic scaling of excitatory  
746 synapses on parvalbumin-expressing interneurons. *Nat Neurosci* 13(9):1090–  
747 1097.
- 748 11. Lau CG, Murthy VN (2012) Activity-Dependent Regulation of Inhibition via  
749 GAD67. *J Neurosci* 32(25):8521–8531.
- 750 12. Desai NS, Cudmore RH, Nelson SB, Turrigiano GG (2002) Critical periods for  
751 experience-dependent synaptic scaling in visual cortex. *Nat Neurosci*  
752 5(8):783–789.
- 753 13. Wenner P (2014) Homeostatic synaptic plasticity in developing spinal networks  
754 driven by excitatory GABAergic currents. *Neuropharmacology* 78:55–62.
- 755 14. Destexhe A, Rudolph M, Paré D (2003) The high-conductance state of  
756 neocortical neurons in vivo. *Nat Rev Neurosci* 4(9):739–751.
- 757 15. Kirov SA, Sorra KE, Harris KM (1999) Slices have more synapses than  
758 perfusion-fixed hippocampus from both young and mature rats. *J Neurosci*



- 759 19(8):2876–2886.
- 760 16. Cazakoff BN, Lau BYB, Crump KL, Demmer HS, Shea SD (2014) Broadly  
761 tuned and respiration-independent inhibition in the olfactory bulb of awake  
762 mice. *Nat Neurosci* 17(4):569–576.
- 763 17. Knogler LD, Liao M, Drapeau P (2010) Synaptic scaling and the development  
764 of a motor network. *J Neurosci* 30(26):8871–8881.
- 765 18. Mongeon R, et al. (2008) Synaptic Homeostasis in a Zebrafish Glial Glycine  
766 Transporter Mutant. *J Neurophysiol* 100(4):1716–1723.
- 767 19. Keck T, et al. (2013) Synaptic scaling and homeostatic plasticity in the mouse  
768 visual cortex in vivo. *Neuron* 80(2):327–334.
- 769 20. Barnes SJ, et al. (2015) Subnetwork-Specific Homeostatic Plasticity in Mouse  
770 Visual Cortex In Vivo. *Neuron* 86(5):1290–1303.
- 771 21. Hengen KB, Lambo ME, Van Hooser SD, Katz DB, Turrigiano GG (2013)  
772 Firing rate homeostasis in visual cortex of freely behaving rodents. *Neuron*  
773 80(2):335–342.
- 774 22. Hengen KB, Torrado Pacheco A, McGregor JN, Van Hooser SD, Turrigiano  
775 GG (2016) Neuronal Firing Rate Homeostasis Is Inhibited by Sleep and  
776 Promoted by Wake. *Cell* 165(1):180–191.
- 777 23. Kuhlman SJ, et al. (2013) A disinhibitory microcircuit initiates critical-period  
778 plasticity in the visual cortex. *Nature* 501(7468):543–546.
- 779 24. Greenhill SD, Ranson A, Fox K (2015) Hebbian and Homeostatic Plasticity  
780 Mechanisms in Regular Spiking and Intrinsic Bursting Cells of Cortical Layer 5.  
781 *Neuron* 88(3):539–552.
- 782 25. Amin H, Lin AC (2019) Neuronal mechanisms underlying innate and learned  
783 olfactory processing in *Drosophila*. *Current Opinion in Insect Science* 36:9–17.
- 784 26. Devaud JM, Acebes A, Ferrus A (2001) Odor exposure causes central  
785 adaptation and morphological changes in selected olfactory glomeruli in  
786 *Drosophila*. *J Neurosci* 21(16):6274–6282.
- 787 27. Sachse S, et al. (2007) Activity-dependent plasticity in an olfactory circuit.  
788 *Neuron* 56(5):838–850.
- 789 28. Das S, et al. (2011) Plasticity of local GABAergic interneurons drives olfactory  
790 habituation. *Proc Natl Acad Sci USA* 108(36):E646–E654.
- 791 29. Oswald MC, et al. (2018) Reactive oxygen species regulate activity-dependent  
792 neuronal plasticity in *Drosophila*. *Elife* 7:1321.
- 793 30. Kremer MC, et al. (2010) Structural long-term changes at mushroom body  
794 input synapses. 20(21):1938–1944.

- 795 31. Doll CA, Vita DJ, Broadie K (2017) Fragile X Mental Retardation Protein  
796 Requirements in Activity-Dependent Critical Period Neural Circuit Refinement.  
797 27(15):2318–2330.e3.
- 798 32. Mee CJ, Pym ECG, Moffat KG, Baines RA (2004) Regulation of neuronal  
799 excitability through pumilio-dependent control of a sodium channel gene. *J*  
800 *Neurosci* 24(40):8695–8703.
- 801 33. Davis GW (2013) Homeostatic signaling and the stabilization of neural  
802 function. *Neuron* 80(3):718–728.
- 803 34. Kazama H, Wilson RI (2008) Homeostatic matching and nonlinear  
804 amplification at identified central synapses. *Neuron* 58(3):401–413.
- 805 35. Gruntman E, Turner GC (2013) Integration of the olfactory code across  
806 dendritic claws of single mushroom body neurons. *Nat Neurosci* 16(12):1821–  
807 1829.
- 808 36. Liu X, Davis RL (2008) The GABAergic anterior paired lateral neuron  
809 suppresses and is suppressed by olfactory learning. *Nat Neurosci* 12(1):53–  
810 59.
- 811 37. Lei Z, Chen K, Li H, Liu H, Guo A (2013) The GABA system regulates the  
812 sparse coding of odors in the mushroom bodies of *Drosophila*. *Biochem*  
813 *Biophys Res Commun* 436(1):35–40.
- 814 38. Honegger KS, Campbell RAA, Turner GC (2011) Cellular-resolution population  
815 imaging reveals robust sparse coding in the *Drosophila* mushroom body. *J*  
816 *Neurosci* 31(33):11772–11785.
- 817 39. Mittal AM, Gupta D, Singh A, Lin AC, Gupta N (2020) Multiple network  
818 properties overcome random connectivity to enable stereotypic sensory  
819 responses. *Nature Communications* 11(1):1–15.
- 820 40. Mayseless O, et al. (2018) Developmental Coordination during Olfactory  
821 Circuit Remodeling in *Drosophila*. *Neuron* 99(6):1204–1215.e5.
- 822 41. Pitman JL, et al. (2011) A pair of inhibitory neurons are required to sustain  
823 labile memory in the *Drosophila* mushroom body. *Current Biology* 21(10):855–  
824 861.
- 825 42. Hallem EA, Carlson JR (2006) Coding of Odors by a Receptor Repertoire. *Cell*  
826 125(1):143–160.
- 827 43. Bielopolski N, et al. (2019) Inhibitory muscarinic acetylcholine receptors  
828 enhance aversive olfactory learning in adult *Drosophila*. *Elife* 8:463.
- 829 44. Turner GC, Bazhenov M, Laurent G (2008) Olfactory representations by  
830 *Drosophila* mushroom body neurons. *J Neurophysiol* 99(2):734–746.
- 831 45. Groschner LN, Chan Wah Hak L, Bogacz R, DasGupta S, Miesenböck G  
832 (2018) Dendritic Integration of Sensory Evidence in Perceptual Decision-

- 833 Making. *Cell* 173(4):894–905.e13.
- 834 46. Inada K, Tsuchimoto Y, Kazama H (2017) Origins of Cell-Type-Specific  
835 Olfactory Processing in the *Drosophila* Mushroom Body Circuit. *Neuron*  
836 95(2):357–367.e4.
- 837 47. Hamada FN, et al. (2008) An internal thermal sensor controlling temperature  
838 preference in *Drosophila*. *Nature* 454(7201):217–220.
- 839 48. Frenkel MY, Bear MF (2004) How Monocular Deprivation Shifts Ocular  
840 Dominance in Visual Cortex of Young Mice. *Neuron* 44(6):917–923.
- 841 49. Wu C-L, Shih M-FM, Lee P-T, Chiang A-S (2013) An octopamine-mushroom  
842 body circuit modulates the formation of anesthesia-resistant memory in  
843 *Drosophila*. *Current Biology* 23(23):2346–2354.
- 844 50. Barnes SJ, et al. (2017) Deprivation-Induced Homeostatic Spine Scaling  
845 In Vivo Is Localized to Dendritic Branches that Have Undergone Recent Spine  
846 Loss. *Neuron* 96(4):871–882.e5.
- 847 51. Gainey MA, Aman JW, Feldman DE (2018) Rapid Disinhibition by Adjustment  
848 of PV Intrinsic Excitability during Whisker Map Plasticity in Mouse S1. *J*  
849 *Neurosci* 38(20):4749–4761.
- 850 52. Turrigiano GG, Leslie KR, Desai NS, Rutherford LC, Nelson SB (1998)  
851 Activity-dependent scaling of quantal amplitude in neocortical neurons. *Nature*  
852 391(6670):892–896.
- 853 53. Pantazis A, et al. (2008) Distinct roles for two histamine receptors (hclA and  
854 hclB) at the *Drosophila* photoreceptor synapse. *J Neurosci* 28(29):7250–7259.
- 855 54. Liu WW, Wilson RI (2013) Transient and specific inactivation of *Drosophila*  
856 neurons in vivo using a native ligand-gated ion channel. 23(13):1202–1208.
- 857 55. Pollack I, Hofbauer A (1991) Histamine-like immunoreactivity in the visual  
858 system and brain of *Drosophila melanogaster*. *Cell Tissue Res* 266(2):391–  
859 398.
- 860 56. Aso Y, et al. (2019) Nitric oxide acts as a cotransmitter in a subset of  
861 dopaminergic neurons to diversify memory dynamics. *Elife* 8:e49257.
- 862 57. Croset V, Treiber CD, Waddell S (2018) Cellular diversity in the *Drosophila*  
863 midbrain revealed by single-cell transcriptomics. *Elife* 7:e34550.
- 864 58. Davie K, et al. (2018) A Single-Cell Transcriptome Atlas of the Aging  
865 *Drosophila* Brain. *Cell* 174(4):982–998.e20.
- 866 59. Shih M-FM, Davis FP, Henry GL, Dubnau J (2019) Nuclear Transcriptomes of  
867 the Seven Neuronal Cell Types That Constitute the *Drosophila* Mushroom  
868 Bodies. *G3 (Bethesda)* 9(1):81–94.
- 869 60. Crocker A, Guan X-J, Murphy CT, Murthy M (2016) Cell-Type-Specific

- 870 Transcriptome Analysis in the Drosophila Mushroom Body Reveals Memory-  
871 Related Changes in Gene Expression. *Cell Rep* 15(7):1580–1596.
- 872 61. Duffy JB (2002) GAL4 system in Drosophila: a fly geneticist's Swiss army  
873 knife. *genesis* 34(1-2):1–15.
- 874 62. Sim S, et al. (2013) Increased cell-intrinsic excitability induces synaptic  
875 changes in new neurons in the adult dentate gyrus that require Npas4. *J*  
876 *Neurosci* 33(18):7928–7940.
- 877 63. Peng Y-R, et al. (2010) Postsynaptic spiking homeostatically induces cell-  
878 autonomous regulation of inhibitory inputs via retrograde signaling. *J Neurosci*  
879 30(48):16220–16231.
- 880 64. Xue M, Atallah BV, Scanziani M (2014) Equalizing excitation-inhibition ratios  
881 across visual cortical neurons. *Nature* 511(7511):596–600.
- 882 65. Howard MA, Rubenstein JLR, Baraban SC (2014) Bidirectional homeostatic  
883 plasticity induced by interneuron cell death and transplantation in vivo. *Proc*  
884 *Natl Acad Sci USA* 111(1):492–497.
- 885 66. Papadopoulou M, Cassenaer S, Nowotny T, Laurent G (2011) Normalization  
886 for sparse encoding of odors by a wide-field interneuron. *Science*  
887 332(6030):721–725.
- 888 67. Bartley AF, Huang ZJ, Huber KM, Gibson JR (2008) Differential Activity-  
889 Dependent, Homeostatic Plasticity of Two Neocortical Inhibitory Circuits. *J*  
890 *Neurophysiol* 100(4):1983–1994.
- 891 68. Rutherford LC, Nelson SB, Turrigiano GG (1998) BDNF Has Opposite Effects  
892 on the Quantal Amplitude of Pyramidal Neuron and Interneuron Excitatory  
893 Synapses. *Neuron* 21(3):521–530.
- 894 69. Desai NS, Rutherford LC, Turrigiano GG (1999) BDNF regulates the intrinsic  
895 excitability of cortical neurons. *Learn Mem* 6(3):284–291.
- 896 70. Wenner P (2011) Mechanisms of GABAergic Homeostatic Plasticity. *Neural*  
897 *Plast* 2011(5161):1–6.
- 898 71. Burrone J, O'Byrne M, Murthy VN (2002) Multiple forms of synaptic plasticity  
899 triggered by selective suppression of activity in individual neurons. *Nature*  
900 420(6914):414–418.
- 901 72. Ibata K, Sun Q, Turrigiano GG (2008) Rapid synaptic scaling induced by  
902 changes in postsynaptic firing. *Neuron* 57(6):819–826.
- 903 73. Hartman KN, Pal SK, Burrone J, Murthy VN (2006) Activity-dependent  
904 regulation of inhibitory synaptic transmission in hippocampal neurons. *Nat*  
905 *Neurosci* 9(5):642–649.
- 906 74. Anggono V, Huganir RL (2012) Regulation of AMPA receptor trafficking and  
907 synaptic plasticity. *Curr Opin Neurobiol* 22(3):461–469.

- 908 75. Wierenga CJ, Ibata K, Turrigiano GG (2005) Postsynaptic expression of  
909 homeostatic plasticity at neocortical synapses. *J Neurosci* 25(11):2895–2905.
- 910 76. Grubb MS, Burrone J (2010) Activity-dependent relocation of the axon initial  
911 segment fine-tunes neuronal excitability. *Nature* 465(7301):1070–1074.
- 912 77. Trunova S, Baek B, Giniger E (2011) Cdk5 regulates the size of an axon initial  
913 segment-like compartment in mushroom body neurons of the *Drosophila*  
914 central brain. *J Neurosci* 31(29):10451–10462.
- 915 78. Takemura S-Y, et al. (2017) A connectome of a learning and memory center in  
916 the adult *Drosophila* brain. *Elife* 6:5643.
- 917 79. Haynes PR, Christmann BL, Griffith LC (2015) A single pair of neurons links  
918 sleep to memory consolidation in *Drosophila melanogaster*. *Elife* 4.  
919 doi:10.7554/eLife.03868.
- 920 80. Wu C-L, et al. (2011) Heterotypic gap junctions between two neurons in the  
921 *drosophila* brain are critical for memory. *21(10):848–854*.
- 922 81. Kaneko M, Stellwagen D, Malenka RC, Stryker MP (2008) Tumor Necrosis  
923 Factor- $\alpha$  Mediates One Component of Competitive, Experience-Dependent  
924 Plasticity in Developing Visual Cortex. *Neuron* 58(5):673–680.
- 925 82. Luo SX, Axel R, Abbott LF (2010) Generating sparse and selective third-order  
926 responses in the olfactory system of the fly. *Proc Natl Acad Sci USA*  
927 107(23):10713–10718.
- 928 83. Dubbs A, Guevara J, Yuste R (2016) moco: Fast Motion Correction for  
929 Calcium Imaging. *Front Neuroinform* 10:6.
- 930 84. Ho J, Tumkaya T, Aryal S, Choi H, Claridge-Chang A (2019) Moving beyond P  
931 values: data analysis with estimation graphics. *Nat Methods* 16(7):565–566.
- 932

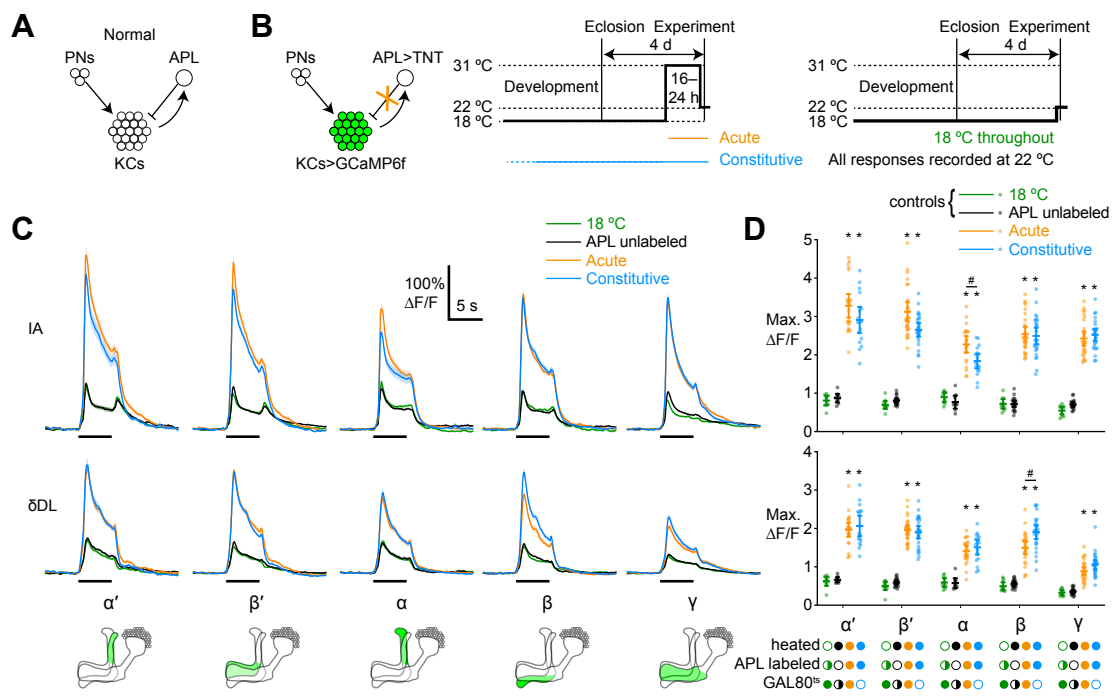


Figure 1

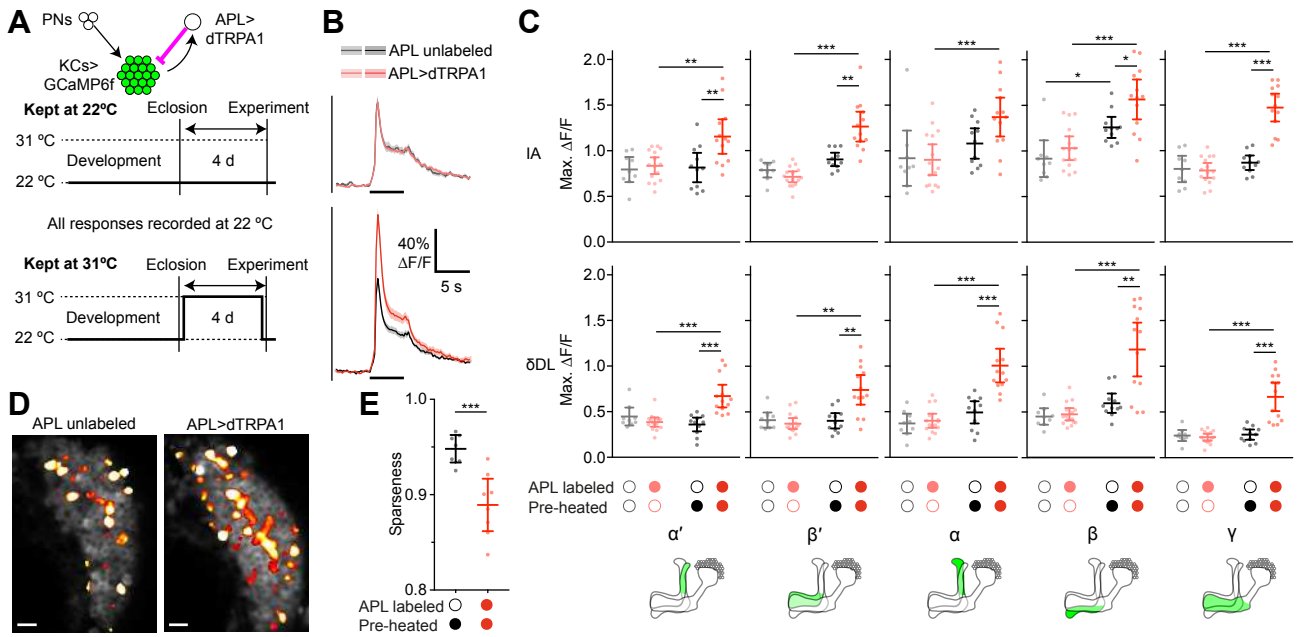


Figure 2

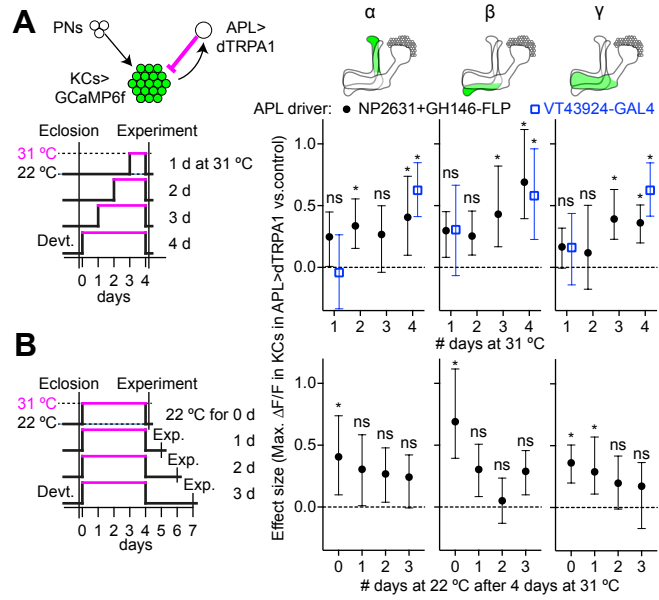


Figure 3



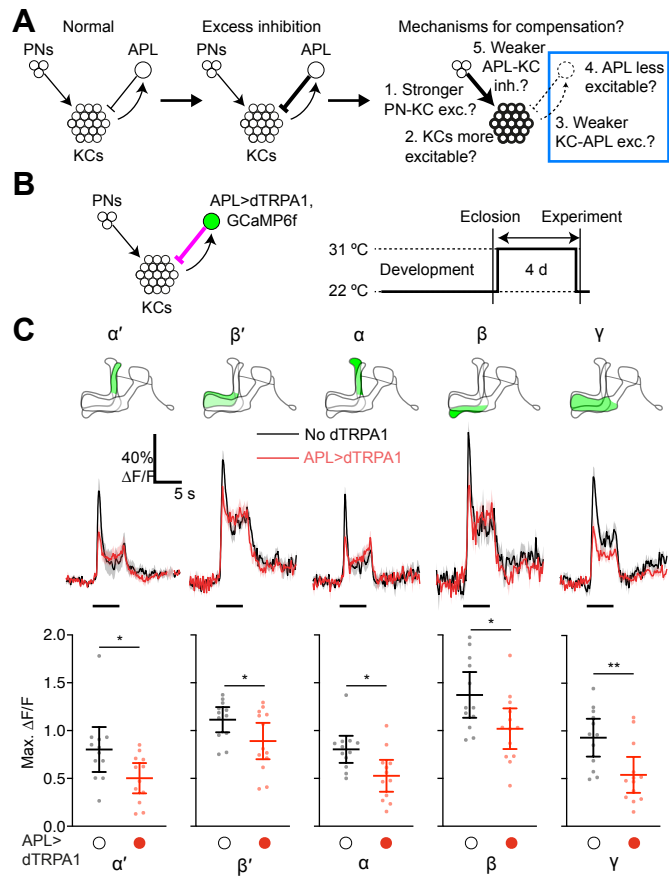


Figure 4

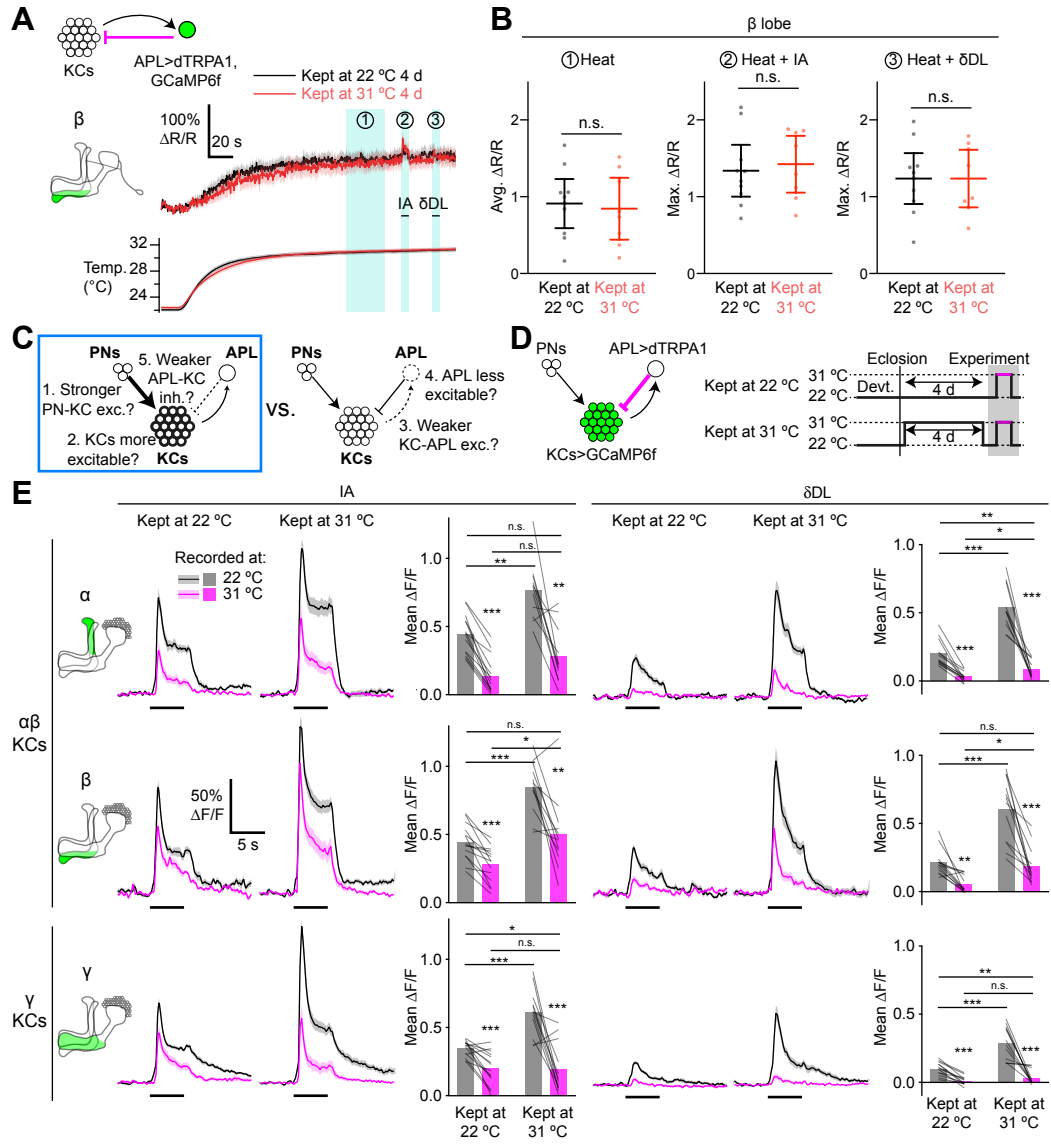


Figure 5

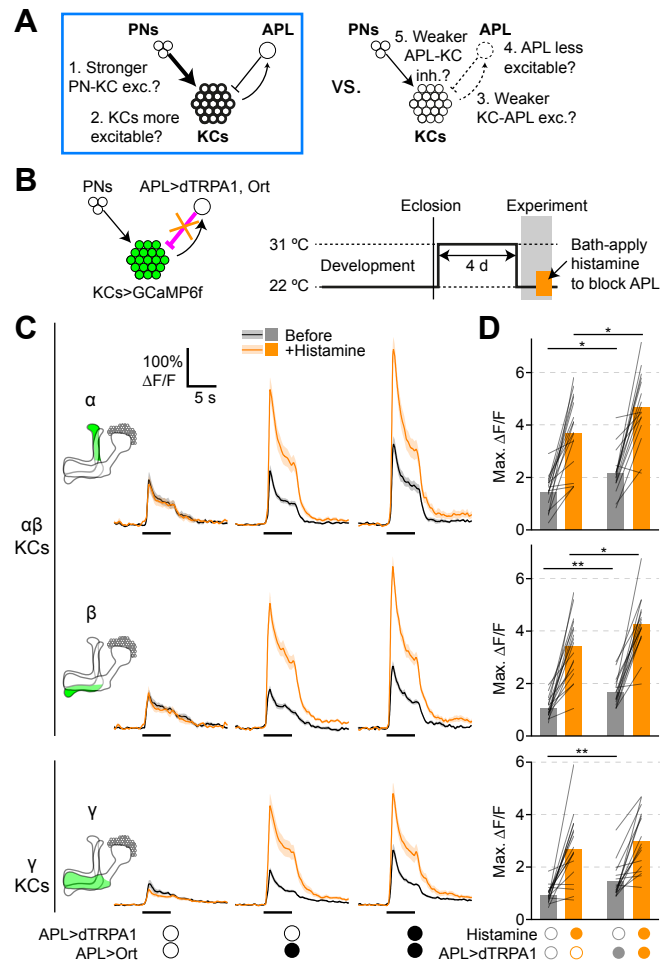


Figure 6

# PNAS

[www.pnas.org](http://www.pnas.org)

Supplementary Information for

Mechanisms underlying homeostatic plasticity in the *Drosophila* mushroom body *in vivo*

Anthi A. Apostolopoulou, Andrew C. Lin

Department of Biomedical Science, University of Sheffield, Sheffield S10 2TN, UK

Neuroscience Institute, University of Sheffield, Sheffield S10 2TN, UK

For correspondence: Andrew C. Lin

Email: [andrew.lin@sheffield.ac.uk](mailto:andrew.lin@sheffield.ac.uk)

**This PDF file includes:**

Supplementary text

Figures S1 to S19

Table S1

SI References

Table S2 appears after the references

## Supplementary Information Text

### Supplementary Methods

#### Fly strains

Fly strains (see below) were raised on standard cornmeal agar (80 g medium cornmeal, 18 g dried yeast, 10 g soya flour, 80 g malt extract, 40 g molasses, 8 g agar, 25 ml 10% nipagin in ethanol, 4 ml propionic acid per 1 L water), at 25 °C for preparatory fly crosses, and at 18 °C (GAL80<sup>ts</sup> flies) or 22 °C (dTRPA1 flies) as described, and in some cases heated to 31 °C after eclosion as described. Flies were imaged at the ages specified in the Results section.

The following transgenic strains were used: NP2631-GAL4 (1), GH146-FLP (2), tubP-FRT-GAL80-FRT (for dTRPA1, on chromosome 2: (3); for TNT, on chromosome 2 or 3: (4)), UAS-TNT (5), tubP-GAL80<sup>ts</sup> (6), UAS-CD8::GFP (7), UAS-mCherry-CAAX (8), MB247-LexA::VP16 (9), lexAop-GCaMP6f (10), lexAop-GCaMP3 (11), UAS-dTRPA1 (12), VT43924-GAL4 (13) (note that we did not include UAS-GAL4), UAS-Ort (14) (gift from Chi-hon Lee).

#### Functional imaging

Calcium imaging was performed as described (11, 15). Cuticle and trachea in a window overlying the mushroom body were removed, and the exposed brain was superfused (perfusion pump Watson-Marlow 120S DM2, ~2.7 ml/min) with carbogenated (95% O<sub>2</sub>, 5% CO<sub>2</sub>) solution containing 103 mM NaCl, 3 mM KCl, 5 mM trehalose, 10 mM glucose, 26 mM NaHCO<sub>3</sub>, 1 mM NaH<sub>2</sub>PO<sub>4</sub>, 3 mM CaCl<sub>2</sub>, 4 mM MgCl<sub>2</sub>, 5 mM N-Tris (TES), pH 7.3. Odors (10<sup>-2</sup> for isoamyl acetate,  $\delta$ -decalactone; 10<sup>-1</sup> for ethyl butyrate, benzaldehyde, 4-methylcyclohexanol, 3-octanol) were delivered by switching mass-flow controlled carrier and stimulus streams (Sensirion) via software controlled solenoid valves (The Lee Company). The flow rate at the fly was ~0.5 L/min. Flies were heated during imaging using a perfusion heater (Scientifica, SM-4600). Histamine (2 mM, Sigma H7250) was added 5 min before imaging in APL>Ort experiments. Although histamine was reported to effectively suppress activity in Ort-expressing neurons at 100  $\mu$ M (14), in preliminary experiments we found that 100  $\mu$ M histamine did not increase KC odor responses in APL>Ort flies but 2 mM histamine did (Fig. 6), possibly because a mere reduction in APL activity (as opposed to a total blockade) would be canceled out by increased KC activity due to the KC-APL negative feedback loop.

Brains were imaged by two-photon microscopy (16, 17). Fluorescence was excited by 75-80 fs pulses (pulse width measured by APE Carpe autocorrelator) of 910 nm light at 80 MHz from a Ti:Sapphire laser (Spectra-Physics eHP DS), attenuated by a Pockels cell (Conoptics, Model 350-80LA) and coupled to a galvo-resonant scanner on a Movable Objective Microscope (Sutter Instruments). Excitation light was focused by a 20X, 1.0 NA objective (Olympus XLUMPLFLN20XW), and emitted photons were passed through a 750 nm short pass filter (to exclude excitation light) and bandpass filters (green: 525/50; red: 605/70), and detected by GaAsP photomultiplier tubes (Hamamatsu Photonics, H10770PA-40SEL), whose currents were amplified (Thorlabs, TIA60) and transferred to the imaging computer running ScanImage 5 (Vidrio Technologies). Volume imaging was performed using a piezo objective stage (nPFocus400, nPoint) using ScanImage's FastZ control in sawtooth mode (typically 10-16 z slices, volume rate ~3 Hz).

Movies were motion-corrected in X-Y using the moco ImageJ plugin (18), with pre-processing to collapse volume movies in Z and to smooth the image with a Gaussian filter (standard deviation = 4 pixels; the displacements generated from the smoothed movie were then applied to the original, unsmoothed movie), and motion-corrected in Z by maximizing the pixel-by-pixel correlation between each volume and the average volume across time points (15).  $\Delta F/F$  traces were calculated in ImageJ using manually-drawn ROIs for the background and brain structure of interest, and smoothed with a 0.2 s boxcar filter in Igor Pro 7 (WaveMetrics).  $\Delta R/R$  in Fig. 5, Fig. S14 was calculated by dividing GCaMP6f signal by dsRed signal, to remove motion artifacts caused by heating. Where traces with different frame times needed to be averaged, traces were linearly interpolated to a frame time of 0.018 s, except for Fig. 5a, Fig. S14c, where they were interpolated to 0.2878 s due to software limitations. Flies were excluded if the neurons of interest did not respond to odor, the GCaMP6f signal was too low/noisy, or the brain moved too much to correct for motion artifacts.

Activity maps were generated as in (11, 15). Briefly, movies were smoothed with a 5-pixel-square Gaussian filter (standard deviation 2). Baseline fluorescence was taken as the average fluorescence during the pre-stimulus period. Frames with sudden, large axial movements were discarded by correlating each frame to the baseline image and discarding it if the correlation fell below a threshold value, which was manually selected for each brain by noting the constant high correlation value when the brain was stationary and sudden drops in correlation when the brain moved.  $\Delta F/F$  was calculated for each pixel as the difference between mean fluorescence during the stimulus period vs. the baseline fluorescence ( $\Delta F$ ), divided by the baseline fluorescence. For pixels where  $\Delta F$  did not exceed 2 times the standard deviation over time of that pixel's intensity during the pre-stimulus period, the pixel was considered non-responsive. We excluded non-responsive flies and flies whose motion could not be corrected.

Inter-odor correlations were calculated by first aligning the activity maps of each odor response by maximizing the inter-odor correlations of baseline fluorescence, and then converting image matrices of the activity maps of each odor response into linear vectors and calculating the Pearson correlation coefficients between each "odor vector". Where a pair of volume movies did not fully align in z, a subset of z-slices was chosen that did align. A threshold for baseline fluorescence was applied as a mask to the activity map to exclude pixels with no baseline GCaMP6f signal. Areas with non-GCaMP6f fluorescence (e.g., cuticle) or non-KC-soma areas (e.g., calyx) were manually excluded. Population sparseness was calculated for activity maps using the following equation (19, 20):

$$S_p = \frac{1}{1 - \frac{1}{N}} \left( 1 - \frac{\left( \sum_{i=1}^N \frac{r_i}{N} \right)^2}{\sum_{i=1}^N \frac{r_i^2}{N}} \right)$$

where  $N$  is the number of pixels and  $r_i$  is the response of each pixel. Analysis code is available at <https://github.com/aclinlab/calcium-imaging>.

### Structural imaging

To visualize tetanus toxin expression in APL>TNT flies, we either included UAS-mCherry in the genotype as in (15) or immunostained with anti-TNT antibody (Abcam, ab53829, formerly known as POL 016 from Statens Serum Institut). mCherry expression in APL was distinguished from 3XP3-driven dsRed from the GH146-FLP transgene by using separate filter cubes for dsRed (49004, Chroma: 545/25 excitation; 565 dichroic; 605/70 emission) and mCherry (LED-mCherry-A-000, Semrock: 578/21 excitation; 596 dichroic; 641/75 emission). Immunostaining was carried out as described in (11, 21). Dissected brains were fixed in 4% (wt/vol) paraformaldehyde in PBT (100 mM Na<sub>2</sub>PO<sub>4</sub>, 0.3% Triton-X-100, pH 7.2), washed in PBT (2 quick washes, then 3 20 min washes), blocked with 5% goat serum (Sigma, G6767) in PBT, incubated in primary antibody (1:100 in blocking solution) at 4 °C over 2-3 nights, washed in PBT (2 quick washes, then 3 20 min washes), incubated in secondary antibody (goat anti-rabbit Alexa 546, 1:500, ThermoFisher A11071), washed in PBT (2 quick washes, then 3 20 min washes), and mounted in Vectashield (Vector Laboratories, H-1000). mCherry expression or anti-TNT staining was scored using epifluorescence.

### Statistics

Statistical analyses were performed in Prism 8 (GraphPad) and MATLAB. Bootstrap-coupled estimation statistics (22) were analysed using the DABEST package (<https://github.com/ACCLAB/DABEST-python>). Parametric (t-test, ANOVA) or non-parametric tests (Mann-Whitney, Friedman, Kruskal-Wallis) were used depending on whether raw data (for pairwise comparisons) or residuals (for ANOVAs) passed the D'Agostino-Pearson normality test. For ANOVAs and unpaired t-tests, Welch or Greenhouse-Geisser corrections were applied when variances were significantly different between groups. Random assignment to experimental groups was not used as all manipulations were genetic. In general, no statistical tests were done to pre-determine sample size, but where a conclusion relied on the absence of a significant effect, a power analysis was performed to confirm if the sample size was sufficient to detect an effect of the expected size; if not, the lack of statistical power was explicitly noted. The experimenter was blind to which APL neurons were labeled before post-experimental dissection (Fig. 1-3,5-6) and for some acute vs. constitutive experiments in Fig. S2c, but not otherwise.

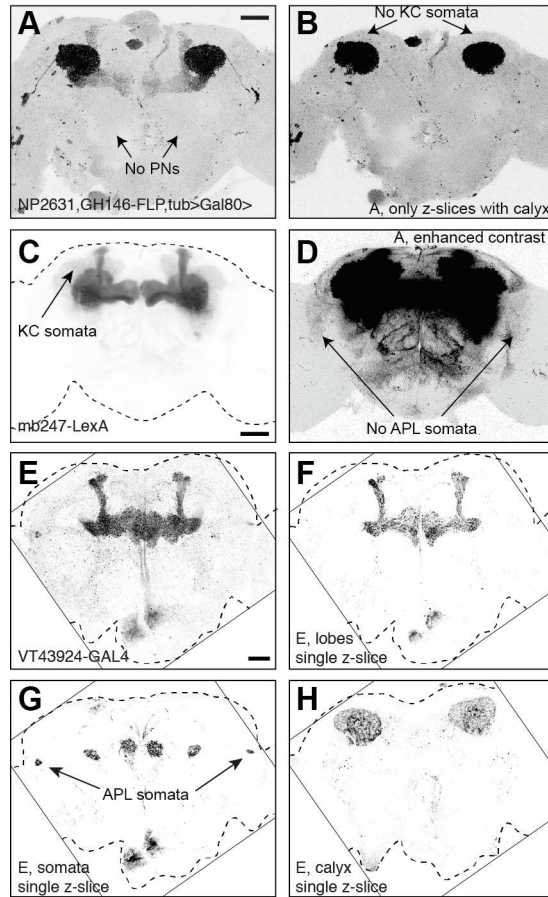


**Fig. S1 (related to all figures). Expression pattern of APL and KC drivers**

- (A) Expression pattern of the intersection of NP2631-GAL4 and GH146-FLP where both APL neurons are labeled (data from ref. 11, Fig. 4c). Projection neurons (PNs) are not labeled.
- (B) Image in A with maximum intensity projection through only the z-slices containing the calyx. No KC somata are labelled (should appear dorsally and laterally to the calyx, as visible in panel C, but even stronger here as this brain was imaged posterior side up).
- (C) Expression pattern of MB247-LexA (data from ref. 11, Fig. 1e).
- (D) Image in C with enhanced contrast, to show that APL is not labelled by MB247-LexA.
- (E) Expression pattern of VT43924-GAL4 driving UAS-CD8::GFP. Maximum intensity projection of z-stack of unfixed brain captured on a two-photon microscope. The non-APL expression along the midline and in the periesophageal neuropils can also be seen in Fig. 1C of (13). Note the lack of expression in the antennal lobes.
- (F) Single z-slice of (E) 30  $\mu$ m deep revealing the typical neurite structure of APL in the mushroom body lobes, indicating that other mushroom body neurons are not labeled. Contrast in (F-H) differs from (E) and from each other to compensate for decreased signal deep in uncleared tissue.
- (G) Single z-slice of (E) 48  $\mu$ m deep showing the APL cell bodies.
- (H) Single z-slice of (E) 134  $\mu$ m deep showing APL in the calyces.

Scale bars 50  $\mu$ m. Dashed outlines outline the brain. Thin diagonal lines outline the boundaries of the rotated field of view.

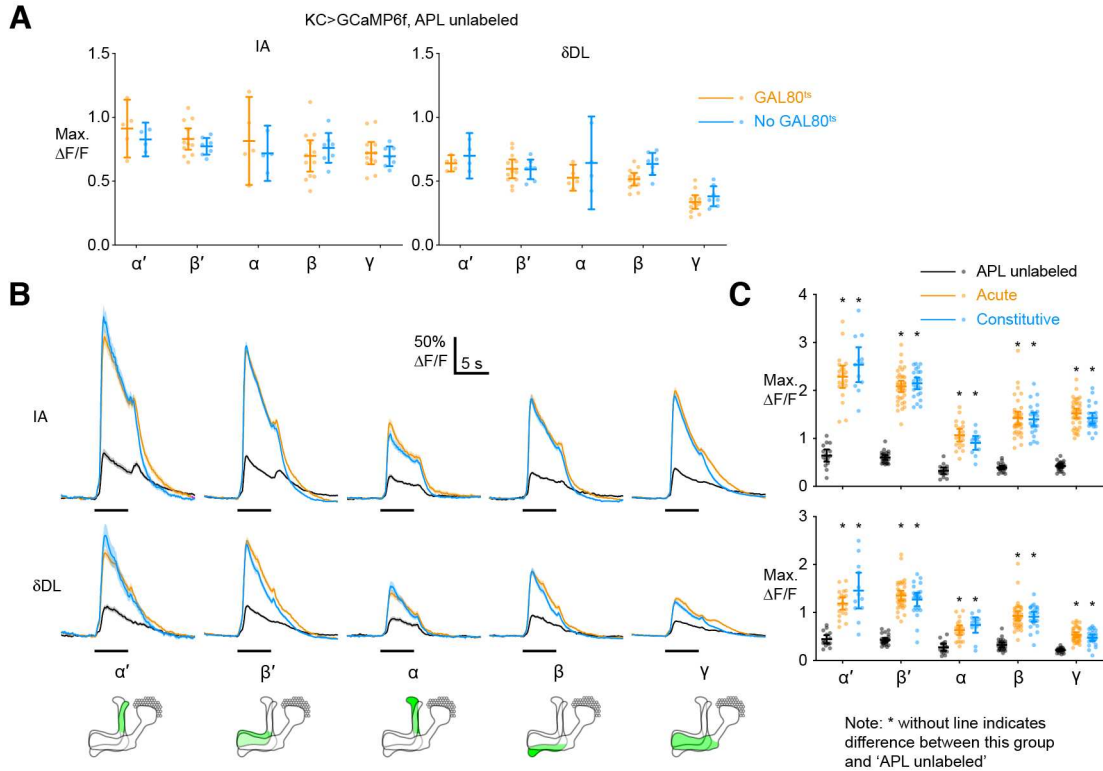


**Fig. S2 (related to Fig. 1). Additional data for APL>TNT**

- (A) KC>GCaMP6f odor responses in APL-unlabeled control hemispheres are the same in flies with (orange) and without (blue) GAL80<sup>ts</sup>. Graph shows maximum  $\Delta F/F$  (data taken from **Fig. 1C**, “APL unlabeled”), mean  $\pm$  95% confidence interval. n, given as # hemispheres (# flies): GAL80<sup>ts</sup>,  $\alpha'$  and  $\alpha$ , 5 (4),  $\beta'$ ,  $\beta$  and  $\gamma$ , 7 (5); no GAL80<sup>ts</sup>,  $\alpha'$  and  $\alpha$ , 4 (3),  $\beta'$ ,  $\beta$  and  $\gamma$ , 12 (9). Mixed-effects model (matching across lobes) finds no significant effect of genotype (GAL80<sup>ts</sup> vs. no GAL80<sup>ts</sup>) ( $p > 0.05$ ).
- (B) Responses of different Kenyon cell lobes to isoamyl acetate (IA, upper) or  $\delta$ -decalactone ( $\delta$ DL, lower), imaged with GCaMP3 instead of GCaMP6f. Horizontal bar shows time of odor presentation. Error shading shows s.e.m. Data for ‘acute’ and ‘APL unlabeled’ (with GAL80<sup>ts</sup>) flies from ref. 23.
- (C) Maximum  $\Delta F/F$  of data from panel B. Mean  $\pm$  95% confidence interval. #  $p < 0.05$  between acute vs. constitutive, \*  $p < 0.001$ , Welch ANOVA with Dunnett’s T3 multiple comparisons test, or Kruskal-Wallis ANOVA with Dunn’s multiple comparisons test. n, given as # hemispheres (# flies), left to right within each graph:  $\alpha'$  and  $\alpha$ , 11 (10), 20 (14), 12 (9);  $\beta'$ ,  $\beta$  and  $\gamma$ , 18 (15), 36 (24), 24 (16).

In all panels, \* without line indicates different from APL unlabeled. Detailed statistical analysis given in **Table S2**.



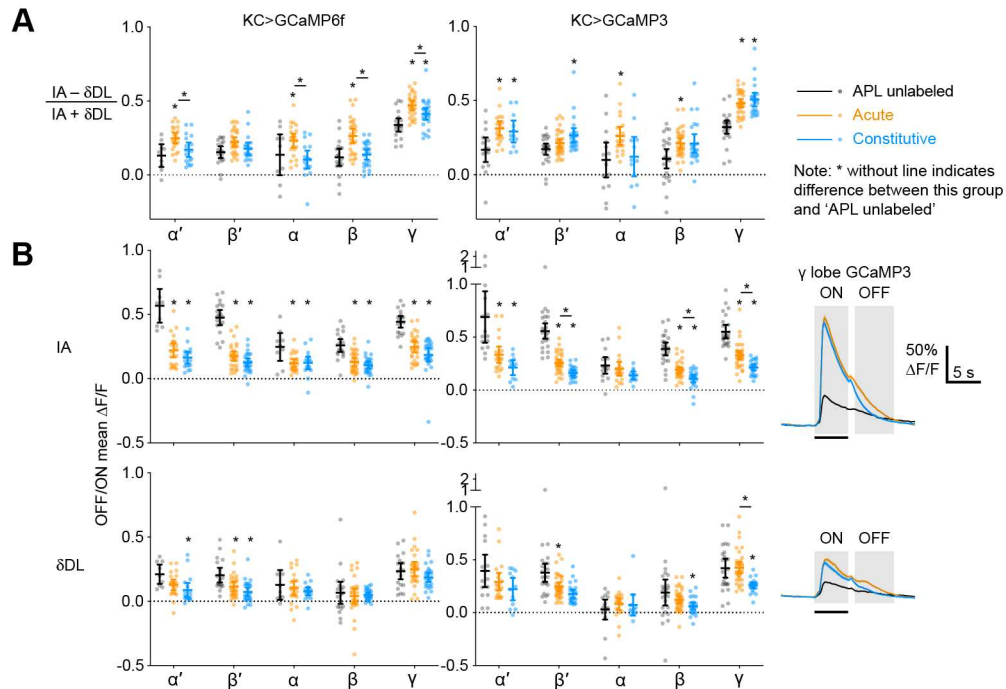


**Fig. S3 (related to Fig. 1). Dynamics of KC odor responses with APL>TNT**

- (A) Normalized difference between maximum  $\Delta F/F$  response to IA vs.  $\delta DL$ , taken as  $(IA - \delta DL)/(IA + \delta DL)$ , for data from **Fig. 1C** (KC>GCaMP6f, left) and **Fig. S2C** (KC>GCaMP3, right).  $n$  as in those panels. For GCaMP6f, but not GCaMP3, the normalized difference is higher with acute APL>TNT than both APL unlabeled controls and constitutive APL>TNT. \*  $p < 0.05$ , mixed-effects model (matching across lobes) with Geisser-Greenhouse correction and Holm-Sidak multiple comparisons test (GCaMP6f), Welch's 1-way ANOVA with Holm-Sidak multiple comparisons or Kruskal-Wallis ANOVA with Dunn's multiple comparisons test (GCaMP3).
- (B) Post-odor GCaMP signal (KC>GCaMP6f, left; KC>GCaMP3, right), for IA (top) and  $\delta DL$  (bottom), analysed as mean  $\Delta F/F$  1-6 s after the end of the odor pulse divided by mean  $\Delta F/F$  during the 5 s odor pulse (ON and OFF periods shown in right panel as shading superimposed on  $\gamma$  lobe responses). Data from **Fig. 1C** and **Fig. S2B** ( $n$  as in those panels). \*  $p < 0.05$ , ordinary 1-way ANOVA with Holm-Sidak multiple comparisons test or Kruskal-Wallis ANOVA with Dunn's multiple comparisons test.

In all panels, \* without line indicates different from APL unlabeled. Detailed statistical analysis given in **Table S2**.

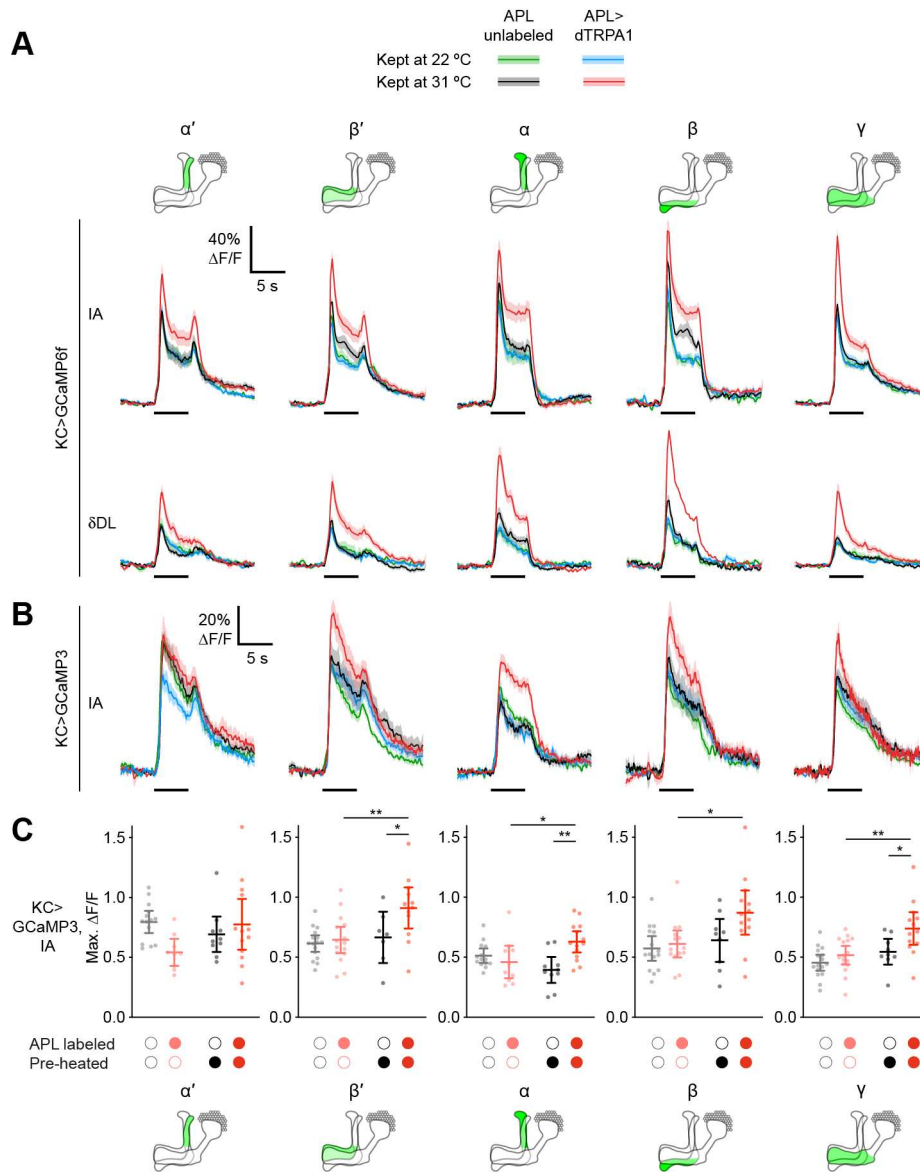


**Fig. S4 (related to Fig. 2). Odor response traces and GCaMP3 data for Fig. 2 (Kenyon cell odor responses are increased following excess activation of the inhibitory APL neuron)**

- (A) Responses of all lobes to isoamyl acetate (IA) and  $\delta$ -decalactone ( $\delta$ DL) for KC>GCaMP6f, APL>dTRPA1 flies kept at 22 °C or 31 °C, where APL was unlabeled or expressed dTRPA1, recorded at 22 °C. Legend shows 2x2 grid: APL unlabeled, kept at 22 °C (green), APL>dTRPA1, kept at 22 °C (blue), APL unlabeled, kept at 31 °C (black), APL>dTRPA1, kept at 31 °C (red). Horizontal bars show time of odor presentation. Error shading shows s.e.m. Diagrams of the mushroom body show the  $\alpha'$ ,  $\beta'$ ,  $\alpha$ ,  $\beta$  and  $\gamma$  lobes. n as in Fig. 2.
- (B) Same as (A) except measured with KC>GCaMP3 instead of KC>GCaMP6f.
- (C) Maximum  $\Delta F/F$  response from panel B. Mean  $\pm$  95% confidence interval. \*  $p < 0.05$ , \*\*  $p < 0.01$ , ordinary 1-way ANOVA with Holm-Sidak multiple comparisons test or Kruskal-Wallis test with Dunn's multiple comparisons test, comparing only conditions where a single variable changed (see Table S2 for details). n, given as # hemispheres (# flies), left to right within each graph:  $\alpha'$ , 14 (9), 9 (7), 10 (9), 13 (11);  $\beta'$ , 16 (11), 15 (11), 7 (6), 12 (10);  $\alpha$ , 14 (9), 10 (7), 10 (9), 14 (11);  $\beta$ , 15 (10), 14 (11), 9 (8), 13 (11);  $\gamma$ , 16 (11), 16 (12), 9 (8), 13 (11).

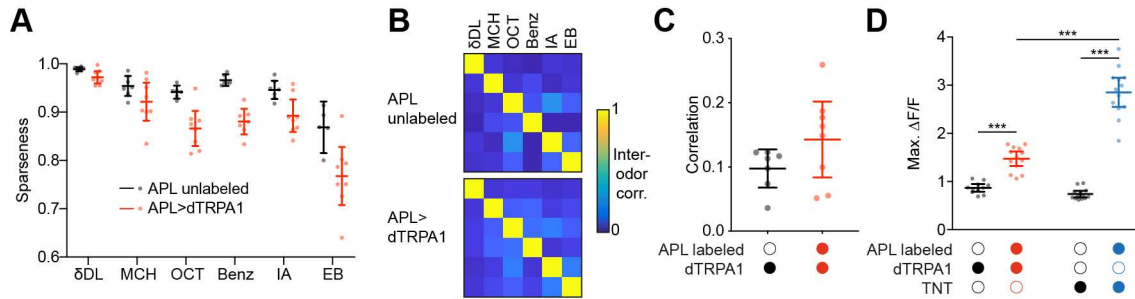


**Fig. S5 (related to Fig. 2). Sparseness and inter-odor correlation of KC odor responses after adaptation to APL>dTRPA1 adaptation**

- (A) Population sparseness of activity maps of KC somatic responses to a panel of 6 odors:  $\delta$ -decalactone, 4-methylcyclohexanol, 3-octanol, benzaldehyde, isoamyl acetate, ethyl butyrate.  $\delta$ -decalactone and isoamyl acetate were at  $10^{-2}$  dilution for consistency with the rest of the study; the others were at  $10^{-1}$  to ease detection of broader odor responses. All flies were kept at 31 °C for 4 d before imaging at 22 °C as in **Fig. 2**. APL unlabeled,  $n = 7$  (6 flies); APL>dTRPA1,  $n = 8$  (6 flies).  $p = 0.0004$ , significant main effect of genotype in mixed-effects model.
- (B) Pairwise correlations between activity maps of KC somatic responses to the odors in A.
- (C) Mean inter-odor correlation (mean of all non-diagonal squares in B) does not significantly differ between APL unlabeled and APL>dTRPA1 hemispheres.  $n$  as in (A).  $p = 0.15$ , unpaired t-test.  $p = 0.18$ , main effect of genotype in mixed-effects model when considering each odor pair separately.  $p < 0.0001$ , main effect of odor-pair identity, indicating that our data reliably report that some odor pairs are more similar than others (see grids in B).
- (D) Maximum  $\Delta F/F$  of  $\gamma$  lobe responses to isoamyl acetate, duplicated from **Fig. 1C, 2C**. Odor responses are higher with APL blocked by TNT (blue) than after adaptation following 4 d APL activation by dTRPA1 (red), possibly explaining why adaptation to APL>dTRPA1 does not affect inter-odor correlations, whereas blocking APL with TNT does (11). \*\*\*  $p < 0.001$ , Welch ANOVA with Holm-Sidak multiple comparisons test (see **Table S2** for details).

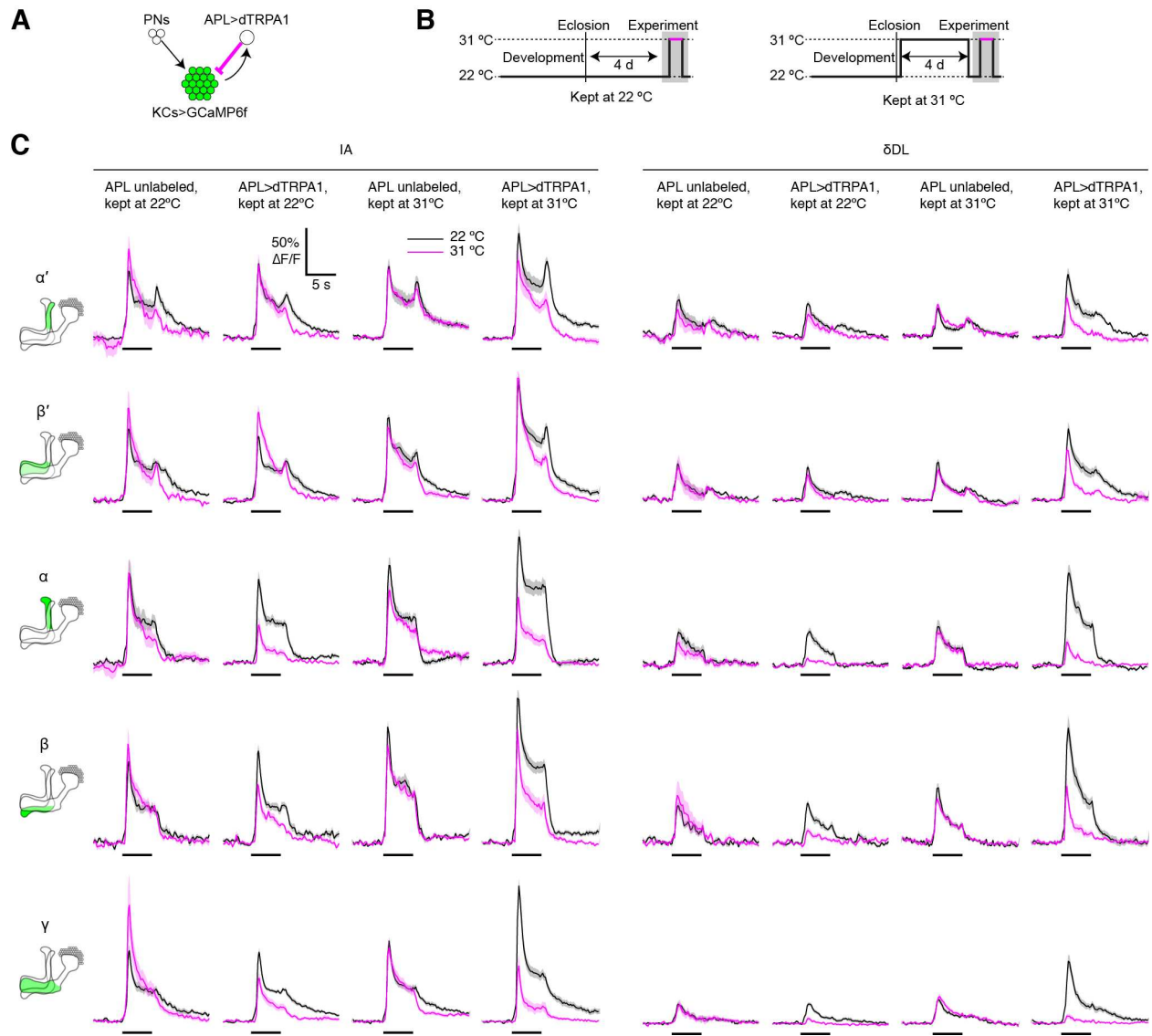


**Fig. S6 (related to Fig. 2). APL remains functional after prolonged activation**

- (A) Diagram of genotype (green shows GCaMP6f expression; magenta shows activation with dTRPA1).
- (B) Diagrams show experimental protocol: Flies were raised at 22 °C, collected 0–1 d after eclosion, kept at 22 °C (control) or 31 °C (pre-heated) for 4 d, and returned to 22 °C before the imaging experiment.
- (C) Responses of all lobes to isoamyl acetate (IA) and  $\delta$ -decalactone ( $\delta$ DL) for KC>GCaMP6f, APL>dTRPA1 flies kept at 22 °C or 31 °C, where APL was unlabeled or expressed dTRPA1, recorded at 22 °C (black) or 31 °C (magenta). Horizontal bars show time of odor presentation. Error shading shows s.e.m. Diagrams of the mushroom body show the  $\alpha'$ ,  $\beta'$ ,  $\alpha$ ,  $\beta$  and  $\gamma$  lobes.

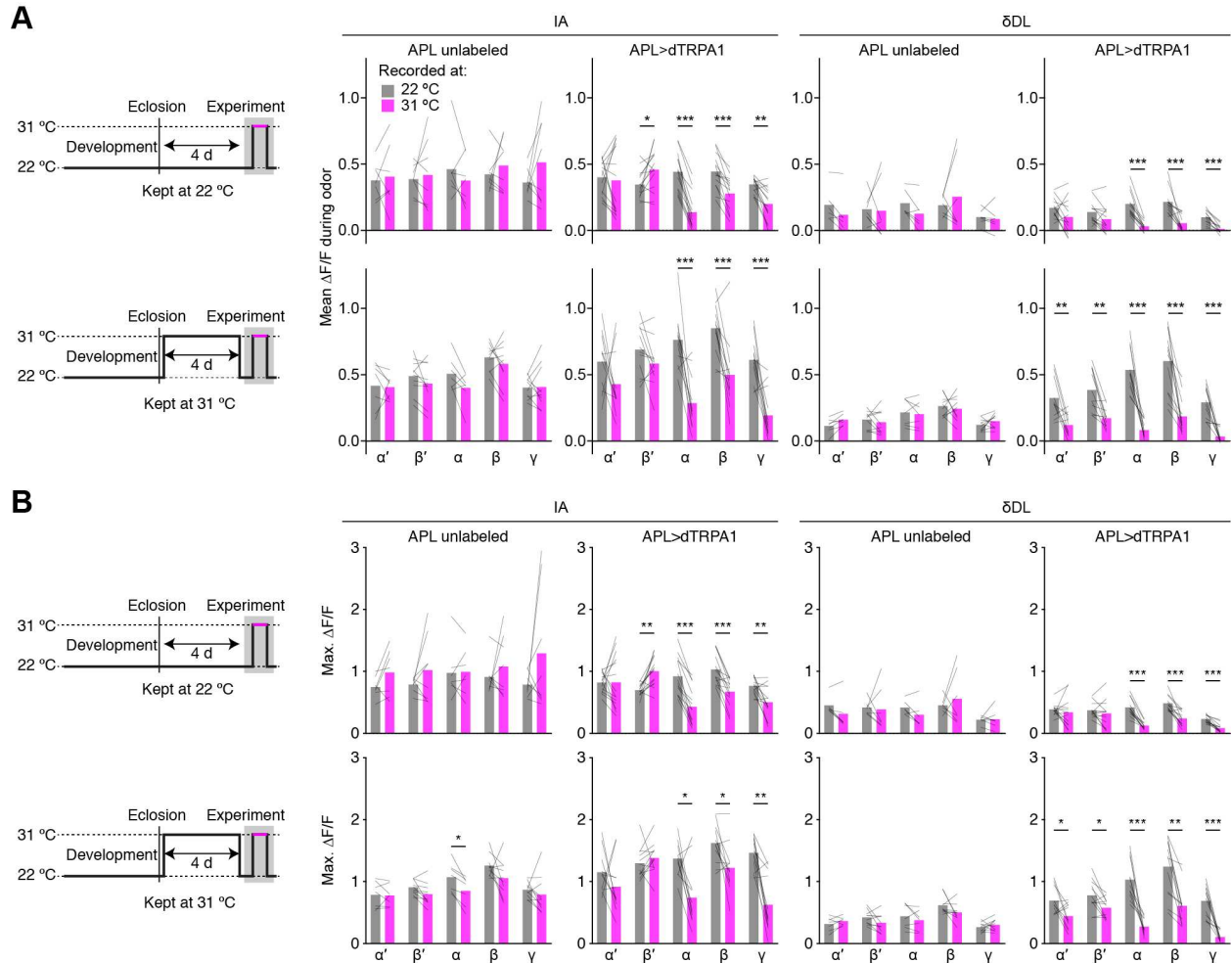


**Fig. S7 (related to Fig. 2). APL remains functional after prolonged activation, quantification**

(A) Mean  $\Delta F/F$  during odor recorded at 22 °C (grey) vs. recorded at 31 °C (magenta), for APL unlabeled or APL>dTRPA1 hemispheres, kept at 22 °C or kept at 31 °C, for odors isoamyl acetate or  $\delta$ -decalactone. Here we quantified odor responses using mean  $\Delta F/F$  rather than maximum  $\Delta F/F$  because in some cases activating APL with dTRPA1 changed the dynamics of the KC odor responses, such that the decrease in mean  $\Delta F/F$  was more obvious than the decrease in maximum  $\Delta F/F$ . Bars show mean, thin lines show paired data (recorded at 22 °C and 31 °C). \*  $p < 0.05$ , \*\*  $p < 0.01$ , \*\*\*  $p < 0.001$ , 2-way repeated measures ANOVA or mixed-effects model with Geisser-Greenhouse correction with Holm-Sidak multiple comparisons test (see **Table S2** for details). n, given as # hemispheres (# flies) in the order APL unlabeled, kept at 22 °C; APL>dTRPA1, kept at 22 °C; APL unlabeled, kept at 31 °C; APL>dTRPA1, kept at 31 °C (n for IA and  $\delta$ DL equal except where noted):  $\alpha'$  and  $\alpha$ , 7 (7) [6 (6) for  $\delta$ DL], 14 (10) [13 (9) for  $\delta$ DL], 7 (4), 11 (6);  $\beta'$ ,  $\beta$  and  $\gamma$ , 8 (7) [7 (6) for  $\delta$ DL], 14 (10) [13 (9) for  $\delta$ DL], 10 (6), 12 (7). Responses recorded at 22 °C are the same as in **Fig. 2** except excluding flies without a response at 31 °C (fly died, motion artifacts, etc.).

(B) Same as panel A except with maximum  $\Delta F/F$  instead of mean  $\Delta F/F$ .

Note: The lesser effect of activating APL with dTRPA1 on  $\alpha'\beta'$  odor responses, compared to  $\alpha\beta$  and  $\gamma$  responses, is consistent with our previous data (11) and with findings that  $\alpha'\beta'$  KCs are more excitable (24, 25) and have higher spontaneous activity than  $\alpha\beta$  and  $\gamma$  KCs (spontaneous activity  $\sim 0.3$  Hz in  $\alpha'\beta'$  KCs vs. 0 Hz in  $\alpha\beta$  and  $\gamma$  KCs; (26)). Although all three types of KCs respond equally to optogenetic activation of APL (25), it may be that APL activation suppresses spontaneous activity in  $\alpha'\beta'$  KCs, which would make the inhibitory effect on the odor-evoked  $\Delta F/F$  less apparent due to the lower baseline GCaMP6f fluorescence.

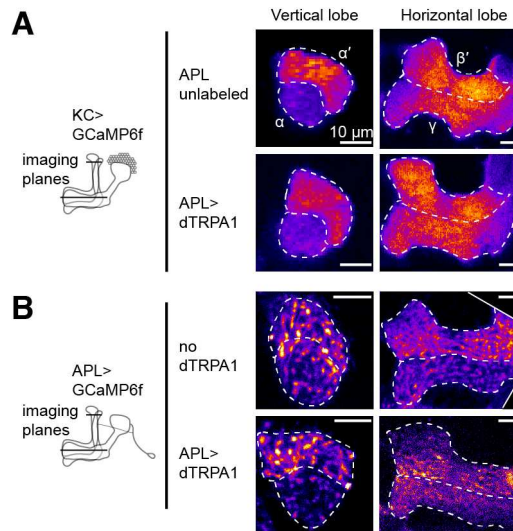


**Fig. S8 (related to Fig. 2). Gross morphology of APL and KCs is unaffected by APL>dTRPA1 adaptation**

- (A) Example single optical sections of KCs expressing GCaMP6f in the vertical (left) and horizontal (right) lobes, in control APL-unlabeled hemispheres (upper) and APL>dTRPA1 hemispheres (lower), kept at 31 °C for 4 d.
- (B) Example single optical sections of APL expressing GCaMP6f in the vertical (left) and horizontal (right) lobes, in APL>GCaMP6f only (no dTRPA1) flies (upper) and APL>GCaMP6f,dTRPA1 flies (lower), kept at 31 °C for 4 d. Diagonal lines indicate the edge of the rotated field of view. Note typical APL neurite morphology, parallel to KC axons (hence perpendicular to the imaging plane in the vertical, and running left and right in the horizontal lobe).

Diagrams illustrate approximate z-depth of imaging planes of each optical section. Scale bars 10  $\mu$ m.



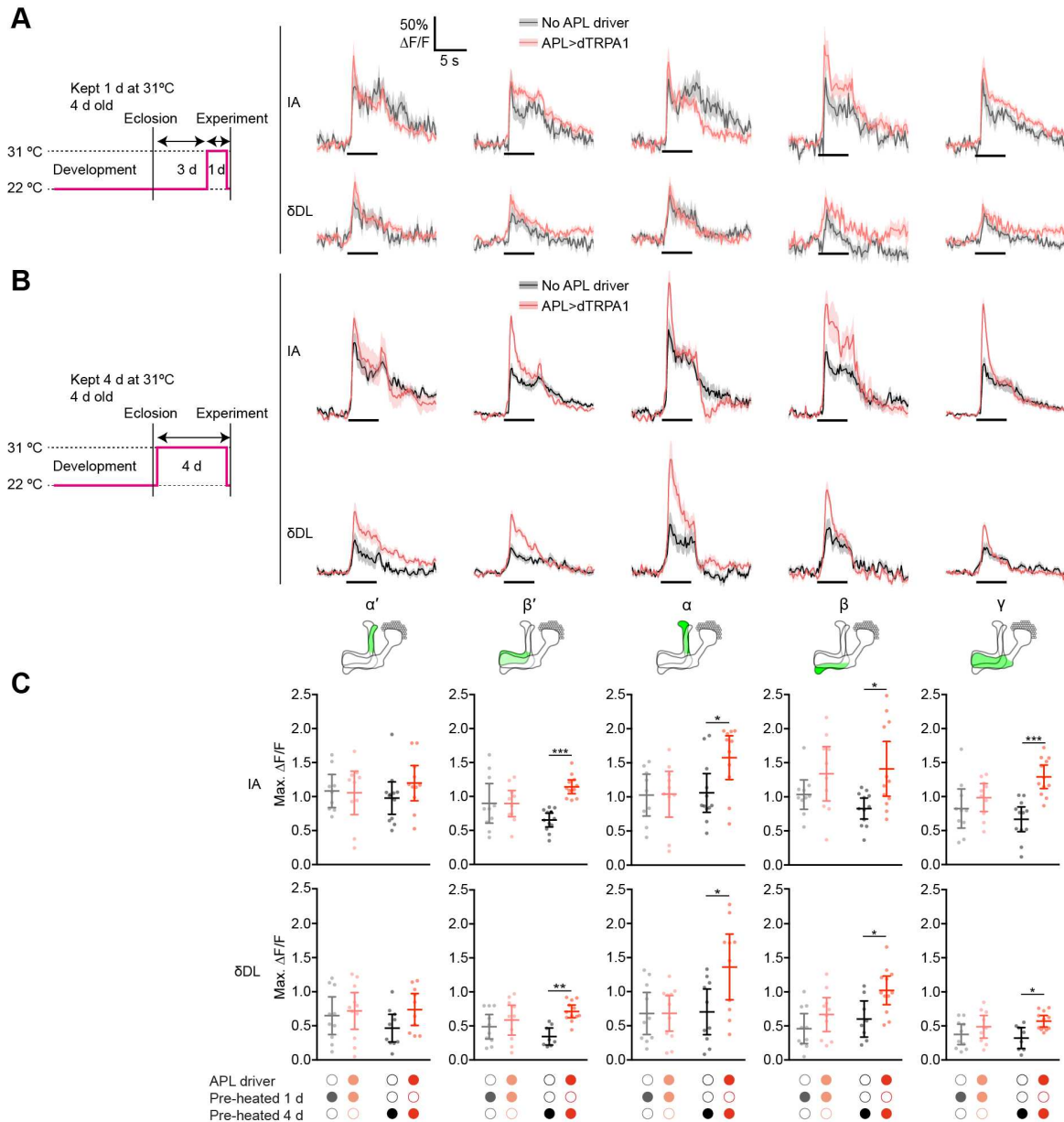


**Fig. S9 (related to Fig. 3). Stronger adaptation to APL activation after 4 days than 1 day (using VT43924-GAL4)**

(A) Responses of different lobes of the mushroom body to isoamyl acetate (IA) and  $\delta$ -decalactone ( $\delta$ DL) for 1 d adapted (4 d old) flies, where APL did not express (grey) or expressed dTRPA1 (pink) driven by VT43924-GAL4. Horizontal bar shows time of odor presentation. Error shading shows s.e.m. Diagram at left shows experimental protocol: Flies were raised at 22 °C and collected 0–1 d after eclosion, then kept at 22 °C for 3 days and moved to 31 °C for 1 d (4 d old). All flies were imaged at 22 °C.

(B) As A, except flies kept at 31 °C for 4 d after eclosion.

(C) Maximum  $\Delta F/F$  of traces in (B-C). \*  $p < 0.05$ , \*\*  $p < 0.01$ , \*\*\*  $p < 0.001$ , 1-way ANOVA with Holm-Sidak multiple comparisons test or Kruskal-Wallis test with Dunn's multiple comparisons test, comparing only conditions where a single variable changed. 2-way ANOVAs revealed interactions between genotype and length of pre-heating in the  $\beta'$  and  $\gamma$  lobes (see **Table S2** for details). n, given as # hemispheres (# flies), left to right within each graph: IA,  $\alpha$  and  $\alpha'$ , 9 (5), 10 (5), 12 (6), 11 (6);  $\beta$ ,  $\beta'$  and  $\gamma$ , 10 (5), 10 (5), 12 (6), 12 (6);  $\delta$ DL,  $\alpha$  and  $\alpha'$ , 10 (5), 11 (6), 10 (5), 10 (5);  $\beta$ ,  $\beta'$  and  $\gamma$ , 10 (5), 10 (5), 8 (4), 12 (6).

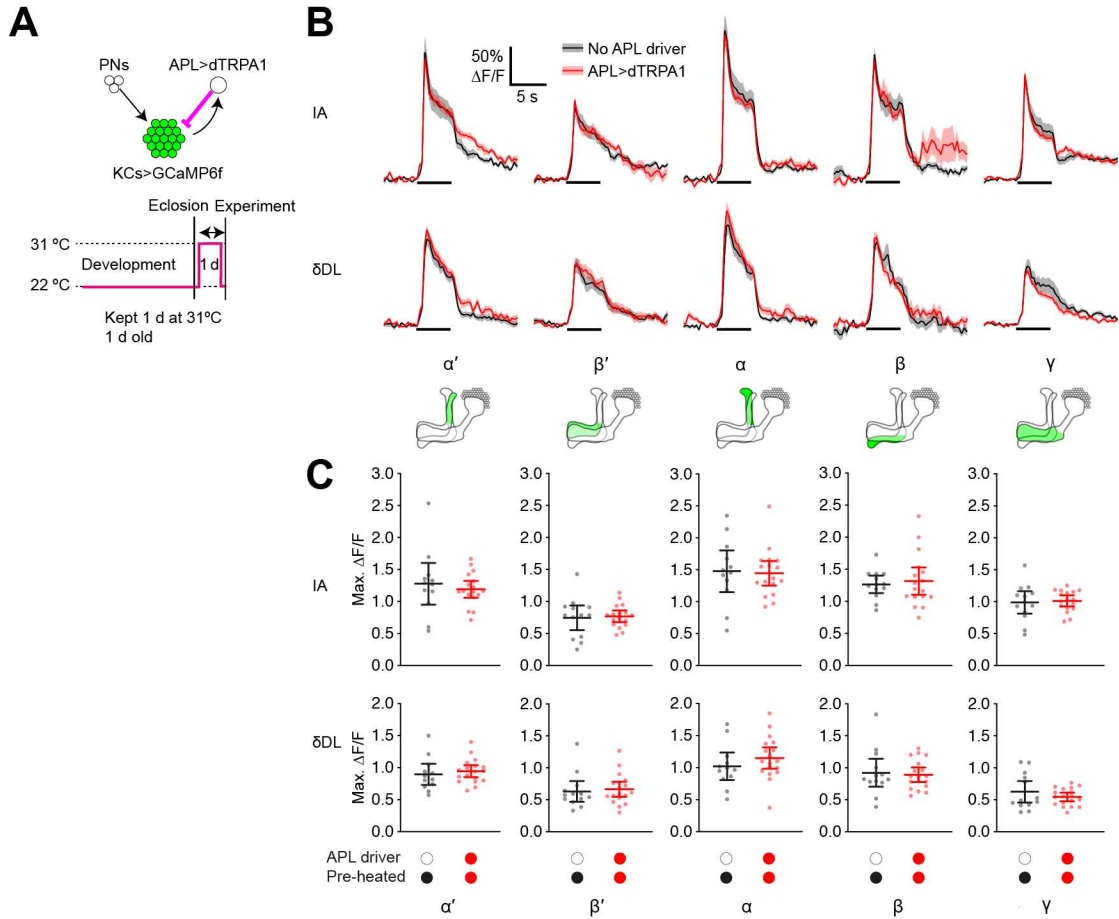


**Fig. S10 (related to Fig. 3). No adaptation after 1 d APL activation in 1 d old flies (using VT43924-GAL4)**

- (A) Diagram of experimental protocol. Flies were raised at 22 °C and collected 0–1 d after eclosion, then immediately moved to 31 °C for 1 d, and then imaged at 22 °C.
- (B) Responses of different lobes of the mushroom body to isoamyl acetate and  $\delta$ -decalactone in 1 d old flies kept at 31 °C for 1 d (diagram in A), where APL did not express (grey) or expressed dTRPA1 (orange) driven by VT43924-GAL4. Horizontal bar shows time of odor presentation. Error shading shows s.e.m.
- (C) Maximum  $\Delta F/F$  from panel B. Mean  $\pm$  95% confidence interval. n, given as # hemispheres (# flies) in the order UAS-TRPA alone; APL>dTRPA1: IA,  $\alpha'$  and  $\alpha$ , 12(7), 17(10);  $\beta'$ ,  $\beta$  and  $\gamma$ , 13(7), 17(10);  $\delta$ DL,  $\alpha'$  and  $\alpha$ , 12(7), 18(10);  $\beta'$ ,  $\beta$  and  $\gamma$ , 13(7), 18(10).  $p > 0.05$  for all comparisons, unpaired t-test or Mann-Whitney test (see **Table S2** for details).



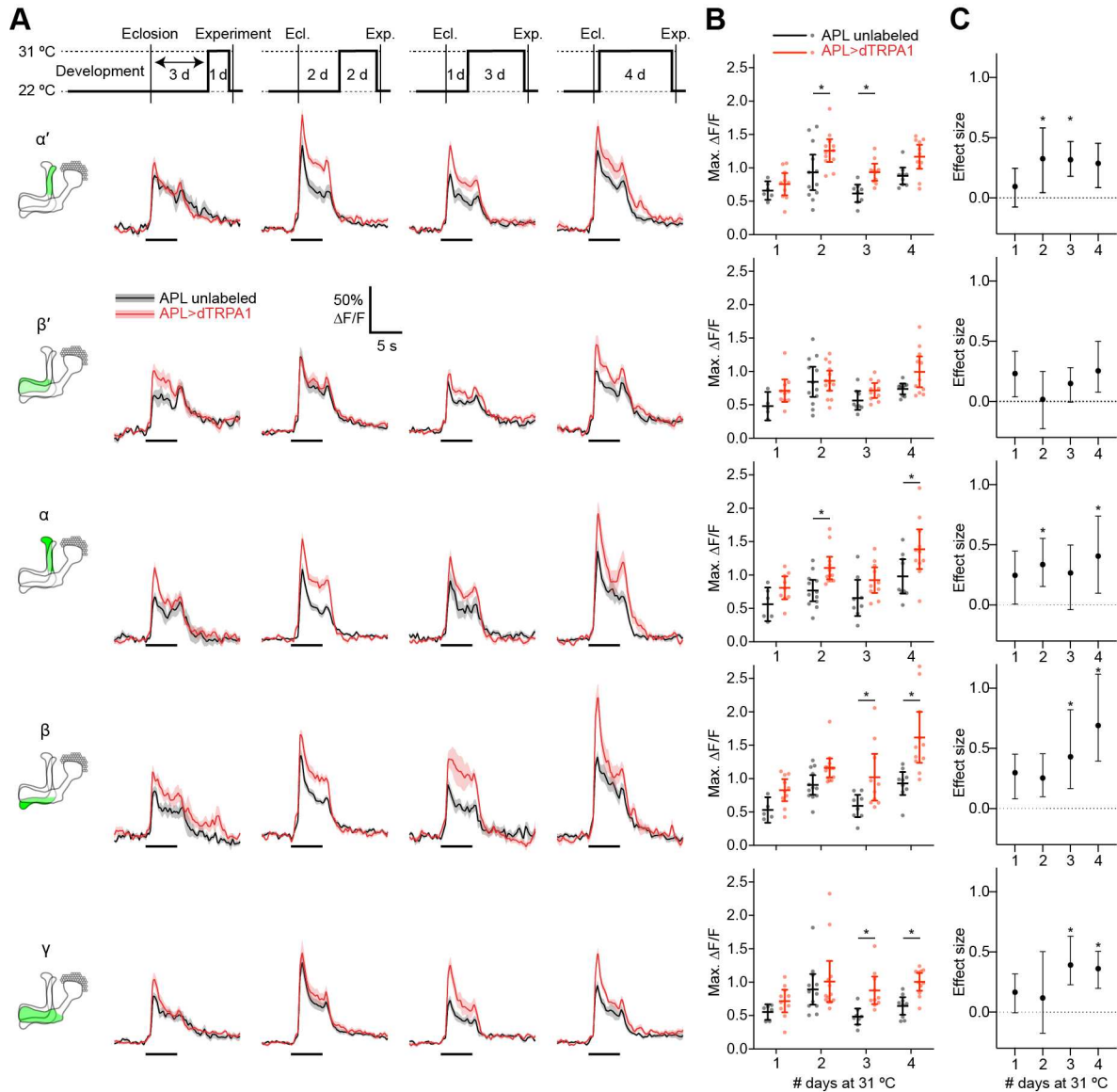


**Fig. S11 (related to Fig. 3). Adaptation after 1, 2, 3, and 4 d pre-activation of APL**

- (A) Responses of all lobes to isoamyl acetate for  $KC > GCaMP6f$ ,  $APL > dTRPA1$  flies kept at 31 °C for 1, 2, 3 or 4 d (as shown on diagrams at top), where APL was unlabeled (black) or expressed dTRPA1 (red). Horizontal bars show time of odor presentation. Error shading shows s.e.m. Diagrams of the mushroom body show the  $\alpha'$ ,  $\beta'$ ,  $\alpha$ ,  $\beta$  and  $\gamma$  lobes.
- (B) Maximum  $\Delta F/F$  response from panel A. Mean  $\pm$  95% confidence interval. \*  $p < 0.05$ , 2-way ANOVA with Sidak's multiple comparisons test. n, given as # hemispheres (# flies), left to right within each graph: 1 d: 6 (5) [5 (4) for  $\beta$  and  $\beta'$ ], 10 [9 for  $\alpha$ ] (7); 2 d: 12 (9), 12 (8); 3 d: 8 (6), 10 (7); 4 d: 9 (7), 11 (8).
- (C) Effect size of adaptation (KC response with  $APL > dTRPA1$  minus KC response with APL unlabeled), calculated using bootstrap-coupled estimation statistics (22). Error bars, 95% confidence intervals.

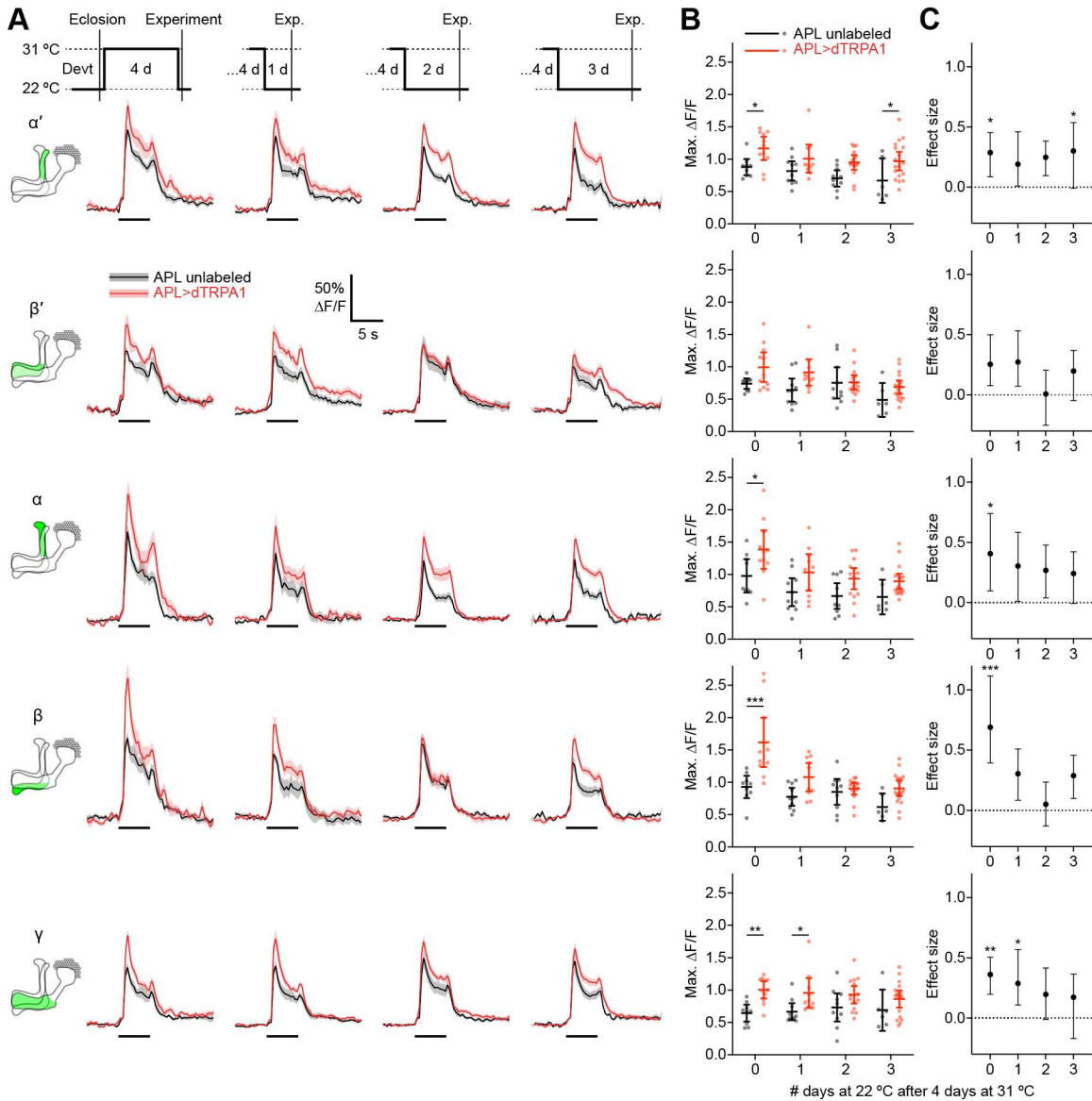


**Fig. S12 (related to Fig. 3). Loss of adaptation 0, 1, 2, and 3 d after the end of pre-activation of APL**

(A) Responses of all lobes to isoamyl acetate for KC>GCaMP6f, APL>dTRPA1 flies kept at 31 °C for 4 d and then 22 °C for 0, 1, 2, or 3 d (as shown on diagrams at top), where APL was unlabeled (black) or expressed dTRPA1 (red). Horizontal bars show time of odor presentation. Error shading shows s.e.m. Diagrams of the mushroom body show the  $\alpha'$ ,  $\beta'$ ,  $\alpha$ ,  $\beta$  and  $\gamma$  lobes.

(B) Maximum  $\Delta F/F$  response from panel A. Mean  $\pm$  95% confidence interval. \*  $p < 0.05$ , 2-way ANOVA with Sidak's multiple comparisons test. n, given as # hemispheres (# flies), left to right within each graph: 0 d: 9 (7), 11 (8); 1 d: 10 (9), 10 (9); 2 d: 10 (9), 15 (11); 3 d: 6 (4), 18 (10).  $p < 0.01$  for the  $\beta$  lobe, interaction between genotype (APL unlabeled vs. APL>dTRPA1) and time (# days at 22 °C) (see **Table S2**).

(C) Effect size of adaptation (KC response with APL>dTRPA1 minus KC response with APL unlabeled), calculated using bootstrap-coupled estimation statistics (22). Error bars, 95% confidence intervals.

Data for 0 d repeated from condition '4 d' in **Fig. S11** for comparison.

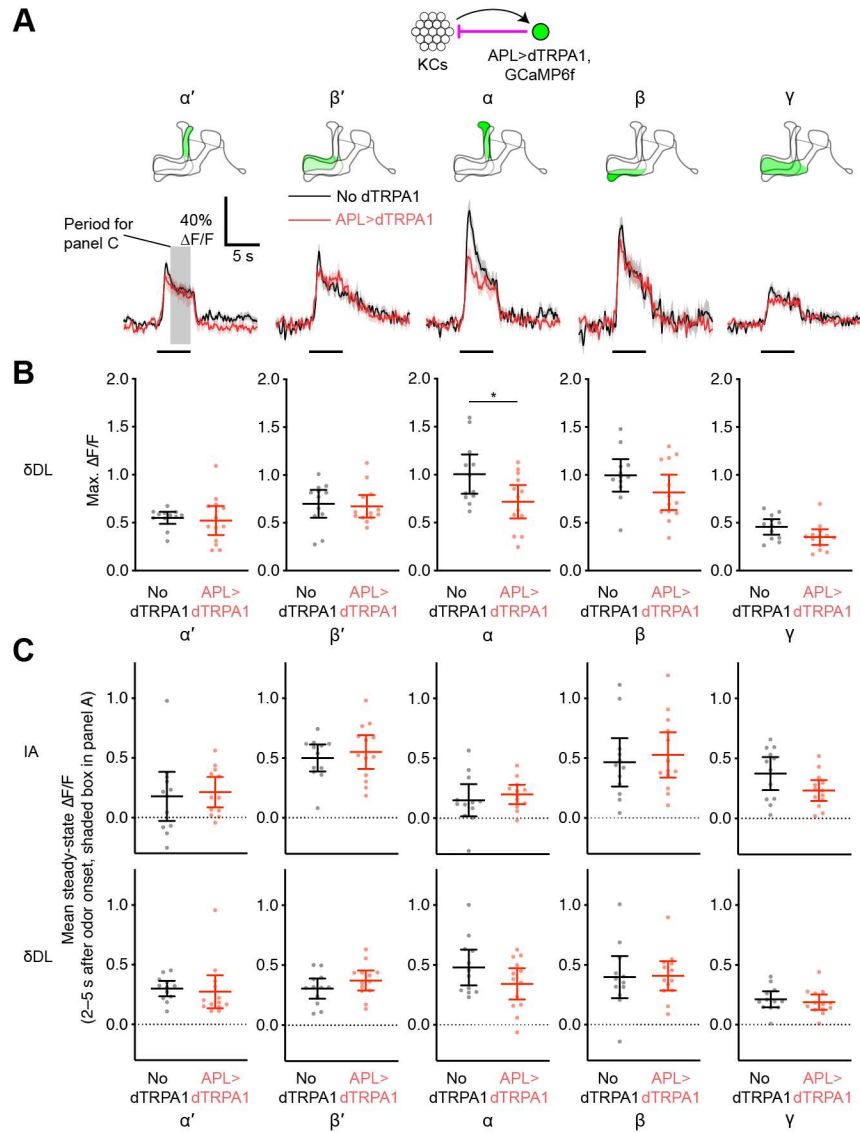


**Fig. S13 (related to Fig. 4). APL responses to  $\delta$ -decalactone, and quantification of APL steady-state responses, following adaptation.**

- (A) Traces show responses of different lobes of APL (as determined by the anatomical marker MB247-dsRed) to  $\delta$ -decalactone in APL>GCaMP6f (“no dTRPA1”) or APL>dTRPA1,GCaMP6f (“APL>dTRPA1”) flies kept at 31 °C for 4 d. Shading shows s.e.m. Grey rectangle shows “steady-state” period for (C).
- (B) Maximum  $\Delta F/F$  of traces from (A). Mean  $\pm$  95% confidence interval. \*  $p < 0.05$ , unpaired t-test. n, given as # hemispheres (# flies): no dTRPA1, 12 (9); APL>dTRPA1, 13 (8). Most lobes show decreased responses in adapted APL>dTRPA1 flies, but unlike responses to isoamyl acetate (Fig. 4), in most cases this is not statistically significant, possibly due to the lower amplitude responses (to  $\delta$ -decalactone compared to isoamyl acetate) combined with the overall noisy GCaMP6f signal (due to recording from only the single APL neuron).
- (C) Mean steady-state  $\Delta F/F$  of traces from (A) and Fig. 4, during 2 – 5 s after odor onset (grey rectangle in (A)). Mean  $\pm$  95% confidence interval. n as in those panels.  $p > 0.05$  for all comparisons, unpaired t-test or Mann-Whitney test (see Table S2 for details).

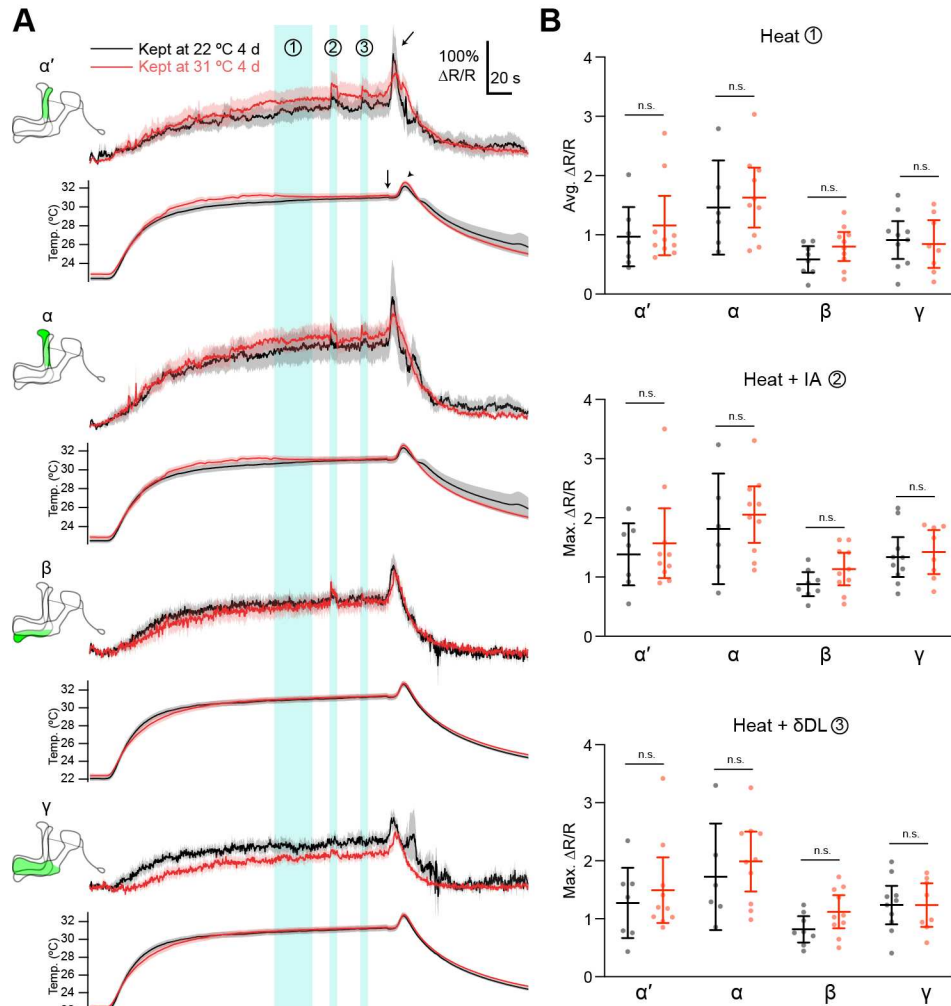


**Fig. S14 (related to Fig. 5). Additional data for activation of APL following adaptation**

(A) Data as in **Fig. 5A,B** but including  $\alpha'$ ,  $\alpha$  and  $\gamma$  APL lobes. n, given as # hemispheres (# flies), left to right within each graph:  $\alpha'$ , 7(5), 10(6);  $\alpha$ , 4(5), 9(6);  $\beta$ , 10(8), 8(6);  $\gamma$ , 10(8), 8(6). We omitted the  $\beta'$  lobe because due to technical limitations in this experiment we could only image one focal plane at a time, and whereas the  $\alpha'$  and  $\alpha$  lobes can be captured in one plane, as can the  $\beta$  and  $\gamma$  lobes, the  $\beta'$  lobe requires another movie, which we deemed non-essential given that **Fig. 5** does not address the  $\beta'$  lobe. The peak after  $\delta$ -decalactone presentation (diagonal arrow) is most likely an artifact of our perfusion protocol. To accelerate cooling, upon turning off the heater, we sped up the perfusion from  $\sim 2.7$  ml/min to  $\sim 9.8$  ml/min. In doing so, we inadvertently briefly increased the saline temperature (arrowhead) because heated saline from the heater had less time to cool down before reaching the fly. Note that the secondary increase in GCaMP6f signal (arrow) aligns not with the secondary rise temperature (arrowhead) but with a slight discontinuity in temperature at the vertical arrow, which reflects the change in perfusion speed. The most likely explanation is that, due to turbulence in the perfusion chamber, the fly received the brief pulse of heat before the thermometer did. Note that this artifact does not affect our interpretation, because the key result of this experiment is only the activation of APL during heating.

(B) Quantification of data from panel A, as in **Fig. 5B**.

Detailed statistical analysis given in **Table S2**.

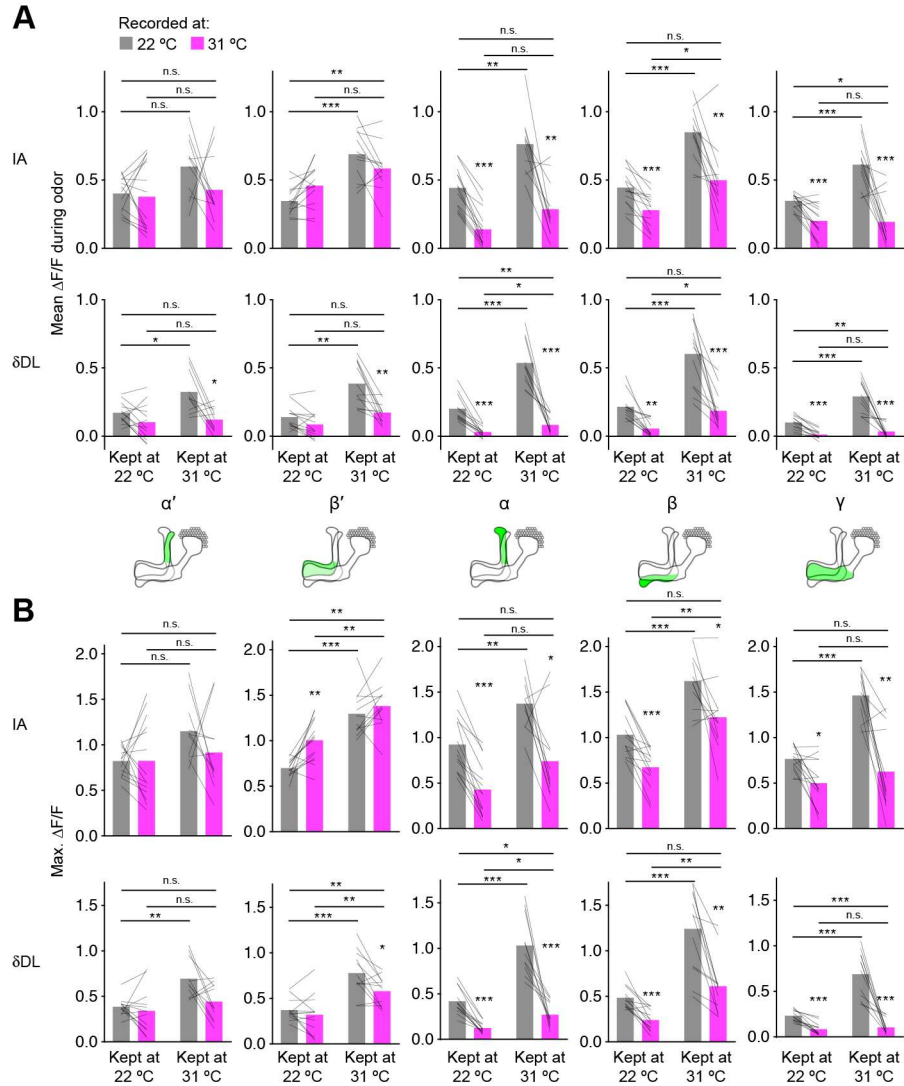


**Fig. S15 (related to Fig. 5). Additional data for activation of APL following adaptation**

(A) Data as in Fig. 5E but including  $\alpha\beta'$  KCs

(B) Data as in panel A, but showing maximum  $\Delta F/F$  during odor response instead of mean  $\Delta F/F$ .

All data from traces in Fig. S6, n as in that figure. Detailed statistical analysis given in Table S2.

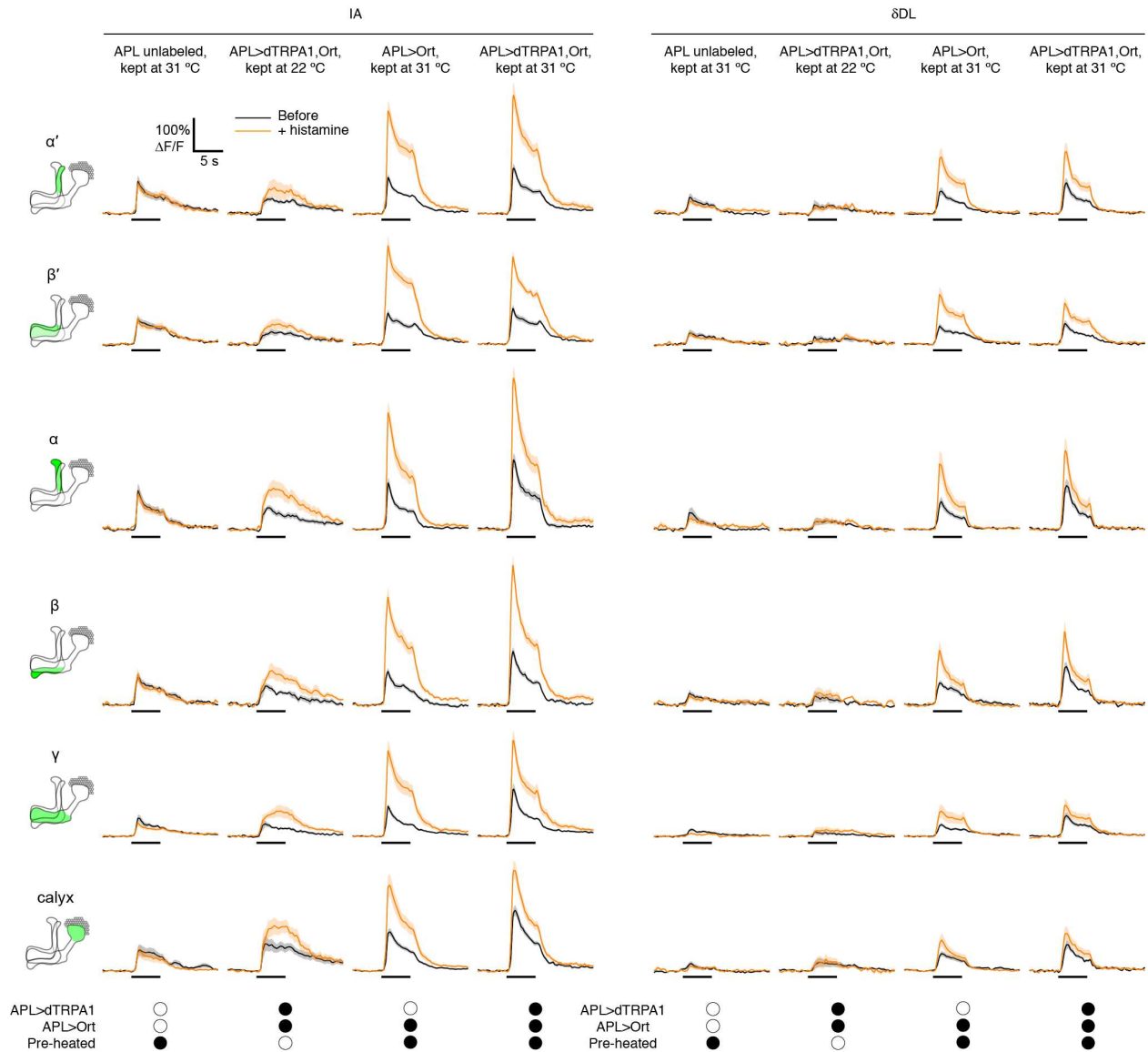


**Fig. S16 (related to Fig. 6). KC odor responses with APL>Ort.**

Average responses of all lobes to isoamyl acetate (IA) or  $\delta$ -decalactone ( $\delta$ DL), before (black) and after (orange) bath-applying 2 mM histamine. Error shading shows s.e.m. Genotypes as described on the Fig. (see **Table S1** for details); “APL unlabeled” is a mixture of hemispheres from APL>Ort and APL>dTRPA1,Ort flies where APL was unlabeled. n, given as # hemispheres (# flies), left to right for each lobe: 10 (9), 6 (4), 17 (11), 16 (11) [15 (10) for  $\delta$ DL].



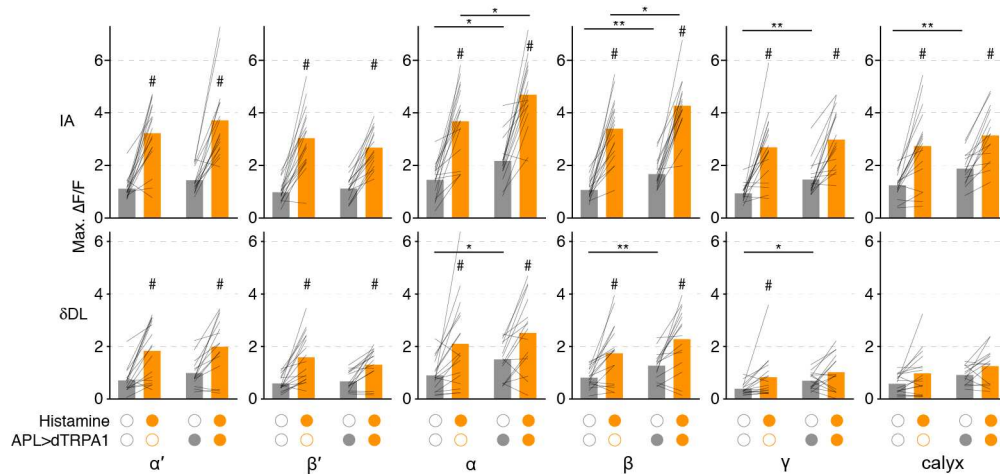


**Fig. S17 (related to Fig. 6). Responses in all KC lobes with APL>Ort.**

Maximum  $\Delta F/F$  for odor responses in all lobes to isoamyl acetate or  $\delta$ -decalactone, before (gray) and after (orange) bath-applying 2 mM histamine. Genotypes: APL>Ort (left), APL>dTRPA1,Ort (right). Bars show mean, thin lines show paired data (same hemisphere before and after histamine). # p < 0.05 effect of histamine, paired t-test or Wilcoxon matched-pairs signed rank test; \* p < 0.05, \*\* p < 0.01, unpaired t-test or Mann-Whitney test, Holm-Bonferroni correction for multiple comparisons (see **Table S2** for details). n, given as # hemispheres (# flies): no dTRPA1, 17 (11); APL>dTRPA1, 16 (11) [15 (10) for  $\delta DL$ ]. Responses from the calyx are shown for completeness but it is difficult to draw conclusions from the calyx as it combines all three types of KCs. Note that for the  $\alpha$  and  $\beta$  lobes, unlike for the strong odor isoamyl acetate, for the weak odor  $\delta$ -decalactone, while APL>dTRPA1,Ort responses were higher than APL>Ort responses after adding histamine, the difference was not statistically significant. This might be due to experimental variability: in some cases even the effect of histamine was not statistically significant for  $\delta$ -decalactone, suggesting that our experimental manipulation was less reliable with a weaker sensory stimulus.

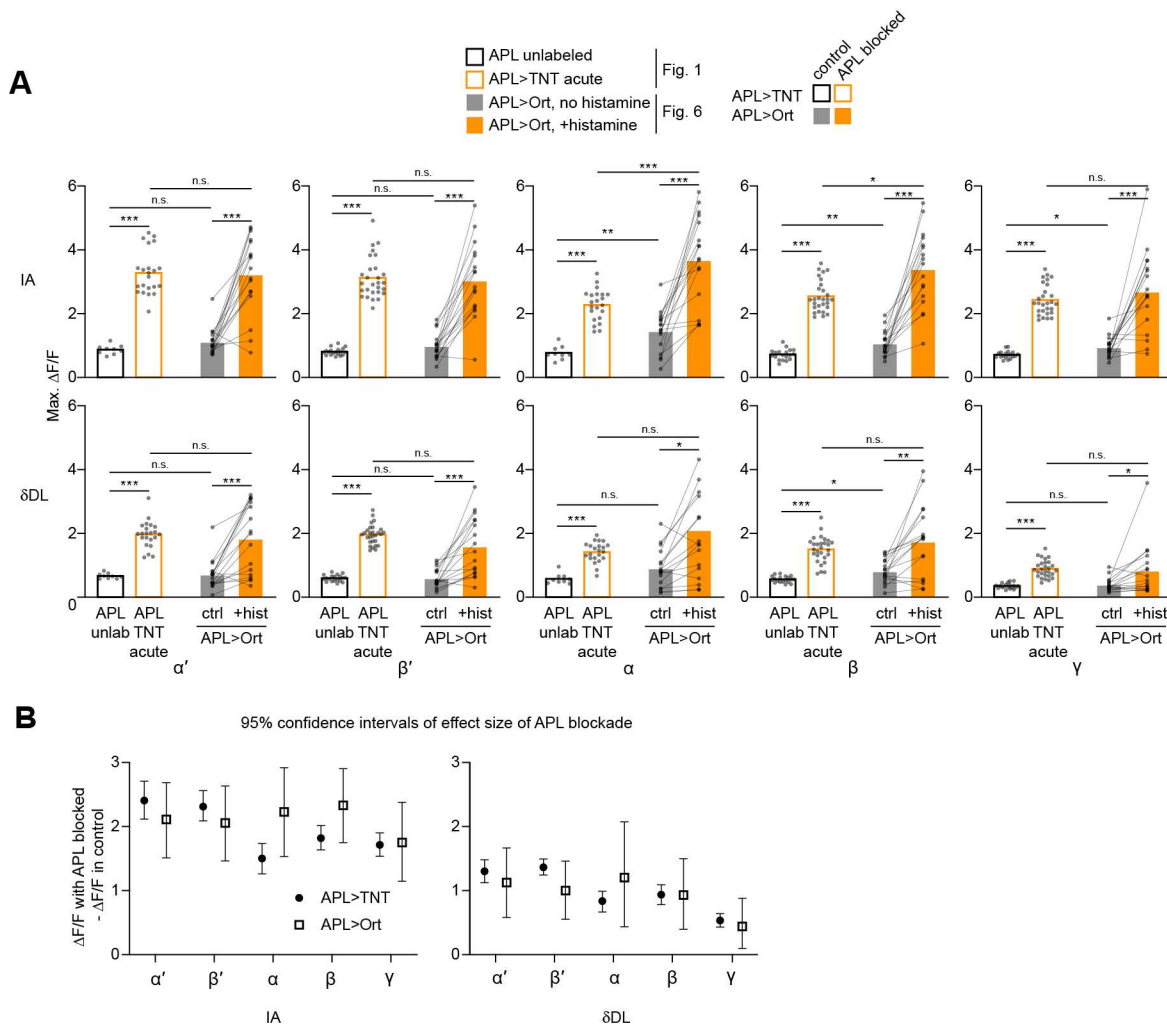


**Fig. S18 (related to Fig. 6). Blocking APL with Ort or TNT causes similar increases in KC odor responses**

- (A) The effect of histamine on APL>Ort (no dTRPA1) flies (filled bars) has similar magnitude as the effect of acute (16-24 h) APL>TNT expression (open bars). Greater variability in APL>Ort flies compared to APL>TNT flies may reflect the more invasive dissection (the perineural sheath had to be removed in APL>Ort flies to allow histamine to penetrate) or variability in penetration of histamine into the brain.  $\alpha\beta$  KC responses were generally higher in APL>Ort flies than APL>TNT flies (independent of whether APL was blocked or not), for unknown reasons. Bars show mean, thin lines show paired data (same hemisphere before and after histamine). \*  $p < 0.05$ , \*\*  $p < 0.01$ , unpaired t-test or Mann-Whitney test, Holm-Bonferroni correction for multiple comparisons (see **Table S2** for details). n as in **Fig. 1** and **6**.
- (B) Effect sizes of blocking APL with APL>TNT or with histamine on APL>Ort flies, calculated using bootstrap-coupled estimation statistics (22). The overlapping error bars for APL>TNT and APL>Ort show the overlap between the 95% confidence intervals of the mean difference between control and APL-blocked conditions, for the two manipulations.



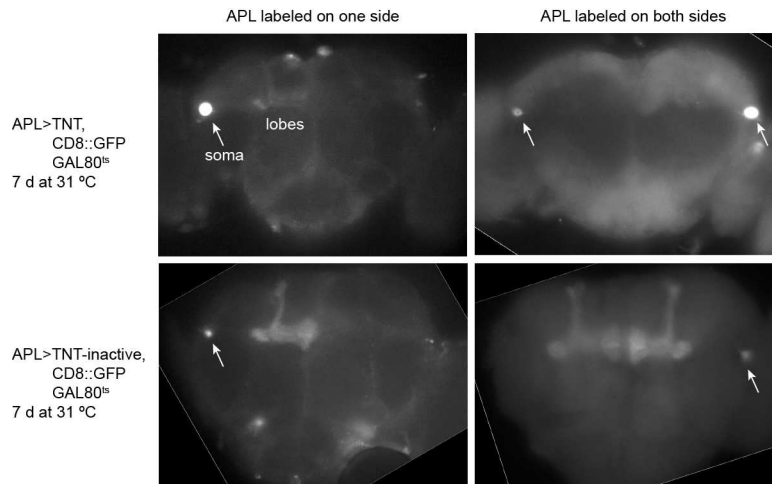


**Fig. S19 (related to Fig. 6). Prolonged expression of tetanus toxin in APL may damage its morphology.** The panels show epifluorescence images of live dissected brains from flies expressing TNT (upper panels) or TNT-inactive (lower panels) and CD8::GFP in APL driven by NP2631-GAL4, GH146-FLP, with tubP-GAL80<sup>ts</sup>, kept at 31 °C for 7 d. Arrows indicate the APL cell bodies. APL neurons expressing TNT show extremely bright cell bodies and dim or no fluorescence in the mushroom body lobes, suggesting that the neurites in the lobes may have degenerated, consistent with previous reports from photoreceptors (27). Scale bars not available.

**Table S1. List of genotypes used**

Figure	Shorthand name / Purpose	Full genotype
(text)	APL>TNT, GFP, GAL80 <sup>ts</sup>	NP2631-GAL4, GH146-FLP/tub-FRT-GAL80-FRT, UAS-TNT, tubP-GAL80 <sup>ts</sup> ; UAS-CD8::GFP/UAS-mCherry
1, S3	APL>TNT, GAL80 <sup>ts</sup>	NP2631-GAL4, GH146-FLP/tub-FRT-GAL80-FRT, UAS-TNT, tubP-GAL80 <sup>ts</sup> ; MB247-LexA, lexAop-GCaMP6f/UAS-mCherry or NP2631-GAL4, GH146-FLP/UAS-TNT, tubP-GAL80 <sup>ts</sup> ; MB247-LexA, lexAop-GCaMP6f/tub-FRT-GAL80-FRT
1, S3	APL>TNT	NP2631-GAL4, GH146-FLP/tub-FRT-GAL80-FRT, UAS-TNT, UAS-mCherry; MB247-LexA, lexAop-GCaMP6f/+
S1	VT43924>GFP	UAS-CD8::GFP/CyO; VT43924-GAL4
S2, S3	APL>TNT, GAL80 <sup>ts</sup> , KC>GCaMP3	NP2631-GAL4, GH146-FLP/tub-FRT-GAL80-FRT, UAS-TNT, tubP-GAL80 <sup>ts</sup> ; MB247-LexA, lexAop-GCaMP3/UAS-mCherry or NP2631-GAL4, GH146-FLP/UAS-TNT, tubP-GAL80 <sup>ts</sup> ; MB247-LexA, lexAop-GCaMP3/tub-FRT-GAL80-FRT
S2, S3	APL>TNT, KC>GCaMP3	NP2631-GAL4, GH146-FLP/UAS-TNT; MB247-LexA, lexAop-GCaMP3,tub-FRT-GAL80-FRT/UAS-mCherry
2, 3, 5, S4-8, S11-12, S15	APL>dTRPA1	NP2631-GAL4, GH146-FLP/tubP-FRT-GAL80-FRT, UAS-dTRPA1, UAS-mCherry; MB247-LexA, lexAop-GCaMP6f/+
S4	APL>dTRPA1, KC>GCaMP3	NP2631-GAL4, GH146-FLP/tubP-FRT-GAL80-FRT, UAS-dTRPA1, UAS-mCherry; MB247-LexA, lexAop-GCaMP3/+
3, S9, S10	APL>dTRPA1	UAS-dTRPA1/+; MB247-LexA, lexAop-GCaMP6f/VT43924-GAL4(attP2)
3, S9, S10	UAS-dTRPA1/+	UAS-dTRPA1/+; MB247-LexA, lexAop-GCaMP6f/+
4, 5, S8, S14	APL>dTRPA1, GCaMP6f	NP2631-GAL4, GH146-FLP, MB247-dsRed/tubP-FRT-GAL80-FRT, UAS-dTRPA1; UAS-GCaMP6f/+
4, S8	APL>GCaMP6f	NP2631-GAL4, GH146-FLP, MB247-dsRed/tubP-FRT-GAL80-FRT; UAS-GCaMP6f/+
6, S16, S17	APL>dTRPA1, Ort	NP2631-GAL4, GH146-FLP/tubP-FRT-GAL80-FRT, UAS-dTRPA1, UAS-Ort; MB247-LexA, lexAop-GCaMP6f/UAS-mCherry
6, S16-18	APL>Ort	NP2631-GAL4, GH146-FLP/tubP-FRT-GAL80-FRT, UAS-Ort; MB247-LexA, lexAop-GCaMP6f/UAS-mCherry
S19	APL>TNT(-inactive),GFP, Gal80 <sup>ts</sup>	NP2631, GH146-FLP/UAS-TNT(-inactive), tubP-GAL80 <sup>ts</sup> ; UAS-CD8:GFP/tub-FRT-GAL80-FRT

**Table S2. Details of statistical analyses:** Appended after references

## SI References

1. Tanaka NK, Tanimoto H, Ito K (2008) Neuronal assemblies of the *Drosophila* mushroom body. *J Comp Neurol* 508(5):711–755.
2. Hong W, et al. (2009) Leucine-rich repeat transmembrane proteins instruct discrete dendrite targeting in an olfactory map. *Nat Neurosci* 12(12):1542–1550.
3. Gao S, et al. (2008) The neural substrate of spectral preference in *Drosophila*. 60(2):328–342.
4. Gordon MD, Scott K (2009) Motor control in a *Drosophila* taste circuit. *Neuron* 61(3):373–384.
5. Sweeney ST, Broadie K, Keane J, Niemann H, O’Kane CJ (1995) Targeted expression of tetanus toxin light chain in *Drosophila* specifically eliminates synaptic transmission and causes behavioral defects. *Neuron* 14(2):341–351.
6. Mao Z, Roman G, Zong L, Davis RL (2004) Pharmacogenetic rescue in time and space of the rutabaga memory impairment by using Gene-Switch. *Proc Natl Acad Sci USA* 101(1):198–203.
7. Lee T, Lee A, Luo L (1999) Development of the *Drosophila* mushroom bodies: sequential generation of three distinct types of neurons from a neuroblast. *Development* 126(18):4065–4076.
8. Kakihara K, Shinmyozu K, Kato K, Wada H, Hayashi S (2008) Conversion of plasma membrane topology during epithelial tube connection requires Arf-like 3 small GTPase in *Drosophila*. *Mechanisms of Development* 125(3-4):325–336.
9. Pitman JL, et al. (2011) A pair of inhibitory neurons are required to sustain labile memory in the *Drosophila* mushroom body. *Current Biology* 21(10):855–861.
10. Barnstedt O, et al. (2016) Memory-Relevant Mushroom Body Output Synapses Are Cholinergic. *Neuron* 89(6):1237–1247.
11. Lin AC, Bygrave AM, de Calignon A, Lee T, Miesenböck G (2014) Sparse, decorrelated odor coding in the mushroom body enhances learned odor discrimination. *Nat Neurosci* 17(4):559–568.
12. Hamada FN, et al. (2008) An internal thermal sensor controlling temperature preference in *Drosophila*. *Nature* 454(7201):217–220.
13. Wu C-L, Shih M-FM, Lee P-T, Chiang A-S (2013) An octopamine-mushroom body circuit modulates the formation of anesthesia-resistant memory in *Drosophila*. *Current Biology* 23(23):2346–2354.
14. Liu WW, Wilson RI (2013) Transient and specific inactivation of *Drosophila* neurons in vivo using a native ligand-gated ion channel. 23(13):1202–1208.
15. Bielopolski N, et al. (2019) Inhibitory muscarinic acetylcholine receptors enhance aversive olfactory learning in adult *Drosophila*. *Elife* 8:463.
16. Ng MM, et al. (2002) Transmission of olfactory information between three populations of neurons in the antennal lobe of the fly. *Neuron* 36(3):463–474.
17. Wang JW, Wong AM, Flores J, Vosshall LB, Axel R (2003) Two-photon calcium imaging reveals an odor-evoked map of activity in the fly brain. *Cell* 112(2):271–282.
18. Dubbs A, Guevara J, Yuste R (2016) moco: Fast Motion Correction for Calcium Imaging. *Front*

*Neuroinform* 10:6.

19. Vinje WE, Gallant JL (2000) Sparse coding and decorrelation in primary visual cortex during natural vision. *Science* 287(5456):1273–1276.
20. Willmore B, Tolhurst DJ (2001) Characterizing the sparseness of neural codes. *Network* 12(3):255–270.
21. Wu JS, Luo L (2006) A protocol for dissecting *Drosophila melanogaster* brains for live imaging or immunostaining. *Nat Protoc* 1(4):2110–2115.
22. Ho J, Tumkaya T, Aryal S, Choi H, Claridge-Chang A (2019) Moving beyond P values: data analysis with estimation graphics. *Nat Methods* 16(7):565–566.
23. Mittal AM, Gupta D, Singh A, Lin AC, Gupta N (2020) Multiple network properties overcome random connectivity to enable stereotypic sensory responses. *Nature Communications* 11(1):1–15.
24. Groschner LN, Chan Wah Hak L, Bogacz R, DasGupta S, Miesenböck G (2018) Dendritic Integration of Sensory Evidence in Perceptual Decision-Making. *Cell* 173(4):894–905.e13.
25. Inada K, Tsuchimoto Y, Kazama H (2017) Origins of Cell-Type-Specific Olfactory Processing in the *Drosophila* Mushroom Body Circuit. *Neuron* 95(2):357–367.e4.
26. Turner GC, Bazhenov M, Laurent G (2008) Olfactory representations by *Drosophila* mushroom body neurons. *J Neurophysiol* 99(2):734–746.
27. Haberman A, et al. (2012) The synaptic vesicle SNARE neuronal Synaptobrevin promotes endolysosomal degradation and prevents neurodegeneration. - PubMed - NCBI. *J Cell Biol* 196(2):261–276.

Table S2: Details of statistics

Figure	Data	Statistical test	Comparison	P-value	Significance
1C: APL>TNT, IA	alpha', IA	Welch's ANOVA		<0.0001	****
		Dunnett's T3 multiple comparisons test	18 °C vs. APL unlabeled	0.9372	ns
			18 °C vs. acute	<0.0001	****
			18 °C vs. constitutive	<0.0001	****
			APL unlabeled vs. acute	<0.0001	****
			APL unlabeled vs. constitutive	<0.0001	****
	acute vs. constitutive	0.4529	ns		
	alpha', IA, separating APL unlabeled, Gal80ts vs. no Gal80ts	Dunnett's T3 multiple comparisons test	18 °C vs. APL unlabeled, Gal80ts	0.9209	ns
			18 °C vs. acute	<0.0001	****
			18 °C vs. APL unlabeled, no Gal80ts	>0.9999	ns
			18 °C vs. constitutive	<0.0001	****
			APL unlabeled, Gal80ts vs. acute	<0.0001	****
			APL unlabeled, Gal80ts vs. APL unlabeled, no Gal80ts	0.9477	ns
			APL unlabeled, no Gal80ts vs. constitutive	<0.0001	****
	acute vs. constitutive	0.5461	ns		
	beta', IA	Kruskal-Wallis test		<0.0001	****
		Dunn's multiple comparisons test	18 °C vs. APL unlabeled	>0.9999	ns
			18 °C vs. acute	<0.0001	****
			18 °C vs. constitutive	<0.0001	****
			APL unlabeled vs. acute	<0.0001	****
			APL unlabeled vs. constitutive	<0.0001	****
	acute vs. constitutive	0.4911	ns		
	beta', IA, separating APL unlabeled, Gal80ts vs. no Gal80ts	Dunn's multiple comparisons test	18 °C vs. APL unlabeled, Gal80ts	>0.9999	ns
			18 °C vs. acute	<0.0001	****
			18 °C vs. APL unlabeled, no Gal80ts	>0.9999	ns
			18 °C vs. constitutive	<0.0001	****
			APL unlabeled, Gal80ts vs. acute	<0.0001	****
			APL unlabeled, Gal80ts vs. APL unlabeled, no Gal80ts	>0.9999	ns
			APL unlabeled, no Gal80ts vs. constitutive	0.007	**
	acute vs. constitutive	0.6548	ns		
	alpha, IA	Welch's ANOVA		<0.0001	****
		Dunnett's T3 multiple comparisons test	18 °C vs. APL unlabeled	0.6682	ns
			18 °C vs. acute	<0.0001	****
			18 °C vs. constitutive	<0.0001	****
			APL unlabeled vs. acute	<0.0001	****
			APL unlabeled vs. constitutive	<0.0001	****
	acute vs. constitutive	0.0204	*		
	alpha, IA, separating APL unlabeled, Gal80ts vs. no Gal80ts	Dunnett's T3 multiple comparisons test	18 °C vs. APL unlabeled, Gal80ts	0.9944	ns
			18 °C vs. acute	<0.0001	****
			18 °C vs. APL unlabeled, no Gal80ts	0.3794	ns
			18 °C vs. constitutive	<0.0001	****
			APL unlabeled, Gal80ts vs. acute	<0.0001	****
			APL unlabeled, Gal80ts vs. APL unlabeled, no Gal80ts	0.9901	ns
			APL unlabeled, no Gal80ts vs. constitutive	<0.0001	****
	acute vs. constitutive	0.0269	*		
	beta, IA	Welch's ANOVA		<0.0001	****
		Dunnett's T3 multiple comparisons test	18 °C vs. APL unlabeled	>0.9999	ns
18 °C vs. acute			<0.0001	****	
18 °C vs. constitutive			<0.0001	****	
APL unlabeled vs. acute			<0.0001	****	
APL unlabeled vs. constitutive			<0.0001	****	
acute vs. constitutive	0.9997	ns			
beta, IA, separating APL unlabeled, Gal80ts vs. no Gal80ts	Dunnett's T3 multiple comparisons test	18 °C vs. APL unlabeled, Gal80ts	>0.9999	ns	
		18 °C vs. acute	<0.0001	****	
		18 °C vs. APL unlabeled, no Gal80ts	0.9993	ns	
		18 °C vs. constitutive	<0.0001	****	
		APL unlabeled, Gal80ts vs. acute	<0.0001	****	
		APL unlabeled, Gal80ts vs. APL unlabeled, no Gal80ts	0.9759	ns	
		APL unlabeled, no Gal80ts vs. constitutive	<0.0001	****	
acute vs. constitutive	>0.9999	ns			
gamma, IA	Welch's ANOVA		<0.0001	****	
	Dunnett's T3 multiple comparisons test	18 °C vs. APL unlabeled	0.0285	*	
		18 °C vs. acute	<0.0001	****	
		18 °C vs. constitutive	<0.0001	****	
		APL unlabeled vs. acute	<0.0001	****	
		APL unlabeled vs. constitutive	<0.0001	****	
acute vs. constitutive	0.9578	ns			
		18 °C vs. APL unlabeled, Gal80ts	0.0569	ns	
		18 °C vs. acute	<0.0001	****	

Table S2: Details of statistics

Figure	Data	Statistical test	Comparison	P-value	Significance
1C: APL>TNT, d-DL	gamma, IA, separating APL unlabeled, Gal80ts vs. no Gal80ts	Dunnett's T3 multiple comparisons test	18 °C vs. APL unlabeled, no Gal80ts	0.0931	ns
			18 °C vs. constitutive	<0.0001	****
			APL unlabeled, Gal80ts vs. acute	<0.0001	****
			APL unlabeled, Gal80ts vs. APL unlabeled, no Gal80ts	0.9993	ns
			APL unlabeled, no Gal80ts vs. constitutive	<0.0001	****
			acute vs. constitutive	0.9846	ns
	alpha', d-DL	Kruskal-Wallis test		<0.0001	****
			18 °C vs. APL unlabeled	>0.9999	ns
		Dunn's multiple comparisons test	18 °C vs. acute	0.0001	***
			18 °C vs. constitutive	<0.0001	****
			APL unlabeled vs. acute	0.0002	***
			APL unlabeled vs. constitutive	0.0001	***
			acute vs. constitutive	>0.9999	ns
			Dunn's multiple comparisons test	18 °C vs. APL unlabeled, Gal80ts	>0.9999
		18 °C vs. acute		0.0001	***
		18 °C vs. APL unlabeled, no Gal80ts		>0.9999	ns
		18 °C vs. constitutive		0.0001	***
		APL unlabeled, Gal80ts vs. acute		0.0037	**
	APL unlabeled, Gal80ts vs. APL unlabeled, no Gal80ts	>0.9999		ns	
	beta', d-DL	Kruskal-Wallis test		<0.0001	****
			18 °C vs. APL unlabeled	>0.9999	ns
		Dunn's multiple comparisons test	18 °C vs. acute	<0.0001	****
			18 °C vs. constitutive	<0.0001	****
			APL unlabeled vs. acute	<0.0001	****
			APL unlabeled vs. constitutive	<0.0001	****
			acute vs. constitutive	>0.9999	ns
			Dunn's multiple comparisons test	18 °C vs. APL unlabeled, Gal80ts	>0.9999
18 °C vs. acute		<0.0001		****	
18 °C vs. APL unlabeled, no Gal80ts		>0.9999		ns	
18 °C vs. constitutive		<0.0001		****	
APL unlabeled, Gal80ts vs. acute		<0.0001		****	
APL unlabeled, Gal80ts vs. APL unlabeled, no Gal80ts	>0.9999	ns			
alpha, d-DL	Kruskal-Wallis test		<0.0001	****	
		18 °C vs. APL unlabeled	>0.9999	ns	
	Dunn's multiple comparisons test	18 °C vs. acute	0.0005	***	
		18 °C vs. constitutive	<0.0001	****	
		APL unlabeled vs. acute	0.0003	***	
		APL unlabeled vs. constitutive	<0.0001	****	
		acute vs. constitutive	>0.9999	ns	
		Dunn's multiple comparisons test	18 °C vs. APL unlabeled, Gal80ts	>0.9999	ns
	18 °C vs. acute		0.0006	***	
	18 °C vs. APL unlabeled, no Gal80ts		>0.9999	ns	
	18 °C vs. constitutive		0.0001	***	
	APL unlabeled, Gal80ts vs. acute		0.0044	**	
APL unlabeled, Gal80ts vs. APL unlabeled, no Gal80ts	>0.9999		ns		
beta, d-DL	Welch's ANOVA		<0.0001	****	
		18 °C vs. APL unlabeled	0.759	ns	
	Dunnett's T3 multiple comparisons test	18 °C vs. acute	<0.0001	****	
		18 °C vs. constitutive	<0.0001	****	
		APL unlabeled vs. acute	<0.0001	****	
		APL unlabeled vs. constitutive	<0.0001	****	
		acute vs. constitutive	0.0055	**	
		Dunnett's T3 multiple comparisons test	18 °C vs. APL unlabeled, Gal80ts	>0.9999	ns
	18 °C vs. acute		<0.0001	****	
	18 °C vs. APL unlabeled, no Gal80ts		0.1759	ns	
	18 °C vs. constitutive		<0.0001	****	
	APL unlabeled, Gal80ts vs. acute		<0.0001	****	
APL unlabeled, Gal80ts vs. APL unlabeled, no Gal80ts	0.1014		ns		
beta, d-DL, separating APL unlabeled, Gal80ts vs. no Gal80ts	Kruskal-Wallis test		<0.0001	****	
		18 °C vs. APL unlabeled	>0.9999	ns	
	Dunn's multiple comparisons test	18 °C vs. acute	<0.0001	****	
		18 °C vs. constitutive	<0.0001	****	
		APL unlabeled, Gal80ts vs. acute	<0.0001	****	
		APL unlabeled, Gal80ts vs. APL unlabeled, no Gal80ts	0.1014	ns	
		APL unlabeled, no Gal80ts vs. constitutive	<0.0001	****	
		acute vs. constitutive	0.0073	**	
	Kruskal-Wallis test		<0.0001	****	
		18 °C vs. APL unlabeled	>0.9999	ns	
		18 °C vs. acute	<0.0001	****	

Table S2: Details of statistics

Figure	Data	Statistical test	Comparison	P-value	Significance	
	gamma, d-DL	Dunn's multiple comparisons test	18 °C vs. constitutive	<0.0001	****	
			APL unlabeled vs. acute	<0.0001	****	
			APL unlabeled vs. constitutive	<0.0001	****	
			acute vs. constitutive	0.8711	ns	
	gamma, dDL, separating APL unlabeled, Gal80ts vs. no Gal80ts	Dunn's multiple comparisons test	18 °C vs. APL unlabeled, Gal80ts	>0.9999	ns	
			18 °C vs. acute	<0.0001	****	
			18 °C vs. APL unlabeled, no Gal80ts	>0.9999	ns	
			18 °C vs. constitutive	<0.0001	****	
			APL unlabeled, Gal80ts vs. acute	<0.0001	****	
			APL unlabeled, Gal80ts vs. APL unlabeled, no Gal80ts	>0.9999	ns	
			APL unlabeled, no Gal80ts vs. constitutive	0.0003	***	
			acute vs. constitutive	>0.9999	ns	
S2A: KC>GCaMP6f, APL unlabeled, with vs. without GAL80ts	IA	Mixed-effects model with Geisser-Greenhouse correction (matching across lobes)	Lobe	0.0973	ns	
			Genotype	0.6698	ns	
	dDL	Mixed-effects model with Geisser-Greenhouse correction (matching across lobes)	Lobe	<0.0001	****	
			Genotype	0.0802	ns	
S2C: KC>GCaMP3, APL>TNT, IA	alpha', IA	Welch's ANOVA		<0.0001	****	
		Dunnett's T3 multiple comparisons test	APL unlabeled vs. acute	<0.0001	****	
			APL unlabeled vs. constitutive	<0.0001	****	
	beta', IA	Welch's ANOVA		<0.0001	****	
		Dunnett's T3 multiple comparisons test	APL unlabeled vs. acute	<0.0001	****	
			APL unlabeled vs. constitutive	<0.0001	****	
	alpha, IA	Welch's ANOVA		<0.0001	****	
		Dunnett's T3 multiple comparisons test	APL unlabeled vs. acute	<0.0001	****	
			APL unlabeled vs. constitutive	<0.0001	****	
	beta, IA	Kruskal-Wallis test		<0.0001	****	
		Dunn's multiple comparisons test	APL unlabeled vs. acute	<0.0001	****	
			APL unlabeled vs. constitutive	<0.0001	****	
	gamma, IA	Welch's ANOVA		<0.0001	****	
		Dunnett's T3 multiple comparisons test	APL unlabeled vs. acute	<0.0001	****	
			APL unlabeled vs. constitutive	<0.0001	****	
	S2C: KC>GCaMP3, APL>TNT, d-DL	alpha', d-DL	Welch's ANOVA		<0.0001	****
			Dunnett's T3 multiple comparisons test	APL unlabeled vs. acute	<0.0001	****
				APL unlabeled vs. constitutive	0.0002	***
		beta', d-DL	Kruskal-Wallis test		<0.0001	****
			Dunn's multiple comparisons test	APL unlabeled vs. acute	<0.0001	****
				APL unlabeled vs. constitutive	<0.0001	****
		alpha, d-DL	Welch's ANOVA		<0.0001	****
			Dunnett's T3 multiple comparisons test	APL unlabeled vs. acute	<0.0001	****
				APL unlabeled vs. constitutive	<0.0001	****
beta, d-DL		Kruskal-Wallis test		<0.0001	****	
		Dunn's multiple comparisons test	APL unlabeled vs. acute	<0.0001	****	
			APL unlabeled vs. constitutive	<0.0001	****	
gamma, d-DL		Welch's ANOVA		<0.0001	****	
		Dunnett's T3 multiple comparisons test	APL unlabeled vs. acute	<0.0001	****	
			APL unlabeled vs. constitutive	<0.0001	****	
S3A: (IA-dDL)/(IA+dDL), KC>GCaMP6f		Mixed-effects model with Geisser-Greenhouse correction (matching across lobes)		Lobe	<0.0001	****
				Genotype	<0.0001	****
				Lobe x Genotype	0.0262	*
		alpha'	Holm-Sidak multiple comparison tests	APL unlabeled vs. acute	0.024	*
				APL unlabeled vs. constitutive	0.3438	ns
		beta'	Holm-Sidak multiple comparison tests	acute vs. constitutive	0.024	*
				APL unlabeled vs. acute	0.0177	*
		alpha	Holm-Sidak multiple comparison tests	APL unlabeled vs. constitutive	0.563	ns
				acute vs. constitutive	0.0319	*
			APL unlabeled vs. acute	0.3056	ns	
			APL unlabeled vs. constitutive	0.6328	ns	

Table S2: Details of statistics

Figure	Data	Statistical test	Comparison	P-value	Significance	
	beta	Holm-Sidak multiple comparison tests	acute vs. constitutive	0.0039	**	
			APL unlabeled vs. acute	0.0005	***	
			APL unlabeled vs. constitutive	0.575	ns	
	gamma	Holm-Sidak multiple comparison tests	acute vs. constitutive	0.0001	***	
			APL unlabeled vs. acute	<0.0001	****	
			APL unlabeled vs. constitutive	0.0274	*	
			acute vs. constitutive	0.0274	*	
S3A: (IA-dDL)/(IA+dDL), KC>GCaMP3	2-way ANOVA		N/A: residuals not normal			
	alpha'	ordinary 1-way ANOVA		0.0034	**	
		Holm-Sidak multiple comparisons test	APL unlabeled vs. acute	0.0036	**	
			APL unlabeled vs. constitutive	0.0248	*	
	acute vs. constitutive		0.6375	ns		
	beta'	Kruskal-Wallis test		0.0127	*	
		Dunn's multiple comparisons test	APL unlabeled vs. acute	0.9179	ns	
			APL unlabeled vs. constitutive	0.0117	*	
	acute vs. constitutive		0.1072	ns		
	alpha	Kruskal-Wallis test		0.0157	*	
		Dunn's multiple comparisons test	APL unlabeled vs. acute	0.0246	*	
			APL unlabeled vs. constitutive	>0.9999	ns	
	acute vs. constitutive		0.1044	ns		
	beta	Kruskal-Wallis test		0.0236	*	
		Dunn's multiple comparisons test	APL unlabeled vs. acute	0.0208	*	
			APL unlabeled vs. constitutive	0.2035	ns	
	acute vs. constitutive		>0.9999	ns		
	gamma	Kruskal-Wallis test		<0.0001	****	
		Dunn's multiple comparisons test	APL unlabeled vs. acute	<0.0001	****	
			APL unlabeled vs. constitutive	<0.0001	****	
	acute vs. constitutive		>0.9999	ns		
	S1e: OFF/ON, KC>GCaMP6f	alpha', IA	Ordinary 1-way ANOVA		<0.0001	****
			Holm-Sidak multiple comparisons test	APL unlabeled vs. acute	<0.0001	****
				APL unlabeled vs. constitutive	<0.0001	****
		acute vs. constitutive		0.1596	ns	
		beta', IA	Ordinary 1-way ANOVA		<0.0001	****
			Holm-Sidak multiple comparisons test	APL unlabeled vs. acute	<0.0001	****
				APL unlabeled vs. constitutive	<0.0001	****
acute vs. constitutive		0.0651		ns		
alpha, IA		Ordinary 1-way ANOVA		0.0039	**	
		Holm-Sidak multiple comparisons test	APL unlabeled vs. acute	0.0054	**	
			APL unlabeled vs. constitutive	0.0054	**	
acute vs. constitutive			0.9967	ns		
beta, IA		Ordinary 1-way ANOVA		<0.0001	****	
		Holm-Sidak multiple comparisons test	APL unlabeled vs. acute	<0.0001	****	
			APL unlabeled vs. constitutive	<0.0001	****	
acute vs. constitutive			0.2841	ns		
gamma, IA		Kruskal-Wallis test		<0.0001	****	
		Dunn's multiple comparisons test	APL unlabeled vs. acute	<0.0001	****	
			APL unlabeled vs. constitutive	<0.0001	****	
acute vs. constitutive			0.5456	ns		
S3B: OFF/ON, KC>GCaMP6f		alpha', d-DL	Kruskal-Wallis test		0.0087	**
			Dunn's multiple comparisons test	APL unlabeled vs. acute	0.2945	ns
				APL unlabeled vs. constitutive	0.0074	**
				acute vs. constitutive	0.1976	ns
	beta', d-DL	Kruskal-Wallis test		0.0004	***	
		Dunn's multiple comparisons test	APL unlabeled vs. acute	0.041	*	
			APL unlabeled vs. constitutive	0.0002	***	
acute vs. constitutive	0.2542		ns			
alpha, d-DL	Kruskal-Wallis test		0.8892	ns		
beta, d-DL	Kruskal-Wallis test		0.8892	ns		
gamma, d-DL	Kruskal-Wallis test		0.1644	ns		
S3B: OFF/ON, KC>GCaMP3	alpha', IA	Kruskal-Wallis test		<0.0001	****	
		Dunn's multiple comparisons test	APL unlabeled vs. acute	0.0019	**	
			APL unlabeled vs. constitutive	<0.0001	****	
	acute vs. constitutive		0.2982	ns		
	beta', IA	Welch's ANOVA		<0.0001	****	
		Dunnnett's T3 multiple comparisons test	APL unlabeled vs. acute	<0.0001	****	
APL unlabeled vs. constitutive			<0.0001	****		
acute vs. constitutive	<0.0001		****			
alpha, IA	Kruskal-Wallis test		0.0736	ns		
	Kruskal-Wallis test		<0.0001	****		



Table S2: Details of statistics

Figure	Data	Statistical test	Comparison	P-value	Significance	
	beta, IA	Dunn's multiple comparisons test	APL unlabeled vs. acute	<0.0001	****	
			APL unlabeled vs. constitutive	<0.0001	****	
			acute vs. constitutive	0.017	*	
	gamma, IA	Kruskal-Wallis test		<0.0001	****	
			Dunn's multiple comparisons test	APL unlabeled vs. acute	<0.0001	****
				APL unlabeled vs. constitutive	<0.0001	****
		acute vs. constitutive	0.0022	**		
S3B: OFF/ON, KC>GCaMP3	alpha', d-DL	Kruskal-Wallis test		0.218	ns	
				<0.0001	****	
	beta', d-DL	Dunnett's T3 multiple comparisons test	APL unlabeled vs. acute	0.032	*	
			APL unlabeled vs. constitutive	<0.0001	****	
			acute vs. constitutive	0.0599	ns	
	alpha, d-DL	Kruskal-Wallis test		0.4053	ns	
				0.0191	****	
	beta, d-DL	Dunn's multiple comparisons test	APL unlabeled vs. acute	>0.9999	ns	
			APL unlabeled vs. constitutive	0.0192	*	
			acute vs. constitutive	0.1087	ns	
	gamma, d-DL	Kruskal-Wallis test		<0.0001	****	
			Dunn's multiple comparisons test	APL unlabeled vs. acute	>0.9999	ns
				APL unlabeled vs. constitutive	0.0015	**
			acute vs. constitutive	<0.0001	****	
	2C: APL>dTRPA1 adaptation, IA	alpha', IA	2-way ANOVA	interaction	0.0354	*
kept at 22 C vs. kept at 31 C				0.0168	*	
APL unlabeled vs. APL labeled				0.008	**	
Ordinary 1-way ANOVA				0.0009	***	
			Holm-Sidak's multiple comparisons test	APL unlab, kept 22°C vs. APL>dTRPA1, kept 22°C	0.8942	ns
				APL unlab, kept 22°C vs. APL unlab, kept 31°C	0.8942	ns
APL>dTRPA1, kept 22°C vs. APL>dTRPA1, kept 31°C		0.0031		**		
			APL unlab, kept 31°C vs. APL>dTRPA1, kept 31°C	0.0031	**	
beta', IA		2-way ANOVA	n/a (residuals not normal)			
			Welch's ANOVA	<0.0001	****	
		Dunnett's T3 multiple comparisons test	APL unlab, kept 22°C vs. APL>dTRPA1, kept 22°C	0.3687	ns	
			APL unlab, kept 22°C vs. APL unlab, kept 31°C	0.097	ns	
			APL>dTRPA1, kept 22°C vs. APL>dTRPA1, kept 31°C	<0.0001	****	
			APL unlab, kept 31°C vs. APL>dTRPA1, kept 31°C	0.0018	**	
alpha, IA		2-way ANOVA	interaction	0.1146	ns	
			kept at 22 C vs. kept at 31 C	0.002	**	
			APL unlabeled vs. APL labeled	0.1613	ns	
		Kruskal-Wallis test		0.0009	***	
			Dunn's multiple comparisons test	APL unlab, kept 22°C vs. APL>dTRPA1, kept 22°C	>0.9999	ns
		APL unlab, kept 22°C vs. APL unlab, kept 31°C		0.731	ns	
		APL>dTRPA1, kept 22°C vs. APL>dTRPA1, kept 31°C		0.0039	**	
		APL unlab, kept 31°C vs. APL>dTRPA1, kept 31°C		0.4608	ns	
		Ordinary 1-way ANOVA		(NB: D'Agostino-Pearson test on residuals p=0.0501)	0.0023	**
		Holm-Sidak's multiple comparisons test	APL unlab, kept 22°C vs. APL>dTRPA1, kept 22°C	0.898	ns	
APL unlab, kept 22°C vs. APL unlab, kept 31°C			0.4796	ns		
APL>dTRPA1, kept 22°C vs. APL>dTRPA1, kept 31°C			0.0018	**		
APL unlab, kept 31°C vs. APL>dTRPA1, kept 31°C			0.101	ns		
beta, IA		2-way ANOVA	interaction	0.2336	ns	
			kept at 22 C vs. kept at 31 C	<0.0001	****	
			APL unlabeled vs. APL labeled	0.0109	*	
		Ordinary 1-way ANOVA		<0.0001	****	
			Holm-Sidak's multiple comparisons test	APL unlab, kept 22°C vs. APL>dTRPA1, kept 22°C	0.3174	ns
		APL unlab, kept 22°C vs. APL unlab, kept 31°C		0.0208	*	
APL>dTRPA1, kept 22°C vs. APL>dTRPA1, kept 31°C		<0.0001		****		
			APL unlab, kept 31°C vs. APL>dTRPA1, kept 31°C	0.0208	*	
gamma, IA		2-way ANOVA	interaction	<0.0001	****	
	kept at 22 C vs. kept at 31 C		<0.0001	****		
	APL unlabeled vs. APL labeled		<0.0001	****		
	Ordinary 1-way ANOVA		<0.0001	****		
		Holm-Sidak's multiple comparisons test	APL unlab, kept 22°C vs. APL>dTRPA1, kept 22°C	0.8358	ns	
	APL unlab, kept 22°C vs. APL unlab, kept 31°C		0.6543	ns		
APL>dTRPA1, kept 22°C vs. APL>dTRPA1, kept 31°C	<0.0001		****			
		APL unlab, kept 31°C vs. APL>dTRPA1, kept 31°C	<0.0001	****		
alpha', d-DL	2-way ANOVA	n/a (residuals not normal)				
		Kruskal-Wallis test	<0.0001	****		
	Dunn's multiple comparisons test	APL unlab, kept 22°C vs. APL>dTRPA1, kept 22°C	>0.9999	ns		
		APL unlab, kept 22°C vs. APL unlab, kept 31°C	>0.9999	ns		
		APL>dTRPA1, kept 22°C vs. APL>dTRPA1, kept 31°C	<0.0001	****		

Table S2: Details of statistics

Figure	Data	Statistical test	Comparison	P-value	Significance	
2C: APL>dTRPA1 adaptation, d-DL	beta', d-DL	2-way ANOVA	APL unlab, kept 31°C vs. APL>dTRPA1, kept 31°C	0.0003	***	
			interaction	0.0005	***	
			kept at 22 C vs. kept at 31 C	0.0008	***	
			APL unlabeled vs. APL labeled	0.0046	**	
		Welch's ANOVA		0.0019	**	
			Dunnett's T3 multiple comparisons test	APL unlab, kept 22°C vs. APL>dTRPA1, kept 22°C	0.8689	ns
				APL unlab, kept 22°C vs. APL unlab, kept 31°C	0.9998	ns
				APL>dTRPA1, kept 22°C vs. APL>dTRPA1, kept 31°C	0.0013	**
		APL unlab, kept 31°C vs. APL>dTRPA1, kept 31°C		0.0029	**	
		alpha, d-DL	2-way ANOVA	interaction	0.0003	***
				kept at 22 C vs. kept at 31 C	<0.0001	****
				APL unlabeled vs. APL labeled	<0.0001	****
	Welch's ANOVA			<0.0001	****	
	Dunnett's T3 multiple comparisons test		APL unlab, kept 22°C vs. APL>dTRPA1, kept 22°C	0.9744	ns	
			APL unlab, kept 22°C vs. APL unlab, kept 31°C	0.3449	ns	
			APL>dTRPA1, kept 22°C vs. APL>dTRPA1, kept 31°C	<0.0001	****	
			APL unlab, kept 31°C vs. APL>dTRPA1, kept 31°C	0.0002	***	
	beta, d-DL		2-way ANOVA	interaction	0.0013	**
				kept at 22 C vs. kept at 31 C	<0.0001	****
				APL unlabeled vs. APL labeled	0.0005	***
				Welch's ANOVA	0.0002	***
		Dunnett's T3 multiple comparisons test	APL unlab, kept 22°C vs. APL>dTRPA1, kept 22°C	0.9796	ns	
			APL unlab, kept 22°C vs. APL unlab, kept 31°C	0.1068	ns	
			APL>dTRPA1, kept 22°C vs. APL>dTRPA1, kept 31°C	0.0008	***	
APL unlab, kept 31°C vs. APL>dTRPA1, kept 31°C			0.0036	**		
gamma, d-DL		2-way ANOVA	interaction	<0.0001	****	
			kept at 22 C vs. kept at 31 C	<0.0001	****	
			APL unlabeled vs. APL labeled	<0.0001	****	
			Welch's ANOVA	0.0001	***	
	Dunnett's T3 multiple comparisons test	APL unlab, kept 22°C vs. APL>dTRPA1, kept 22°C	0.9551	ns		
		APL unlab, kept 22°C vs. APL unlab, kept 31°C	0.9976	ns		
		APL>dTRPA1, kept 22°C vs. APL>dTRPA1, kept 31°C	0.0002	***		
		APL unlab, kept 31°C vs. APL>dTRPA1, kept 31°C	0.0003	***		
	2E: sparseness	Unpaired t-test	APL unlabeled vs. APL>dTRPA1	0.0003	***	
	S2: KC>GCaMP3, APL>dTRPA1, odor responses after adaptation	alpha', IA	Kruskal-Wallis test		0.0223	*
			Dunn's multiple comparisons test	APL unlab, kept 22°C vs. APL>dTRPA1, kept 22°C	0.0088	**
				APL unlab, kept 22°C vs. APL unlab, kept 31°C	0.6146	ns
APL>dTRPA1, kept 22°C vs. APL>dTRPA1, kept 31°C				0.1445	ns	
APL unlab, kept 31°C vs. APL>dTRPA1, kept 31°C		>0.9999		ns		
beta', IA		Ordinary 1-way ANOVA		0.0022	**	
		Holm-Sidak multiple comparisons test	APL unlab, kept 22°C vs. APL>dTRPA1, kept 22°C	0.8251	ns	
			APL unlab, kept 22°C vs. APL unlab, kept 31°C	0.8251	ns	
			APL>dTRPA1, kept 22°C vs. APL>dTRPA1, kept 31°C	0.0061	**	
APL unlab, kept 31°C vs. APL>dTRPA1, kept 31°C			0.0441	*		
alpha, IA		Ordinary 1-way ANOVA		0.0034	**	
		Holm-Sidak multiple comparisons test	APL unlab, kept 22°C vs. APL>dTRPA1, kept 22°C	0.3967	ns	
			APL unlab, kept 22°C vs. APL unlab, kept 31°C	0.1209	ns	
			APL>dTRPA1, kept 22°C vs. APL>dTRPA1, kept 31°C	0.0277	*	
APL unlab, kept 31°C vs. APL>dTRPA1, kept 31°C			0.0019	**		
beta, IA		Kruskal-Wallis test		0.0174	*	
		Dunn's multiple comparisons test	APL unlab, kept 22°C vs. APL>dTRPA1, kept 22°C	>0.9999	ns	
			APL unlab, kept 22°C vs. APL unlab, kept 31°C	>0.9999	ns	
			APL>dTRPA1, kept 22°C vs. APL>dTRPA1, kept 31°C	0.0436	*	
APL unlab, kept 31°C vs. APL>dTRPA1, kept 31°C			0.2168	ns		
gamma, IA		Ordinary 1-way ANOVA		0.0002	***	
		Holm-Sidak multiple comparisons test	APL unlab, kept 22°C vs. APL>dTRPA1, kept 22°C	0.3343	ns	
			APL unlab, kept 22°C vs. APL unlab, kept 31°C	0.3343	ns	
			APL>dTRPA1, kept 22°C vs. APL>dTRPA1, kept 31°C	0.0023	**	
APL unlab, kept 31°C vs. APL>dTRPA1, kept 31°C	0.0239		*			
Fig. S5A, sparseness for different odor	Mixed-effects model (matching across odors)	main effect APL unlabeled vs. APL>dTRPA1	0.0004	***		
		main effect across odors	<0.0001	****		
		interaction odor x (APL unlabeled vs. APL>dTRPA1)	0.0032	**		
Fig. S5C, inter-odor correlation	Unpaired t-test	APL unlabeled vs. APL>dTRPA1	0.1457	ns		
	Mixed-effects model (matching across odor pairs)	main effect APL unlabeled vs. APL>dTRPA1	0.1808	ns		
		main effect across odor pairs	<0.0001	****		
		interaction odor pairs x (APL unlabeled vs. APL>dTRPA1)	0.3646	ns		
S5D: APL>dTRPA1 vs. APL>dTRPA1	Welch's ANOVA		<0.0001	****		
		APL unlab, dTRPA1, kept 31°C vs. APL>dTRPA1, kept 31°C	<0.0001	****		
		APL unlab, dTRPA1, kept 31°C vs. APL unlab, TNT	0.0769	ns		

Table S2: Details of statistics

Figure	Data	Statistical test	Comparison	P-value	Significance
SSD, APL>TNT vs. APL>dTRPA1 adaptation		Dunnett's T3 multiple comparisons test	APL unlab, dTRPA1, kept 31°C vs. APL>TNT acute	<0.0001	****
			APL>dTRPA1, kept 31°C vs. APL unlab, TNT	<0.0001	****
			APL>dTRPA1, kept 31°C vs. APL>TNT acute	<0.0001	****
			APL unlab, TNT vs. APL>TNT acute	<0.0001	****
S7A: APL>dTRPA1 effect of heating during imaging, mean ΔF/F	APL unlabeled, kept at 22 °C, IA	Mixed-effects model with Geisser-Greenhouse correction (matching across lobes and across temperature at time of measurement)	lobe	0.6803	ns
			temperature	0.4272	ns
			lobe x temperature	0.3621	ns
	APL>dTRPA1, kept at 22 °C, IA	2-way repeated measures ANOVA with Geisser-Greenhouse correction (matching across lobes and across temperature at time of measurement)	lobe	<0.0001	****
			temperature	0.0017	**
			lobe x temperature	<0.0001	****
		Holm-Sidak multiple comparison test (22 °C vs. 31 °C)	alpha'	0.7426	ns
			beta'	0.044	*
			alpha	<0.0001	****
			beta	0.0004	***
	APL unlabeled, kept at 31 °C, IA	Mixed-effects model with Geisser-Greenhouse correction (matching across lobes and across temperature at time of measurement)	lobe	0.0024	**
			temperature	0.1031	ns
			lobe x temperature	0.4676	ns
	APL>dTRPA1, kept at 31 °C, IA	Mixed-effects model with Geisser-Greenhouse correction (matching across lobes and across temperature at time of measurement)	lobe	<0.0001	****
			temperature	0.0018	**
			lobe x temperature	<0.0001	****
		Holm-Sidak multiple comparison test (22 °C vs. 31 °C)	alpha'	0.2072	ns
			beta'	0.1344	ns
			alpha	0.0033	**
			beta	0.0042	**
	APL unlabeled, kept at 22 °C, dDL	2-way repeated measures ANOVA with Geisser-Greenhouse correction (matching across lobes and across temperature at time of measurement)	lobe	0.0006	***
			temperature	0.0002	***
			lobe x temperature	0.0012	**
	APL>dTRPA1, kept at 22 °C, dDL	Holm-Sidak multiple comparison test (22 °C vs. 31 °C)	alpha'	0.071	ns
			beta'	0.052	ns
			alpha	<0.0001	****
			beta	0.0015	**
	APL unlabeled, kept at 31 °C, dDL	Mixed-effects model with Geisser-Greenhouse correction (matching across lobes and across temperature at time of measurement)	lobe	0.0006	***
temperature			0.561	ns	
lobe x temperature			0.0185	*	
APL>dTRPA1, kept at 31 °C, IA	Mixed-effects model with Geisser-Greenhouse correction (matching across lobes and across temperature at time of measurement)	lobe	<0.0001	****	
		temperature	<0.0001	****	
		lobe x temperature	<0.0001	****	
	Holm-Sidak multiple comparison test (22 °C vs. 31 °C)	alpha'	0.0058	**	
		beta'	0.0026	**	
		alpha	0.0002	***	
		beta	0.0005	***	
APL unlabeled, kept at 22 °C, IA	Mixed-effects model with Geisser-Greenhouse correction (matching across lobes and across temperature at time of measurement)	lobe	0.5361	ns	
		temperature	0.1998	ns	
		lobe x temperature	0.3806	ns	
APL>dTRPA1, kept at 22 °C, IA	2-way repeated measures ANOVA with Geisser-Greenhouse correction (matching across lobes and across temperature at time of measurement)	lobe	0.0011	**	
		temperature	0.0103	*	
		lobe x temperature	<0.0001	****	
	Holm-Sidak multiple comparison test (22 °C vs. 31 °C)	alpha'	0.9831	ns	
		beta'	0.0032	**	
		alpha	<0.0001	****	
		beta	0.0003	***	
APL unlabeled, kept at 31 °C, IA	Mixed-effects model with Geisser-Greenhouse correction (matching across lobes and across temperature at time of measurement)	lobe	0.0001	***	
		temperature	0.0464	*	
		lobe x temperature	0.2941	ns	
Holm-Sidak multiple comparison test (22 °C vs. 31 °C)	alpha'	0.8542	ns		
	beta'	0.1352	ns		
	alpha	0.0217	*		
	beta	0.3134	ns		
APL unlabeled, kept at 22 °C, IA	Mixed-effects model with Geisser-Greenhouse correction (matching across lobes and across temperature at time of measurement)	lobe	0.0001	***	
		temperature	0.0088	**	
		lobe x temperature	0.0088	**	

Table S2: Details of statistics

Figure	Data	Statistical test	Comparison	P-value	Significance		
S7B: APL>dTRPA1 effect of heating during imaging - max. ΔF/F	APL>dTRPA1, kept at 31 °C, IA	Holm-Sidak multiple comparison test (22 °C vs. 31 °C)	lobe x temperature	<0.0001	****		
			alpha'	0.4606	ns		
			beta'	0.4606	ns		
			alpha	0.0228	*		
			beta	0.0412	*		
	APL unlabeled, kept at 22 °C, dDL	Mixed-effects model with Geisser-Greenhouse correction (matching across lobes and across temperature at time of measurement)	lobe	0.0034	**		
			temperature	0.9247	ns		
			lobe x temperature	0.3579	ns		
	APL>dTRPA1, kept at 22 °C, dDL	2-way repeated measures ANOVA with Geisser-Greenhouse correction (matching across lobes and across temperature at time of measurement)	lobe	<0.0001	****		
			temperature	0.0002	***		
			lobe x temperature	0.0003	***		
			alpha'	0.533	ns		
			beta'	0.533	ns		
	APL unlabeled, kept at 31 °C, dDL	Mixed-effects model with Geisser-Greenhouse correction (matching across lobes and across temperature at time of measurement)	alpha	<0.0001	****		
			beta	0.0003	***		
			gamma	<0.0001	****		
			lobe	<0.0001	****		
			temperature	0.6791	ns		
	APL>dTRPA1, kept at 31 °C, IA	Mixed-effects model with Geisser-Greenhouse correction (matching across lobes and across temperature at time of measurement)	lobe x temperature	0.0006	***		
			lobe	<0.0001	****		
temperature			0.0001	***			
lobe x temperature			<0.0001	****			
alpha'			0.0289	*			
Fig. S9, APL>dTRPA1 adaptation, IA after 1d and 4d adaptation	alpha', IA	2-way ANOVA	interaction	0.3092	ns		
			1d adaptation vs. 4d adaptation	0.8735	ns		
			UAS TRPA vs. APL TRPA	0.4222	ns		
	beta', IA	Ordinary 1-way ANOVA	Holm-Sidak's multiple comparisons test	UAS TRPA 1d vs. APL TRPA 1d	0.9998	ns	
				UAS TRPA 4d vs. APL TRPA 4d	<0.0001	****	
				interaction	0.0033	**	
		alpha, IA	2-way ANOVA	Holm-Sidak's multiple comparisons test	1d adaptation vs. 4d adaptation	0.9944	ns
					UAS TRPA vs. APL TRPA	0.0036	**
	UAS TRPA 1d vs. APL TRPA 1d				0.9975	ns	
	beta, IA	Ordinary 1-way ANOVA	Holm-Sidak's multiple comparisons test	UAS TRPA 4d vs. APL TRPA 4d	0.0185	*	
UAS TRPA 1d vs. APL TRPA 1d				0.9975	ns		
UAS TRPA 4d vs. APL TRPA 4d				0.0185	*		
gamma, IA		2-way ANOVA	Holm-Sidak's multiple comparisons test	interaction	0.3323	ns	
				1d adaptation vs. 4d adaptation	0.638	ns	
	UAS TRPA vs. APL TRPA			0.0031	**		
	alpha', dDL	Ordinary 1-way ANOVA	Holm-Sidak's multiple comparisons test	UAS TRPA 1d vs. APL TRPA 1d	0.0151	*	
				UAS TRPA 4d vs. APL TRPA 4d	0.2767	ns	
UAS TRPA 4d vs. APL TRPA 4d				0.0078	**		
beta', dDL		2-way ANOVA	Holm-Sidak's multiple comparisons test	UAS TRPA 1d vs. APL TRPA 1d	0.0187	*	
				UAS TRPA 4d vs. APL TRPA 4d	0.4415	ns	
	UAS TRPA vs. APL TRPA			0.0002	***		
	alpha, dDL	Ordinary 1-way ANOVA	Holm-Sidak's multiple comparisons test	UAS TRPA 1d vs. APL TRPA 1d	0.0002	***	
				UAS TRPA 4d vs. APL TRPA 4d	0.4469	ns	
UAS TRPA 4d vs. APL TRPA 4d				<0.0001	****		
Fig. S9, beta, dDL		2-way ANOVA	Holm-Sidak's multiple comparisons test	interaction	0.3624	ns	
				1d adaptation vs. 4d adaptation	0.466	ns	
	UAS TRPA vs. APL TRPA			0.1286	ns		
	alpha, dDL	Ordinary 1-way ANOVA	Holm-Sidak's multiple comparisons test	UAS TRPA 1d vs. APL TRPA 1d	0.3528	ns	
				UAS TRPA 4d vs. APL TRPA 4d	0.0011	**	
UAS TRPA 4d vs. APL TRPA 4d				0.2283	ns		
beta, dDL		2-way ANOVA	Holm-Sidak's multiple comparisons test	UAS TRPA vs. APL TRPA	0.0207	*	
				UAS TRPA 1d vs. APL TRPA 1d	0.0073	**	
	UAS TRPA 4d vs. APL TRPA 4d			0.5612	ns		
	alpha, dDL	Ordinary 1-way ANOVA	Holm-Sidak's multiple comparisons test	UAS TRPA 1d vs. APL TRPA 1d	0.0019	**	
				UAS TRPA 4d vs. APL TRPA 4d	0.0427	*	
UAS TRPA vs. APL TRPA				0.0304	*		
beta, dDL		2-way ANOVA	Holm-Sidak's multiple comparisons test	UAS TRPA 1d vs. APL TRPA 1d	0.0411	*	
				UAS TRPA 4d vs. APL TRPA 4d	0.0411	*	
	UAS TRPA vs. APL TRPA			0.0411	*		

Table S2: Details of statistics

Figure	Data	Statistical test	Comparison	P-value	Significance	
APL>dTRPA1 adaptation, d-DL after 1d and 4d adaptation	alpha, dDL	Ordinary 1-way ANOVA		0.0079	**	
		Holm-Sidak's multiple comparisons test	UAS TRPA 1d vs. APL TRPA 1d UAS TRPA 4d vs. APL TRPA 4d	>0.9999 0.011	ns *	
	beta, dDL	2-way ANOVA	interaction		0.3142	ns
			1d adaptation vs. 4d adaptation		0.0231	*
			UAS TRPA vs. APL TRPA		0.0049	**
	gamma, dDL	Ordinary 1-way ANOVA			0.0022	**
			Holm-Sidak's multiple comparisons test	UAS TRPA 1d vs. APL TRPA 1d UAS TRPA 4d vs. APL TRPA 4d	0.3058 0.0158	ns *
			2-way ANOVA	interaction 1d adaptation vs. 4d adaptation UAS TRPA vs. APL TRPA	0.281 0.8239 0.0056	ns ns **
	Fig S10, APL>dTRPA1 1d adaptation (imaged at 1 d old)	alpha', IA	Mann-Whitney test	no dTRPA1 vs. APL>dTRPA1	0.4985	ns
		beta', IA	Unpaired t-test	no dTRPA1 vs. APL>dTRPA1	0.7981	ns
		alpha, IA	Mann-Whitney test	no dTRPA1 vs. APL>dTRPA1	0.6788	ns
		beta, IA	Unpaired t-test	no dTRPA1 vs. APL>dTRPA1	0.6934	ns
gamma, IA		Unpaired t-test	no dTRPA1 vs. APL>dTRPA1	0.7713	ns	
alpha', d-DL		Unpaired t-test	no dTRPA1 vs. APL>dTRPA1	0.5653	ns	
beta', d-DL		Mann-Whitney test	no dTRPA1 vs. APL>dTRPA1	0.5145	ns	
alpha, d-DL		Unpaired t-test	no dTRPA1 vs. APL>dTRPA1	0.3114	ns	
beta, d-DL		Mann-Whitney test	no dTRPA1 vs. APL>dTRPA1	0.9215	ns	
gamma, d-DL		Mann-Whitney test	no dTRPA1 vs. APL>dTRPA1	0.7374	ns	
Fig 3, S11, APL>dTRPA1 1,2,3,4 d adaptation		alpha', IA	2-way ANOVA	interaction	0.5387	ns
				main effect of days at 31 °C	<0.0001	****
	main effect of APL unlabeled vs. APL>dTRPA1			<0.0001	****	
	Sidak multiple comparisons test		1 d	0.9266	ns	
			2 d	0.0112	*	
			3 d	0.046	*	
	beta', IA	2-way ANOVA	interaction	0.4041	ns	
			main effect of days at 31 °C	0.0018	**	
			main effect of APL unlabeled vs. APL>dTRPA1	0.0074	**	
		Sidak multiple comparisons test	1 d	ns	0.3357	
			2 d	ns	0.9997	
			3 d	ns	0.6155	
	alpha, IA	2-way ANOVA	interaction	0.8591	ns	
			main effect of days at 31 °C	<0.0001	****	
			main effect of APL unlabeled vs. APL>dTRPA1	<0.0001	****	
		Sidak multiple comparisons test	1 d	0.4206	ns	
			2 d	0.0338	*	
			3 d	0.2485	ns	
	beta, IA	2-way ANOVA	interaction	0.1678	ns	
			main effect of days at 31 °C	<0.0001	****	
			main effect of APL unlabeled vs. APL>dTRPA1	<0.0001	****	
		Sidak multiple comparisons test	1 d	0.3706	ns	
			2 d	0.2266	ns	
			3 d	0.0332	*	
gamma, IA	2-way ANOVA	interaction	0.3869	ns		
		main effect of days at 31 °C	0.0065	**		
		main effect of APL unlabeled vs. APL>dTRPA1	0.0005	***		
	Sidak multiple comparisons test	1 d	0.7576	ns		
		2 d	0.8093	ns		
		3 d	0.0338	*		
alpha', IA	2-way ANOVA	interaction	0.8996	ns		
		main effect of days at 31 °C	0.0363	*		
		main effect of APL unlabeled vs. APL>dTRPA1	<0.0001	****		
	Sidak multiple comparisons test	1 d	0.0459	*		
		2 d	0.3131	ns		
		3 d	0.0643	ns		
	2-way ANOVA	4 d	0.0463	*		
		interaction	0.2786	ns		
		main effect of days at 31 °C	0.0106	*		

Table S2: Details of statistics

Figure	Data	Statistical test	Comparison	P-value	Significance
Fig 3, S12, APL>dTRPA1 0, 1,2,3 d loss of adaptation	beta', IA		main effect of APL unlabeled vs. APL>dTRPA1	0.0016	**
		Sidak multiple comparisons test	1 d	0.1053	ns
			2 d	0.0694	ns
			3 d	>0.9999	ns
			4 d	0.343	ns
	alpha, IA	2-way ANOVA	interaction	0.8594	ns
			main effect of days at 31 °C	0.0003	****
			main effect of APL unlabeled vs. APL>dTRPA1	<0.0001	****
		Sidak multiple comparisons test	1 d	0.0228	*
			2 d	0.1343	ns
			3 d	0.1595	ns
			4 d	0.3751	ns
		beta, IA	2-way ANOVA	interaction	0.0073
			main effect of days at 31 °C	<0.0001	****
			main effect of APL unlabeled vs. APL>dTRPA1	<0.0001	****
	Sidak multiple comparisons test		1 d	<0.0001	****
			2 d	0.0901	ns
		3 d	0.9886	ns	
	gamma, IA	2-way ANOVA	interaction	0.6227	ns
			main effect of days at 31 °C	0.9096	ns
		main effect of APL unlabeled vs. APL>dTRPA1	<0.0001	****	
Sidak multiple comparisons test		1 d	0.0081	**	
		2 d	0.0488	*	
		3 d	0.2186	ns	
		4 d	0.4802	ns	
Fig 4: APL>dTRPA, GCaMP6f		alpha', IA	Mann-Whitney test	no dTRPA1 vs. APL>dTRPA1	0.0205
	beta', IA	Unpaired t-test	no dTRPA1 vs. APL>dTRPA1	0.0498	*
	alpha, IA	Unpaired t-test	no dTRPA1 vs. APL>dTRPA1	0.0111	*
	beta, IA	Unpaired t-test	no dTRPA1 vs. APL>dTRPA1	0.0235	*
	gamma, IA	Unpaired t-test	no dTRPA1 vs. APL>dTRPA1	0.0048	**
Fig S13B: APL>dTRPA, GCaMP6f, responses to d-DL	alpha', d-DL	Mann-Whitney test	no dTRPA1 vs. APL>dTRPA1	0.6495	ns
	beta', d-DL	Mann-Whitney test	no dTRPA1 vs. APL>dTRPA1	0.3475	ns
	alpha, d-DL	Unpaired t-test	no dTRPA1 vs. APL>dTRPA1	0.0271	*
	beta, d-DL	Unpaired t-test	no dTRPA1 vs. APL>dTRPA1	0.1355	ns
	gamma, d-DL	Mann-Whitney test	no dTRPA1 vs. APL>dTRPA1	0.0768	ns
Fig S13C: APL>dTRPA1, GCaMP6f, steady state responses	alpha', IA	Mann-Whitney test	no dTRPA1 vs. APL>dTRPA1	0.4776	ns
	beta', IA	Unpaired t-test	no dTRPA1 vs. APL>dTRPA1	0.5483	ns
	alpha, IA	Unpaired t-test	no dTRPA1 vs. APL>dTRPA1	0.4987	ns
	beta, IA	Unpaired t-test	no dTRPA1 vs. APL>dTRPA1	0.6323	ns
	gamma, IA	Unpaired t-test	no dTRPA1 vs. APL>dTRPA1	0.0652	ns
	alpha', d-DL	Mann-Whitney test	no dTRPA1 vs. APL>dTRPA1	0.1366	ns
	beta', d-DL	Unpaired t-test	no dTRPA1 vs. APL>dTRPA1	0.2305	ns
	alpha, d-DL	Unpaired t-test	no dTRPA1 vs. APL>dTRPA1	0.1425	ns
	beta, d-DL	Unpaired t-test	no dTRPA1 vs. APL>dTRPA1	0.9134	ns
	gamma, d-DL	Unpaired t-test	no dTRPA1 vs. APL>dTRPA1	0.5768	ns
Fig 5B, S14: APL>dTRPA, GCaMP6f	alpha', heat	Mann-Whitney test	kept 22°C 4d vs. kept 31°C 4d	0.6009	ns
	alpha', heat + IA	Mann-Whitney test	kept 22°C 4d vs. kept 31°C 4d	0.9623	ns
	dDL	Mann-Whitney test	kept 22°C 4d vs. kept 31°C 4d	0.7396	ns
	alpha, heat	Unpaired t-test	kept 22°C 4d vs. kept 31°C 4d	0.6606	ns
	alpha, heat + IA	Unpaired t-test	kept 22°C 4d vs. kept 31°C 4d	0.5465	ns
	dDL	Unpaired t-test	kept 22°C 4d vs. kept 31°C 4d	0.5223	ns
	beta, heat	Unpaired t-test	kept 22°C 4d vs. kept 31°C 4d	0.7655	ns
	beta, heat + IA	Unpaired t-test	kept 22°C 4d vs. kept 31°C 4d	0.7018	ns
	beta, heat + dDL	Unpaired t-test	kept 22°C 4d vs. kept 31°C 4d	0.9975	ns
	gamma, heat	Unpaired t-test	kept 22°C 4d vs. kept 31°C 4d	0.1617	ns
	gamma, heat + IA	Unpaired t-test	kept 22°C 4d vs. kept 31°C 4d	0.1225	ns
	dDL	Unpaired t-test	kept 22°C 4d vs. kept 31°C 4d	0.0881	ns
	alpha', IA	alpha', IA	Welch's ANOVA		0.1045
beta', IA		Welch's ANOVA	Post hoc tests below with Holm-Bonferroni correction	<0.0001	****
		Paired t-test	Kept at 22 °C, measured at 22 °C v. 31 °C	0.066	ns
		Paired t-test	Kept at 31 °C, measured at 22 °C v. 31 °C	0.0696	ns
		Welch's t-test	Measured at 22 °C, kept at 22 °C v. kept at 31 °C	0.0002	***
		Welch's t-test	Measured at 31 °C, kept at 22 °C v. kept at 31 °C	0.0028	***
		Welch's t-test	Kept @22°C, meas. @22°C v. kept @31°C, meas. @31°C	0.1348	ns
alpha, IA		Welch's ANOVA	Post hoc tests below with Holm-Bonferroni correction	<0.0001	****
		Paired t-test	Kept at 22 °C, measured at 22 °C v. 31 °C	<0.0001	****
		Paired t-test	Kept at 31 °C, measured at 22 °C v. 31 °C	0.0024	**
		Welch's t-test	Measured at 22 °C, kept at 22 °C v. kept at 31 °C	0.0028	**

Table S2: Details of statistics

Figure	Data	Statistical test	Comparison	P-value	Significance
Fig 5E, S15A: APL>dTRPA1, KC>GCaMP6f, responses measured at 31°C (mean ΔF/F)	beta, IA	Welch's t-test	Measured at 31 °C, kept at 22 °C v. kept at 31 °C	0.0609	ns
		Welch's t-test	Kept @22°C, meas. @22°C v. kept @31°C, meas. @31°C	0.104	ns
		Welch's ANOVA	Post hoc tests below with Holm-Bonferroni correction	<0.0001	****
		Paired t-test	Kept at 22 °C, measured at 22 °C v. 31 °C	0.0005	***
		Paired t-test	Kept at 31 °C, measured at 22 °C v. 31 °C	0.0042	**
		Welch's t-test	Measured at 22 °C, kept at 22 °C v. kept at 31 °C	<0.0001	****
	gamma, IA	Welch's t-test	Measured at 31 °C, kept at 22 °C v. kept at 31 °C	0.04	*
		Welch's t-test	Kept @22°C, meas. @22°C v. kept @31°C, meas. @31°C	0.5275	ns
		Welch's ANOVA	Post hoc tests below with Holm-Bonferroni correction	<0.0001	****
		Paired t-test	Kept at 22 °C, measured at 22 °C v. 31 °C	0.002	**
		Paired t-test	Kept at 31 °C, measured at 22 °C v. 31 °C	0.0018	**
		Welch's t-test	Measured at 22 °C, kept at 22 °C v. kept at 31 °C	0.0011	**
	alpha', dDL	Welch's t-test	Measured at 31 °C, kept at 22 °C v. kept at 31 °C	0.9022	ns
		Welch's t-test	Kept @22°C, meas. @22°C v. kept @31°C, meas. @31°C	0.0318	*
		Welch's ANOVA	Post hoc tests below with Holm-Bonferroni correction	<0.0001	****
		Paired t-test	Kept at 22 °C, measured at 22 °C v. 31 °C	0.002	***
		Paired t-test	Kept at 31 °C, measured at 22 °C v. 31 °C	0.213	ns
		Paired t-test	Kept at 31 °C, measured at 22 °C v. 31 °C	0.029	*
	beta', dDL	Welch's t-test	Measured at 22 °C, kept at 22 °C v. kept at 31 °C	0.034	*
		Welch's t-test	Measured at 31 °C, kept at 22 °C v. kept at 31 °C	0.6808	ns
		Welch's t-test	Kept @22°C, meas. @22°C v. kept @31°C, meas. @31°C	0.3088	ns
		Welch's ANOVA	Post hoc tests below with Holm-Bonferroni correction	<0.0001	****
		Paired t-test	Kept at 22 °C, measured at 22 °C v. 31 °C	0.0526	ns
		Paired t-test	Kept at 31 °C, measured at 22 °C v. 31 °C	0.0052	**
	alpha, dDL	Welch's t-test	Measured at 22 °C, kept at 22 °C v. kept at 31 °C	0.001	**
		Welch's t-test	Measured at 31 °C, kept at 22 °C v. kept at 31 °C	0.072	ns
		Welch's t-test	Kept @22°C, meas. @22°C v. kept @31°C, meas. @31°C	0.3252	ns
		Welch's ANOVA	Post hoc tests below with Holm-Bonferroni correction	<0.0001	****
		Paired t-test	Kept at 22 °C, measured at 22 °C v. 31 °C	<0.0001	****
		Paired t-test	Kept at 31 °C, measured at 22 °C v. 31 °C	0.00012	***
	beta, dDL	Welch's t-test	Measured at 22 °C, kept at 22 °C v. kept at 31 °C	<0.0001	****
		Welch's t-test	Measured at 31 °C, kept at 22 °C v. kept at 31 °C	0.0374	*
		Welch's t-test	Kept @22°C, meas. @22°C v. kept @31°C, meas. @31°C	0.0032	**
		Welch's ANOVA	Post hoc tests below with Holm-Bonferroni correction	0.0002	***
		Paired t-test	Kept at 22 °C, measured at 22 °C v. 31 °C	0.0015	**
		Paired t-test	Kept at 31 °C, measured at 22 °C v. 31 °C	0.0005	***
	gamma, dDL	Welch's t-test	Measured at 22 °C, kept at 22 °C v. kept at 31 °C	0.00044	***
		Welch's t-test	Measured at 31 °C, kept at 22 °C v. kept at 31 °C	0.0194	*
		Welch's t-test	Kept @22°C, meas. @22°C v. kept @31°C, meas. @31°C	0.5368	ns
		Welch's ANOVA	Post hoc tests below with Holm-Bonferroni correction	<0.0001	****
		Paired t-test	Kept at 22 °C, measured at 22 °C v. 31 °C	<0.0001	****
		Paired t-test	Kept at 31 °C, measured at 22 °C v. 31 °C	0.0008	***
	alpha', IA	Welch's t-test	Measured at 22 °C, kept at 22 °C v. kept at 31 °C	0.0008	***
		Welch's t-test	Measured at 31 °C, kept at 22 °C v. kept at 31 °C	0.1946	ns
	beta', IA	Welch's t-test	Kept @22°C, meas. @22°C v. kept @31°C, meas. @31°C	0.0084	**
		Welch's ANOVA	Post hoc tests below with Holm-Bonferroni correction	0.0599	ns
		Kruskal-Wallis test	Post hoc tests below with Holm-Bonferroni correction	<0.0001	****
		Paired t-test	Kept at 22 °C, measured at 22 °C v. 31 °C	0.0022	**
		Wilcoxon signed rank test	Kept at 31 °C, measured at 22 °C v. 31 °C	0.2334	ns
		Mann-Whitney test	Measured at 22 °C, kept at 22 °C v. kept at 31 °C	<0.0001	****
	alpha, IA	Welch's t-test	Measured at 31 °C, kept at 22 °C v. kept at 31 °C	0.0024	**
		Welch's t-test	Kept @22°C, meas. @22°C v. kept @31°C, meas. @31°C	<0.0001	****
Welch's ANOVA		Post hoc tests below with Holm-Bonferroni correction	<0.0001	****	
Paired t-test		Kept at 22 °C, measured at 22 °C v. 31 °C	<0.0001	****	
Paired t-test		Kept at 31 °C, measured at 22 °C v. 31 °C	0.0174	*	
Welch's t-test		Measured at 22 °C, kept at 22 °C v. kept at 31 °C	0.0032	**	
beta, IA	Welch's t-test	Measured at 31 °C, kept at 22 °C v. kept at 31 °C	0.1724	ns	
	Welch's t-test	Kept @22°C, meas. @22°C v. kept @31°C, meas. @31°C	0.3025	ns	
	Welch's ANOVA	Post hoc tests below with Holm-Bonferroni correction	<0.0001	****	
	Paired t-test	Kept at 22 °C, measured at 22 °C v. 31 °C	0.0002	***	
	Paired t-test	Kept at 31 °C, measured at 22 °C v. 31 °C	0.0278	*	
	Welch's t-test	Measured at 22 °C, kept at 22 °C v. kept at 31 °C	0.0002	***	
gamma, IA	Welch's t-test	Measured at 31 °C, kept at 22 °C v. kept at 31 °C	0.0015	**	
	Welch's t-test	Kept @22°C, meas. @22°C v. kept @31°C, meas. @31°C	0.1597	ns	
	Welch's ANOVA	Post hoc tests below with Holm-Bonferroni correction	<0.0001	****	
	Paired t-test	Kept at 22 °C, measured at 22 °C v. 31 °C	0.0123	*	
	Paired t-test	Kept at 31 °C, measured at 22 °C v. 31 °C	0.0016	**	
	Welch's t-test	Measured at 22 °C, kept at 22 °C v. kept at 31 °C	<0.0001	****	
gamma, IA	Welch's t-test	Measured at 31 °C, kept at 22 °C v. kept at 31 °C	0.4147	ns	
	Welch's t-test	Kept @22°C, meas. @22°C v. kept @31°C, meas. @31°C	0.6607	ns	

Table S2: Details of statistics

Figure	Data	Statistical test	Comparison	P-value	Significance
Fig S15B: APL>dTRPA1, KC>GCaMP6f, responses measured at 31c (max ΔF/F)	alpha', dDL	Welch's ANOVA	Post hoc tests below with Holm-Bonferroni correction	0.0027	**
		Paired t-test	Kept at 22 °C, measured at 22 °C v. 31 °C	0.4921	ns
		Paired t-test	Kept at 31 °C, measured at 22 °C v. 31 °C	0.1156	ns
		Welch's t-test	Measured at 22 °C, kept at 22 °C v. kept at 31 °C	0.0035	**
		Welch's t-test	Measured at 31 °C, kept at 22 °C v. kept at 31 °C	0.8121	ns
	beta', dDL	Welch's t-test	Kept @22°C, meas. @22°C v. kept @31°C, meas. @31°C	0.8322	ns
		Welch's ANOVA	Post hoc tests below with Holm-Bonferroni correction	<0.0001	****
		Paired t-test	Kept at 22 °C, measured at 22 °C v. 31 °C	0.3166	ns
		Paired t-test	Kept at 31 °C, measured at 22 °C v. 31 °C	0.0248	*
		Welch's t-test	Measured at 22 °C, kept at 22 °C v. kept at 31 °C	0.0005	***
	alpha, dDL	Welch's t-test	Measured at 31 °C, kept at 22 °C v. kept at 31 °C	0.0087	**
		Welch's t-test	Kept @22°C, meas. @22°C v. kept @31°C, meas. @31°C	0.0072	**
		Welch's ANOVA	Post hoc tests below with Holm-Bonferroni correction	<0.0001	****
		Paired t-test	Kept at 22 °C, measured at 22 °C v. 31 °C	<0.0001	****
		Paired t-test	Kept at 31 °C, measured at 22 °C v. 31 °C	0.0006	***
	beta, dDL	Welch's t-test	Measured at 22 °C, kept at 22 °C v. kept at 31 °C	0.0002	***
		Welch's t-test	Measured at 31 °C, kept at 22 °C v. kept at 31 °C	0.0126	*
		Welch's t-test	Kept @22°C, meas. @22°C v. kept @31°C, meas. @31°C	0.0178	*
		Welch's ANOVA	Post hoc tests below with Holm-Bonferroni correction	<0.0001	****
		Paired t-test	Kept at 22 °C, measured at 22 °C v. 31 °C	0.0005	***
	gamma, dDL	Paired t-test	Kept at 31 °C, measured at 22 °C v. 31 °C	0.0015	**
		Welch's t-test	Measured at 22 °C, kept at 22 °C v. kept at 31 °C	0.0004	***
		Welch's t-test	Measured at 31 °C, kept at 22 °C v. kept at 31 °C	0.0042	**
		Welch's t-test	Kept @22°C, meas. @22°C v. kept @31°C, meas. @31°C	0.2224	ns
Welch's ANOVA		Post hoc tests below with Holm-Bonferroni correction	<0.0001	****	
alpha', IA	Paired t-test	Kept at 22 °C, measured at 22 °C v. 31 °C	<0.0001	****	
	Paired t-test	Kept at 31 °C, measured at 22 °C v. 31 °C	0.0002	***	
	Welch's t-test	Measured at 22 °C, kept at 22 °C v. kept at 31 °C	0.0002	***	
	Welch's t-test	Measured at 31 °C, kept at 22 °C v. kept at 31 °C	0.51	ns	
	Welch's t-test	Kept @22°C, meas. @22°C v. kept @31°C, meas. @31°C	0.0008	***	
Note: for Fig 6/S17, pairwise comparisons were Holm-Bonferroni corrected for the 4 comparisons within each lobe (2 paired, 2 unpaired)					
Fig 6, S17: APL>Ort	alpha', IA	Wilcoxon signed-rank test	no dTRPA1: before vs. +histamine	0.0002	***
		Wilcoxon signed-rank test	APL>dTRPA1: before vs. +histamine	0.0002	***
		Mann-Whitney test	before: no dTRPA1 vs. APL>dTRPA1	0.0974	ns
		Mann-Whitney test	+histamine: no dTRPA1 vs. APL>dTRPA1	0.8173	ns
	beta', IA	paired t-test	no dTRPA1: before vs. +histamine	<0.0001	****
		paired t-test	APL>dTRPA1: before vs. +histamine	<0.0001	****
		unpaired t-test	before: no dTRPA1 vs. APL>dTRPA1	0.3371	ns
		unpaired t-test	+histamine: no dTRPA1 vs. APL>dTRPA1	0.6116	ns
	alpha, IA	paired t-test	no dTRPA1: before vs. +histamine	<0.0001	****
		paired t-test	APL>dTRPA1: before vs. +histamine	<0.0001	****
		unpaired t-test	before: no dTRPA1 vs. APL>dTRPA1	0.0214	*
		unpaired t-test	+histamine: no dTRPA1 vs. APL>dTRPA1	0.042	*
	beta, IA	paired t-test	no dTRPA1: before vs. +histamine	<0.0001	****
		paired t-test	APL>dTRPA1: before vs. +histamine	<0.0001	****
		unpaired t-test	before: no dTRPA1 vs. APL>dTRPA1	0.002	**
		unpaired t-test	+histamine: no dTRPA1 vs. APL>dTRPA1	0.0352	*
	gamma, IA	Wilcoxon signed-rank test	no dTRPA1: before vs. +histamine	0.0006	***
		Wilcoxon signed-rank test	APL>dTRPA1: before vs. +histamine	0.0002	***
		Mann-Whitney test	before: no dTRPA1 vs. APL>dTRPA1	0.0038	**
		unpaired t-test	+histamine: no dTRPA1 vs. APL>dTRPA1	0.4998	ns
	calyx, IA	paired t-test	no dTRPA1: before vs. +histamine	0.0006	***
		paired t-test	APL>dTRPA1: before vs. +histamine	0.0002	***
		unpaired t-test	before: no dTRPA1 vs. APL>dTRPA1	0.0046	**
		unpaired t-test	+histamine: no dTRPA1 vs. APL>dTRPA1	0.3891	ns
	alpha', dDL	Wilcoxon signed-rank test	no dTRPA1: before vs. +histamine	0.0008	***
		paired t-test	APL>dTRPA1: before vs. +histamine	0.0018	**
		Mann-Whitney test	before: no dTRPA1 vs. APL>dTRPA1	0.139	ns
		Mann-Whitney test	+histamine: no dTRPA1 vs. APL>dTRPA1	0.7658	ns
	beta', dDL	paired t-test	no dTRPA1: before vs. +histamine	0.0008	***
		paired t-test	APL>dTRPA1: before vs. +histamine	0.0018	**
		unpaired t-test	before: no dTRPA1 vs. APL>dTRPA1	0.5005	ns
		unpaired t-test	+histamine: no dTRPA1 vs. APL>dTRPA1	0.6698	ns
	alpha, dDL	paired t-test	no dTRPA1: before vs. +histamine	0.0147	*
		paired t-test	APL>dTRPA1: before vs. +histamine	0.0132	*
		unpaired t-test	before: no dTRPA1 vs. APL>dTRPA1	0.0254	*
		unpaired t-test	+histamine: no dTRPA1 vs. APL>dTRPA1	0.4561	ns
beta, dDL	paired t-test	no dTRPA1: before vs. +histamine	0.0064	**	
	paired t-test	APL>dTRPA1: before vs. +histamine	0.0057	**	



Table S2: Details of statistics

Figure	Data	Statistical test	Comparison	P-value	Significance
	beta, dDL	unpaired t-test	before: no dTRPA1 vs. APL>dTRPA1	0.002	**
		unpaired t-test	+histamine: no dTRPA1 vs. APL>dTRPA1	0.016	*
	gamma, dDL	Wilcoxon signed-rank test	no dTRPA1: before vs. +histamine	0.033	*
		Wilcoxon signed-rank test	APL>dTRPA1: before vs. +histamine	0.214	ns
		Mann-Whitney test	before: no dTRPA1 vs. APL>dTRPA1	0.0164	*
		unpaired t-test	+histamine: no dTRPA1 vs. APL>dTRPA1	0.2777	ns
	calyx, dDL	paired t-test	no dTRPA1: before vs. +histamine	0.0801	ns
		paired t-test	APL>dTRPA1: before vs. +histamine	0.1358	ns
		unpaired t-test	before: no dTRPA1 vs. APL>dTRPA1	0.0548	ns
		unpaired t-test	+histamine: no dTRPA1 vs. APL>dTRPA1	0.3275	ns
Note: for Fig S18, pairwise comparisons were Holm-Bonferroni corrected for the 4 comparisons within each lobe (2 paired, 2 unpaired)					
Fig S18: APL>TNT vs. APL.Ort	alpha', IA	Welch's t-test	APL unlabeled vs. APL>TNT	<0.0001	****
		Wilcoxon signed rank test	APL>Ort, histamine vs. no histamine	0.0002	***
		Mann-Whitney test	APL unlabeled vs. APL>Ort no histamine	0.102	ns
		Welch's t-test	APL>TNT vs. APL>Ort + histamine	0.8805	ns
	beta', IA	Mann-Whitney test	APL unlabeled vs. APL>TNT	<0.0001	****
		Paired t-test	APL>Ort, histamine vs. no histamine	<0.0001	****
		Welch's t-test	APL unlabeled vs. APL>Ort no histamine	0.2128	ns
		Mann-Whitney test	APL>TNT vs. APL>Ort + histamine	0.6682	ns
	alpha, IA	Welch's t-test	APL unlabeled vs. APL>TNT	<0.0001	****
		Paired t-test	APL>Ort, histamine vs. no histamine	<0.0001	****
		Welch's t-test	APL unlabeled vs. APL>Ort no histamine	0.0016	**
		Welch's t-test	APL>TNT vs. APL>Ort + histamine	0.0008	***
	beta, IA	Welch's t-test	APL unlabeled vs. APL>TNT	<0.0001	****
		Paired t-test	APL>Ort, histamine vs. no histamine	<0.0001	****
		Welch's t-test	APL unlabeled vs. APL>Ort no histamine	0.006	**
		Welch's t-test	APL>TNT vs. APL>Ort + histamine	0.011	*
	gamma, IA	Welch's t-test	APL unlabeled vs. APL>TNT	<0.0001	****
		Wilcoxon signed rank test	APL>Ort, histamine vs. no histamine	0.0006	***
		Mann-Whitney test	APL unlabeled vs. APL>Ort no histamine	0.02	*
		Welch's t-test	APL>TNT vs. APL>Ort + histamine	0.4298	ns
	alpha', dDL	Welch's t-test	APL unlabeled vs. APL>TNT	<0.0001	****
		Wilcoxon signed rank test	APL>Ort, histamine vs. no histamine	0.0006	***
		Mann-Whitney test	APL unlabeled vs. APL>Ort no histamine	>0.99	ns
		Welch's t-test	APL>TNT vs. APL>Ort + histamine	>0.99	ns
	beta', dDL	Welch's t-test	APL unlabeled vs. APL>TNT	<0.0001	****
		Paired t-test	APL>Ort, histamine vs. no histamine	0.0006	***
		Welch's t-test	APL unlabeled vs. APL>Ort no histamine	0.9555	ns
		Welch's t-test	APL>TNT vs. APL>Ort + histamine	0.1324	ns
	alpha, dDL	Welch's t-test	APL unlabeled vs. APL>TNT	<0.0001	****
		Paired t-test	APL>Ort, histamine vs. no histamine	0.0147	*
		Welch's t-test	APL unlabeled vs. APL>Ort no histamine	0.1487	ns
		Welch's t-test	APL>TNT vs. APL>Ort + histamine	0.2208	ns
	beta, dDL	Welch's t-test	APL unlabeled vs. APL>TNT	<0.0001	****
		Paired t-test	APL>Ort, histamine vs. no histamine	0.0038	**
		Welch's t-test	APL unlabeled vs. APL>Ort no histamine	0.03	*
		Welch's t-test	APL>TNT vs. APL>Ort + histamine	0.3994	ns
gamma, dDL	Welch's t-test	APL unlabeled vs. APL>TNT	<0.0001	****	
	Wilcoxon signed rank test	APL>Ort, histamine vs. no histamine	0.033	*	
	Mann-Whitney test	APL unlabeled vs. APL>Ort no histamine	0.8266	ns	
	Welch's t-test	APL>TNT vs. APL>Ort + histamine	0.2188	ns	